Space Science Reviews (2024) 220:54
https://doi.org/10.1007/s11214-024-01085-y

Geophysical Characterization of the Interiors of Ganymede, Callisto and Europa by ESA's JUpiter ICy moons Explorer

Tim Van Hoolst · Gabriel Tobie · Claire Vallat · Nicolas Altobelli · Lorenzo Bruzzone · Hao Cao et al. ***[full author details at the end of the article]***

Received: 1 November 2023 / Accepted: 13 June 2024 / Published online: 11 July 2024

Abstract
The JUpiter ICy moons Explorer (JUICE) of ESA was launched on 14 April 2023 and will arrive at Jupiter and its moons in July 2031. In this review article, we describe how JUICE will investigate the interior of the three icy Galilean moons, Ganymede, Callisto and Europa, during its Jupiter orbital tour and the final orbital phase around Ganymede. Detailed geophysical observations about the interior of the moons can only be performed from close distances to the moons, and best estimates of signatures of the interior, such as an induced magnetic field, tides and rotation variations, and radar reflections, will be obtained during flybys of the moons with altitudes of about 1000 km or less and during the Ganymede orbital phase at an average altitude of 490 km. The 9-month long orbital phase around Ganymede, the first of its kind around another moon than our Moon, will allow an unprecedented and detailed insight into the moon's interior, from the central regions where a magnetic field is generated to the internal ocean and outer ice shell. Multiple flybys of Callisto will clarify the differences in evolution compared to Ganymede and will provide key constraints on the origin and evolution of the Jupiter system. JUICE will visit Europa only during two close flybys and the geophysical investigations will focus on selected areas of the ice shell. A prime goal of JUICE is the characterisation of the ice shell and ocean of the Galilean moons, and we here specifically emphasise the synergistic aspects of the different geophysical investigations, showing how different instruments will work together to probe the hydrosphere. We also describe how synergies between JUICE instruments will contribute to the assessment of the deep interior of the moons, their internal differentiation, dynamics and evolution. In situ measurements and remote sensing observations will support the geophysical instruments to achieve these goals, but will also, together with subsurface radar sounding, provide information about tectonics, potential plumes, and the composition of the surface, which will help understanding the composition of the interior, the structure of the ice shell, and exchange processes between ocean, ice and surface. Accurate tracking of the JUICE spacecraft all along the mission will strongly improve our knowledge of the changing orbital motions of the moons and will provide additional insight into the dissipative processes in the Jupiter system. Finally, we present an overview of how the geophysical investigations will be performed and describe the operational synergies and challenges.

Keywords JUICE · Ganymede · Callisto · Europa · Interior · Evolution · Geophysics

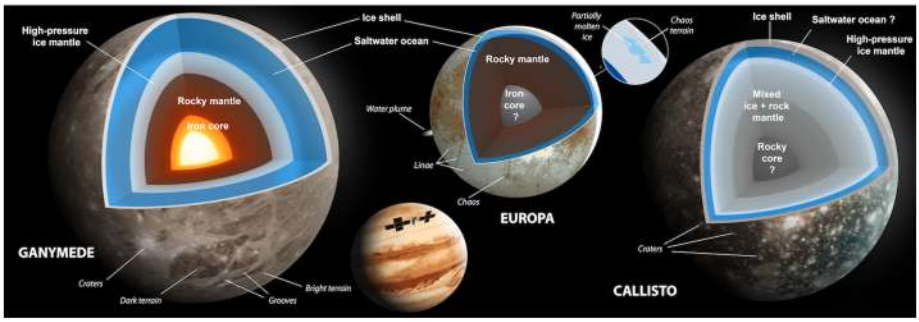

Fig. 1 Schematic possible interior structures of Ganymede, Europa and Callisto based on the Galileo data, and link with surface signatures of internal activity. Ganymede possesses the most differentiated structure with a thick hydrosphere, a rocky mantle and a liquid iron core, while the presence of an iron core inside Europa and the degree of ice-rock separation in the interior of Callisto are still uncertain. The thickness, depth and composition of the saltwater subsurface oceans are still poorly constrained. Galileo data are not fully conclusive about the existence of an ocean in Callisto

1 Introduction

The discovery of the four Jovian moons in 1610 by Galileo Galilei (1610) marked the beginning of modern observational astronomy in which the universe is observed by means of telescopes instead of the naked eye. It also contributed to the acceptance of the heliocentric model of the Solar System (Copernicus 1543) replacing the Earth-centered world view. Not only did the Jupiter system clearly show multiple smaller bodies - the moons that Galileo called Medician stars - orbiting a more massive body (Jupiter), the telescopic observations also indicated that moons can orbit the Sun together with their central planet, something that some contemporaries of Galileo were reluctant to accept for the Earth and Moon (Galilei 1610). During centuries, the Galilean moons just remained tiny bright spots orbiting Jupiter, intriguing astronomers and mathematicians. First resolved images by Pioneer 10 in 1973 and Voyager 1 and 2 in 1979 revolutionized our view of these moons. They revealed the cataclysmic volcanic eruptions of Io and the intensely tectonized surface of Europa. These observations hinted at the possibility of a global ocean underneath Europa's surface. A prediction that was confirmed two decades later by the Galileo mission, which also provided evidence that Ganymede also has a global subsurface ocean and that Callisto might have one. Another major discovery of the Galileo mission was the detection of an intrinsic magnetic field on Ganymede (Fig. 1).

After these first explorations, the ESA Jupiter ICy moons Explorer (JUICE) mission and NASA's Europa Clipper together will open a new chapter of detailed characterization of the Galilean moons. JUICE will be the first mission to explore one of these moons, Ganymede, the largest moon of the Solar System, in detail from orbit. It will investigate the oceanic environments and their habitability in the three icy Galilean moons, Europa, Ganymede and Callisto. Although the main focus will be on Ganymede, JUICE will also significantly advance our understanding of Callisto through multiple flybys and will contribute with two flybys to the in-depth investigation of Europa by Clipper.

This review belongs to a series of papers describing the entire JUICE mission. Besides papers on spacecraft and mission design (Erd et al. 2024, this collection, Witasse et al. 2023, this collection) and on the different science instruments and experiments, the volume of JUICE publications also includes four review articles related to the four major science

themes of JUICE. This article focuses on the interior of the icy moons of Jupiter, including an assessment of the habitability of their hydrosphere. The three other reviews on the major science themes focus on the moons' geology, surface composition and tenuous atmospheres (Tosi et al. 2024, this collection), the magnetosphere (Masters et al. 2024, this collection), and Jupiter's atmosphere (Fletcher et al. 2023, this collection). We also refer to the recent book on Ganymede edited by Volwerk et al. (2024).

We here focus on the current status and scientific advances in moon interiors that JUICE will contribute to, with specific attention to the synergies between the different JUICE instruments. To avoid overlap with other papers in this collection, we often refer to instrument papers and other papers in this collection for information on instruments capabilities, mission constraints, and trajectories and only describe those elements that are needed for our objectives. The most important instruments for our science goals are the radio science instrument 3GM (Iess et al. 2024, this collection), the laser altimeter GALA (Hussmann et al. 2024, this collection), the magnetometer J-MAG (Dougherty et al. 2024, this collection) and the ice penetrating radar RIME (Bruzzone et al. 2024, this collection). Complementary data are provided by the optical camera JANUS (Palumbo et al. 2024, this collection), the visible and infrared imaging spectrometer MAJIS (Poulet et al. 2024, this collection), the UV imaging spectrograph UVS (Gladstone et al. 2024, this collection), the radio and plasma wave instrument RPWI (Wahlund et al. 2024, this collection), and the particle environment package PEP (Barabash et al. 2024, this collection). The Planetary Radio Interferometer and Doppler Experiment PRIDE (Gurvits et al. 2023, this collection) does not have any hardware on board of JUICE but detects and processes the radio signal of the JUICE spacecraft with a network of Earth-based radio telescopes. PRIDE will contribute essential information on the ephemerides of the moons and Jupiter.

The article first describes the science objectives of JUICE from a synergistic point of view and then focuses on the operational aspects and observation synergies. Section 2 provides an overview of how JUICE will characterise the hydrosphere of Ganymede, Callisto and Europa (Fig. 1). We show how three instruments, 3GM, GALA and J-MAG, are essential in probing the hydrosphere, proving the existence of a subsurface ocean, determining the thickness of the ice shell and ocean, and setting important constraints on thermodynamic and transport properties of those two layers. Detailed local information on the structure and composition of the ice shell and on the occurrence of brines or salt-rich deposits at shallow depths will be provided by RIME complemented with the remote sensing instruments. Section 3 reviews the expected advances on the deep interior structure and evolution of the moons (Fig. 1). Of particular interest here are the metallic core of Ganymede, the only moon to possess an internal dynamo magnetic field, and the possibly different internal differentiation of the moons. Although probing deeper layers beneath the hydrosphere is more difficult, we outline how the JUICE geophysical instruments will advance our knowledge of the moons global structure, formation and evolution. Section 4 outlines how JUICE will use surface manifestations of internal processes to investigate moon interiors (Fig. 1). The scientific objectives described in this section rely more on the remote sensing instruments than the previous sections. Section 5 reviews how tracking of the JUICE spacecraft, complemented by other JUICE data, will largely improve the ephemerides of the Galilean moons. Since the orbital motion depends on the tidal dissipation in the moons, accurate determination of the ephemerides is an important complement to the more direct methods of probing the interior of the moons. Finally, Sect. 6 describes the operational aspects and observation synergies of the geophysical investigations of the moons and their complementarity with remote-sensing and in situ investigations.

2 Characterizing the Hydrosphere Structure

The hydrosphere of the icy Galilean moons is not only a possible habitat, and as such of prime interest for JUICE investigations, but its characteristics also play a key role in the evolution of the moons and contain clues about their history. As an example, knowledge of the thickness of the ice shell above a subsurface ocean is required to understand the amount of internal energy (including radiogenic and tidal heating) and the mode of heat transport through the shell, and to assess the possibility of material exchange between the ocean and the surface. JUICE's main methods to determine the basic structural parameters, the thickness and composition of the ice shell, subsurface ocean, and high-pressure ice mantle, are based on measurements of the gravitational interactions by 3GM, GALA and JANUS, and of the electromagnetic field by J-MAG, RPWI and PEP. Section 2.1 focuses on tides and rotation, two consequences of gravitational interactions between the moons and Jupiter. Section 2.2 explains how electromagnetic field measurements are essential in deciphering the hydrosphere structure. Besides probing the average interior structure, those methods also inform on the 3D structure, internal dynamics and heat flow (Sects. 2.3 and 2.4). Throughout the section, we explain why a combination of instruments is required to explore the hydrosphere and we specifically summarise the instrument synergies in Sect. 2.5.

2.1 Gravitational Interaction

Gravitational interaction between Jupiter and the Galilean moons periodically deforms the moons and modifies their rotation. Both tides and rotation have played an important role in deciphering the internal structure of the Earth (e.g. Hough 1895; Jeffreys 1926) and also provide unique insight into moon interiors. A major difference between the Earth and the moons is that they occupy a Cassini state, an equilibrium rotation state in which they have equal spin and revolution periods and a small but non-zero obliquity (e.g. Peale 1969). This state specifies the main characteristics of the tidal potential, which determines the gravitational forcing of tides and rotation. The time-periodic part of that potential, with a main period equal to the orbital period, depends on the orbital eccentricity and obliquity. Because of the small obliquities of the Galilean moons (Baland et al. 2012), the tidal potential due to the non-zero eccentricity is most important.

Tides and rotation variations are different displacements induced by gravitational interaction, but they are not independent. Changes in the rotation rate of the moon, or longitudinal librations, lead to a different orientation of the moon with respect to Jupiter and therefore to a slightly modified tidal potential and tides with a symmetry axis showing a phase shift with respect to the tidal potential at constant rotation rate (Van Hoolst et al. 2013). Librations can be strongly influenced by tides, as is the case for the Galilean moons (Van Hoolst et al. 2013, 2020). Below, we first discuss how tides can provide information on the interior of the icy Galilean moons, and then consider libration.

2.1.1 Tides

Love numbers

Two main tidal effects are accessible to JUICE: (1) the vertical tidal deformation due to the external tidal forcing and (2) the change in the gravitational potential of the moon due to the mass redistribution in the moon associated with the tidal deformation. Although the tidal signal in the gravitational field of the moon is much easier to detect than the surface deformation, JUICE will be able to determine both for Ganymede thanks to the advanced radio system 3GM and the GALA laser altimeter.

Traditionally, the periodic tidal response of a planetary body is described in terms of degree-two Love numbers h_2 and k_2. The vertical displacement ξ of the surface is described by $\xi = h_2 V_T / g$, where V_T is the tidal potential of degree two and g the gravitational acceleration at the surface. The incremental gravitational potential δV due to the mass redistribution in the moon associated with the tidal deformation is given by $\delta V = k_2 V_T$. The tidal potential V_T describes the geometry and the strength of the gravitational interaction, and k_2 and h_2 express the response of the moon. The tidal potential is accurately known from celestial mechanics, apart from the small influence of libration. The measurement of the vertical displacement of the surface and of the incremental gravitational potential can, therefore, be interpreted in terms of the interior characterised by h_2 and k_2.

Relative to the static gravitational potential of the Galilean moon, the amplitude of the time-variable tidal forcing potential scales as the ratio M_J/M_s of the masses of Jupiter (M_J) and the moon (M_s), as the orbital eccentricity, and as the ratio $(R_s/a)^3$ of the radius of the moon (R_s) and the semimajor axis of the orbit (a). The product of these ratios is more than an order of magnitude larger for Io and Europa than for Ganymede and Callisto, showing that they experience a larger tidal forcing, mainly because they are closer to Jupiter. The time-variable part of the tidal potential is different from zero since the eccentricity and obliquity are non-zero. Correct to lowest order, the time-variable tidal potential can be expressed as a sum of a term that is linearly proportional to the small eccentricity (the 'eccentricity tidal potential'), and a term linearly proportional to the small obliquity (the 'obliquity tidal potential') (e.g. Tyler 2011a). Because of the strong decrease of the tidal force with distance to Jupiter, only the degree-two tidal potential is normally considered and higher-degree components of the tidal potential are usually neglected. Nevertheless, the very accurate 3GM measurements (see below) might also enable to detect higher-degree tidal responses to the degree-two forcing caused by flattening of the moon and longitudinal and latitudinal variations in interior structure and rheology (see e.g. Métivier and Konrad 2008 for the Earth, Zhong et al. 2012 for the Moon). As examples, the detection of a degree-three tide could indicate lateral variations in mechanical properties (Zhong et al. 2012), in ice shell thickness (A et al. 2014) and/or the complex nature of the oceanic response (Rovira-Navarro et al. 2023; Aygün and Cadek 2023). A moon like Ganymede will also have different tidal responses at different azimuthal orders because of its deviation from spherical symmetry. Therefore, the dependence of Love numbers on the order will also have to be studied in order to be able to correctly interpret the JUICE tidal data. Further theoretical modelling and data simulations are needed to assess how well the different Love numbers can be determined and to estimate the constraints they put on the interior of Ganymede.

The eccentricity tides of the Galilean moons are thought to be the dominant tides because the eccentricity is thought to be larger than the obliquity, but this is not certain since the obliquity is not well constrained for the moment (Baland et al. 2012). In particular for Ganymede, which has the smallest eccentricity of the four satellites, it may result in a more complex tidal response than for eccentricity tides only (Jara-Orué and Vermeersen 2016; Steinbrügge et al. 2024, Fig. 2), with maximal tidal amplitudes shifted relative to the equator. For an obliquity between 0.03° and 0.1°, which is the expected range (see Sect. 2.1.2), the tidal pattern is significantly affected (Fig. 2). We note that an obliquity of 0.1° corresponds to 1.7×10^{-3} rad, which is close to the mean value of the eccentricity of Ganymede during the time that JUICE is active in the Jupiter system (see Fig. 3). GALA will be able to determine the location of the maximal tidal amplitude, which will provide additional constraints on the rotational response.

As illustrated in Fig. 3, the orbital eccentricity of Ganymede is subject to considerable variations, with a mean orbital eccentricity of 0.0015 which can oscillate from values close

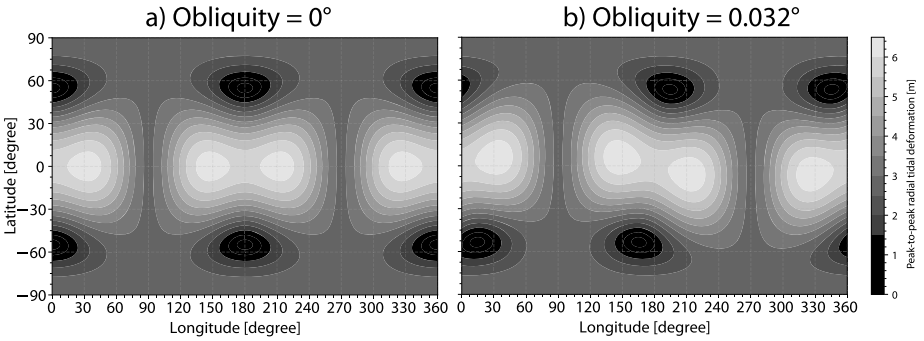

Fig. 2 Maximal radial tidal deformation of Ganymedes' surface during one tidal cycle as a function of the moon latitude and longitude, assuming a tidal Love number h_2 of 1.3 with zero obliquity (a) and an obliquity of 0.032° (b). The plots show the tidal deformation for an eccentricity of 0.0015 (Steinbrügge et al. 2024)

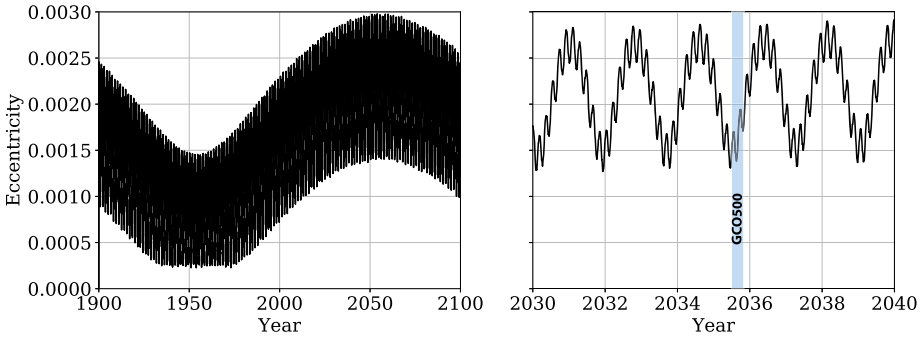

Fig. 3 Variation of Ganymede's eccentricity as a function of time, highlighting the expected eccentricity values during the GCO500 campaign, which is JUICE's main phase for geophysical investigations at an altitude of 490 km. See Sect. 6.1 and Table 1 for a detailed description of the different orbital phases of JUICE

to zero and up to 0.003 on a scale of about 100 years. The best JUICE phases for geophysical investigations (the low altitude circular orbits GCO500 and GCO200, see Sect. 6.1 and Table 1 for a detailed description of the different orbital phases of JUICE.) will start when the eccentricity is near a minimal value in the years 2030-2040, close to the long-term average value of 0.0015. The situation will improve with time and would be particularly favorable if the JUICE mission is extended by a few months. In early 2036, the eccentricity will be almost twice the values at the beginning of GCO500, resulting in much larger tidal distortions and hence more accurate determination of the Love numbers.

Tidal gravitational perturbations

Although Ganymede has a small tidal forcing magnitude due its small orbital eccentricity compared to Europa and Io, the repeated gravity measurements during the circular orbital phases at low altitude (490 km for GCO500 and 200 km for GCO200) will provide very precise estimates of the complex Love number k_2, which will inform mainly on the ice shell and on the subsurface ocean. The presence of a phase shift in the tidal response will provide information on the dissipative nature of Ganymede. The high precision on the Love numbers is made possible by the state-of-the-art Ka-band radio system of 3GM, which provides range rate accuracies of 0.012 mm/s (two-way) at 60 s integration times and allows determining

the position of the spacecraft with respect to Ganymede with an uncertainty of only 5 cm in the radial direction during the GCO500 phase (Cappuccio et al. 2020, their Fig. 7). Considerably better results will be obtained at 200 km, especially with a longer than nominal duration of the orbital phase (see Sect. 6.1 for the mission profile), which seems very likely. Expected accuracies for the real and imaginary part of Ganymede's tidal Love number k_2 are estimated at the level of 10^{-4} based on numerical simulations of the 3GM measurements during the orbital phase at Ganymede (Cappuccio et al. 2020; Iess et al. 2024, this collection). The 3GM accuracy is expected to be sufficient to detect small differences between the different azimuthal numbers at degree two and to detect potential degree 3 and 4 variations, which might indicate lateral variations in mechanical properties of the ice shell, and/or in the dynamic response of the ocean.

The measurement of the Callisto gravity field relies on 21 flybys and, even though the tidal forcing amplitude for Callisto is only smaller by about a factor 2 than that for Ganymede, the determination of the tidal Love number k_2 is more challenging than for Ganymede for which orbital data will be acquired. Numerical simulations indicate that 3GM can determine the real part of the tidal Love number k_2 with an uncertainty of about 0.06 (Cappuccio et al. 2022), which is comparable to what has been achieved at Titan with Cassini (Durante et al. 2019). Unless Callisto is highly dissipative (a tidal quality factor Q, which describes the ratio of the energy dissipated during one tidal cycle to $2\,\pi$ times the peak tidal energy, smaller than about 10), the imaginary part of the tidal Love number cannot be accurately constrained. To be able to measure k_2, flyby observations have to be performed at different tidal phases and thus at different mean anomalies of Callisto (see Sect. 6). Europa Clipper flybys might provide additional tracking opportunities.

Tidal surface displacements

The expected amplitude of the tidal vertical displacement of the surface for an oceanless moon is expected to be a few tens of cm, but can reach values as large as 7 m (peak-to-peak) for thin ice shells above a global subsurface ocean (Moore and Schubert 2000, 2003). GALA will acquire accurate measurements of Ganymede's shape over about 18 tidal cycles (for more detail, see Hussmann et al. 2024, this collection). Due to JUICE's nearly-polar orbit, the laser profiles, formed by consecutive GALA measurements along one orbit, converge in polar regions and form about 500,000 crossing points (see Fig. 18). As two profiles that intersect at a crossover point are typically obtained at different tidal phases, the height difference between the two profiles at the crossover point can be used as an observable to solve for the Love number h_2. The determination of h_2 by GALA requires an accurate knowledge of the orbit of JUICE, which will be provided by 3GM with an uncertainty at the level of 5 cm for the radial direction with respect to Ganymede (see above and also Iess et al. 2024, this collection). The anticipated measurement accuracy of GALA on h_2 is a few percent (Steinbrügge et al. 2015; Hussmann et al. 2024, this collection).

Although GALA will acquire topographic profiles from Europa and Callisto, the obtained measurements will not be sufficient to measure the tidal surface displacements. At most a coarse upper limit for Callisto's Love number h_2 might be obtained as only a few crossing profiles from JUICE flybys will be available. The two flybys of Europa are not sufficient to determine its h_2.

Tidal constraints on the hydrosphere

The Love numbers k_2 and h_2 are the main tidal constraints on the hydrosphere, and each independently can convincingly confirm the existence of a subsurface ocean on Ganymede and will decide upon the existence of such an ocean in Callisto in a more definitive way than previous measurements of the induction response observed by the Galileo magnetometer (Kivelson et al. 1999, 2002a, 2002b) because of the large differences of almost an order

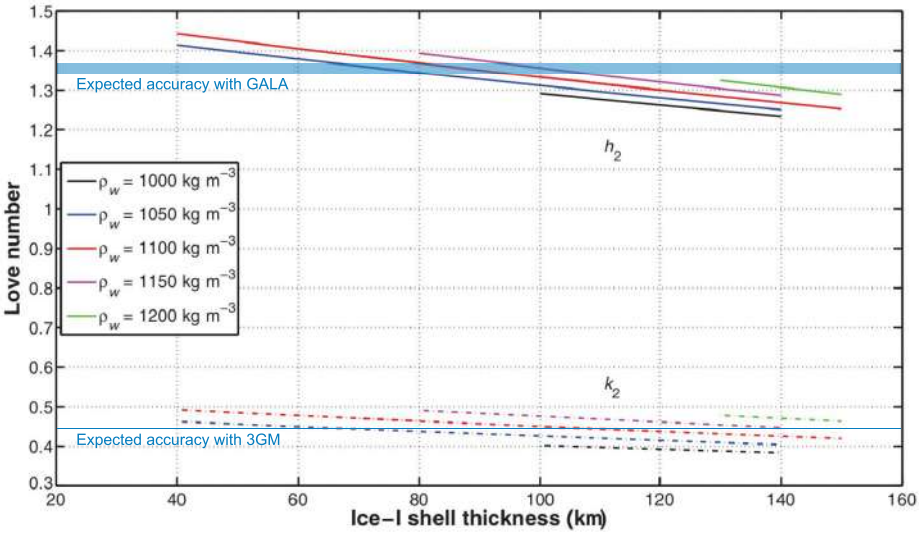

Fig. 4 Predicted tidal Love numbers h_2 (solid lines) and k_2 (dashed lines) as a function of the thickness of the ice shell for models of Ganymede with different average ocean density ρ_w. In all cases the density of the ice-I shell is taken at $\rho_I = 937$ kg/m^3 and the rigidity at $\mu_I = 3.5$ GPa (adapted from Jara-Orué and Vermeersen 2016). The blue lines indicate the expected accuracy on h_2 for GALA (Steinbrügge et al. 2015) and k_2 for 3GM (Cappuccio et al. 2020)

of magnitude in values for a moon with or without a subsurface ocean. As for Titan (Iess et al. 2012; Durante et al. 2020), the k_2 value of Ganymede and Callisto without subsurface ocean ($k_2 \lesssim 0.1$) is expected to be far below the value for a moon with a subsurface ocean ($k_2 \approx 0.3$ to 0.6, see e.g. Moore and Schubert 2000, 2003, Vance et al. 2018). The precise value depends on, in order of importance, ice shell thickness, ocean density (average value and density gradient), ice shell rigidity, ice shell density, and deep interior structure, and will be used to set bounds on these interior parameters (Baland et al. 2014; Mitri et al. 2014; Jara-Orué and Vermeersen 2016; Kamata et al. 2016; Vance et al. 2018; Fig. 4). The Love number h_2 also depends on these quantities, although with different sensitivities to the different parameters. In addition, the Love numbers depend on the visco-elastic behaviour of the satellite's interior.

Both k_2 and h_2 increase with decreasing thickness of the ice shell since the differential pressure forces in the liquid ocean require larger deformations to balance the tidal force than shear stresses in the shell. For expected ice shell thicknesses below about 150 km for Ganymede (Vance et al. 2014, 2018) and for realistic values of shell rigidity and of ice and water density, k_2 increases from about 0.3 to 0.6 and h_2 from about 1.1 to 1.6 (Moore and Schubert 2003; Steinbrügge et al. 2015; Jara-Orué and Vermeersen 2016; Kamata et al. 2016). Their dependence on shell thickness is almost linear, with other parameters causing a significant spread of about 0.1 (Steinbrügge et al. 2015; Jara-Orué and Vermeersen 2016; Kamata et al. 2016). With the anticipated accuracies on h_2 and k_2, the ice-shell thickness can be constrained to about 30 km from h_2, if the rigidity can be assumed to be well known (Steinbrügge et al. 2015), and somewhat less well from k_2. Although fractures close to the surface have a significant but not well-known effect on the local rigidity value, the effect of it on the Love numbers for a satellite with a thick ice shell such as Ganymede is expected to be minor. For a Maxwell visco-elastic model, results of Jara-Orué and Vermeersen (2016) show

that a difference in elastic rigidity of 1 GPa changes the Love numbers by less than a change in shell thickness of 20 km. However, the main source of uncertainty in modeling the tidal response concerns the appropriate visco-elastic model to predict correctly the anelasticity of ice at tidal frequencies (e.g. McCarthy and Castillo-Rogez 2013; McCarthy and Cooper 2016). Future experimental and modeling work are needed to better assess the effective rigidity at tidal frequencies in order to correctly interpret the Love numbers and assess the ice shell thickness. Because of the different sensitivities of k_2 and h_2 on the interior parameters, the best tidal information on the ice shell and ocean parameters will be obtained from a joint inversion of these two tidal quantities. Wahr et al. (2006) for example showed for Europa that the combination $1 + k_2 - h_2$ gives a better constraint on the ice shell thickness since h_2 is less sensitive to the uncertainty in ocean density than k_2. Steinbrügge et al. (2015) confirmed that this is also the case for Ganymede, although uncertainties in the ice rigidity and viscosity reduce the potential to determine the thickness (Kamata et al. 2016).

The Love number k_2 decreases with decreasing ocean density by about 23% for ocean densities in the range of 1000 kg/m^3 to 1200 kg/m^3 whereas h_2 decreases by only 6% (Jara-Orué and Vermeersen 2016, Fig. 4). The Love number k_2 is therefore an excellent constraint on ocean density, as has already been shown for Titan (Mitri et al. 2014; Durante et al. 2019). For Titan, the increase in density throughout the ocean under the effect of pressure has a significant influence on the Love number, enhancing it by about 5% compared to models with constant density (Mitri et al. 2014). Uncertainties in the density and rigidity of the outer ice shell (due to the presence of salts and other impurities) can also change the values of the Love numbers by less than 10% for realistic ranges of these parameters (Mitri et al. 2014; Jara-Orué and Vermeersen 2016, Steinbrügge et al. 2022). The influence of the deeper interior on the Love numbers is below 1% (Jara-Orué and Vermeersen 2016; Kamata et al. 2016).

The viscosity of the ice shell, which is not well known and strongly depends on the temperature, can have a large influence on the Love numbers since the tidal periods can be close to or larger than the Maxwell time scale. Viscosity can then lead to significant dissipation and larger tidal deformations (Moore and Schubert 2003). The influence is notably significant if the ice shell convects (Mitri et al. 2014). In principle, a more viscous rather than elastic response could largely increase the Love numbers for an oceanless moon to values typical of a moon with a subsurface ocean, but that would require very low viscosity values below 10^{13} Pa s in the entire hydrosphere (Moore and Schubert 2003), which appears unrealistic. Since tidal dissipation delays the tidal deformation of the surface with respect to the forcing tidal potential and leads to a phase lag, the moon's dissipative response can be determined from the complex tidal Love numbers. 3GM will have the capability to determine the imaginary part of k_2 with an accuracy of 0.000068 (Cappuccio et al. 2020), thus providing key constraints on the average viscosity of the ice shell and hence on its thermal state. Phase lag differences between h_2 and k_2 could also inform on the rheological state in the deep interior of Ganymede (Hussmann et al. 2016), especially on the viscosity of the high-pressure ice layer. However, for reasonable ranges of viscosities of high-pressure ices ($> 10^{13}$Pa s) (e.g. Kalousová et al. 2018) the phase lag difference would remain below 5°, which will be challenging to detect based on the expected accuracy on h_2.

Additional tides

Besides the main eccentricity tides, JUICE can measure the smaller obliquity tides of Ganymede and Callisto related to the non-zero obliquity resulting in a shift in the pattern of tidal surface displacement (Jara-Orué and Vermeersen 2016; Steinbrügge et al. 2024, Fig. 2). Relative to eccentricity tides, obliquity tides are expected to be larger for Ganymede than for Callisto because of Ganymede's larger obliquity over eccentricity ratio (Baland et al.

2012). Given the 1:1 spin-orbit resonance, the obliquity tides have the same period as the eccentricity tides and have to be considered in the determination of the Love numbers h_2 and k_2 from GALA and 3GM data. Since both the orbital eccentricity and the obliquity can vary significantly (by 10% to almost 100%, Baland et al. 2012; Steinbrügge et al. 2024) over the more than 4 years that JUICE will operate in the Jupiter system, the amplitudes of the eccentricity and obliquity tides as well as their ratio will depend on time, and should be carefully monitored to correctly interpret the interior response.

In addition to the tidal interaction with Jupiter, the Galilean moons are subject to lower amplitude, time-dependent, tidal interactions with the other moons (Hay et al. 2020). Because the mass of the tide-raising satellites are a factor of 10,000 smaller than the mass of Jupiter, a moon-to-moon tide is expected to have a very small vertical displacement amplitude below 1 mm, unless the tidal reaction of the moon is strongly enhanced by internal dynamics such as flow in the ocean (Hay et al. 2020). Since the moon-moon tides have multiple frequencies related to the Io-Ganymede, Europa-Ganymede and Ganymede-Callisto synodic frequencies and their harmonics, resonances can occur between the tidal forcing and eigenmodes of the ocean (Hay et al. 2020; De Marchi et al. 2022). If these resonances succeed in amplifying the Love numbers by more than a factor 100, they could in principle lead to an observable tidal signal. Largest tidal enhancements require a conductive ice shell and a drag at the ocean-ice interfaces that is at the lower end of expected values (Hay et al. 2022). If resonances would occur in Ganymede's ocean and lead to observable moon-moon tides, they can help constrain the visco-elastic behaviour of Ganymede and may provide additional and independent constraints on the thickness of the ocean and shell to within about 10 km (De Marchi et al. 2022; Hay et al. 2022). The best prospects for observing moon-moon tides is by 3GM (De Marchi et al. 2022). By providing the opportunity to estimate k_2 at different frequencies, they can help constrain the visco-elastic behaviour of Ganymede and may provide additional and independent constraints on the thickness of the ocean to within about 10 km if one of the tides is resonant with a surface gravity wave of the ocean (De Marchi et al. 2022; Hay et al. 2022). Lateral variations in ice shell thickness and the dynamical response of subsurface ocean and its coupling with the overlying ice shell (e.g. A et al. 2014; Beuthe 2016, 2018; Vincent et al. 2022; Rovira-Navarro et al. 2023) can make the tidal response much more complex and more challenging to interpret. Even if these effects are second order, JUICE's very high accuracy of tidal monitoring using 3GM and to a lesser extent GALA may reveal deviations from the standard tidal response, which will provide additional insights on the hydrosphere structure and dynamics. Future modeling works dedicated to Ganymede taking into account the complexity of ocean-ice tidal coupling is required to anticipate the interpretation of these future data.

2.1.2 Rotation

Obliquity

The Galilean moons are assumed to be locked in a Cassini state since internal dissipation can drive the moons to such a state of minimum energy in a time much shorter than the age of the solar system (Goldreich and Peale 1966). In a Cassini state, the moon rotates synchronously with its orbital motion, and the spin axis, the normal to the orbit, and the normal to the Laplace plane (the mean orbital plane) lie in the same plane. This also requires the precession rate of the moon to be equal to that of the orbit. The angle between the normal to the orbit and the spin axis, the obliquity, is almost constant and small, but not zero because orbital precession tends to deviate the orbit normal from the spin axis. An analysis based on images from the Voyager-1, Voyager-2, and Galileo missions showed that Ganymede's obliquity is smaller than 0.1° (Zubarev et al. 2015).

JUICE will accurately determine the ephemerides and rotation of Ganymede and to a lesser extent that of Callisto and will thereby be able to confirm whether Ganymede and Callisto occupy the Cassini state. The global mapping of Ganymede's gravity field by the 3GM experiment will yield a formal uncertainty of 0.2 arcsec for the pole obliquity (Cappuccio et al. 2020), a three orders of magnitude improvement with respect to current knowledge. For Callisto, the obliquity can be retrieved with an accuracy of 15 arcmin or 10.7 km on Callisto's equator (Cappuccio et al. 2022). The two close encounters with Europa are insufficient for 3GM to measure the moon's rotation, but the data can be useful as a complement to the dataset of the Europa Clipper mission (Howell and Pappalardo 2020; Roberts et al. 2023).

For a moon without subsurface ocean, the obliquity together with the degree-two gravity coefficients determines the mean moment of inertia (MoI), which can be used to constrain the deep interior structure and differentiation of the moon (Bills 2005). With a subsurface ocean, the situation is more complex and no direct relation between obliquity and moment of inertia exists (Baland et al. 2012). The obliquity depends on the same internal parameters as tides and constraints on those parameters can be obtained by a joint analysis of tides and obliquity. In particular, since tides mainly depend on the properties of the ice shell and ocean, and only marginally on the deeper interior, obliquity can help better constraining the interior below the ocean. In addition, dissipative processes such as tidal dissipation and friction between layers lead to a small offset of the Cassini state from coplanarity (e.g. Williams et al. 2001 for the Moon, Baland et al. 2017 for Mercury). Observation of a deviation from the exact Cassini state would thus provide a useful additional constraint. Three instruments will contribute to obliquity measurements: GALA altimetry and JANUS imaging data will provide accurate measurements of the orientation of the ice shell and 3GM will determine the orientation of the global mass distribution of the moon. Differences between the obliquity of the ice shell, as observed by JANUS and GALA, and the global obliquity as observed by 3GM, will provide additional crucial information on the ice-ocean coupling, complementary to tidal monitoring. Any constant and time-varying difference will provide key insights on the mass distribution and on the mechanical coupling. Future modelling effort is, however, needed to quantify the possible amplitude of the orientation difference and its implications for the hydrosphere structure and dynamics.

Libration

Since the orbital eccentricity of the Galilean moons is non-zero, the moon's long axis is not directed towards Jupiter but approximately to the empty focus of the orbit (Murray and Dermott 1999). As a result, Jupiter exerts a time-variable gravitational torque on the moons, which are significantly flattened in both the polar direction and the direction towards the central planet (see Sect. 2.3 and 3.1). These torques do not destabilize the Cassini state but lead to variations in the rotation speed about the mean speed. The orientation of the long axis will oscillate, or librate, around the direction of the long axis the moon would have if it were rotating at constant speed. For a Keplerian orbit, longitudinal librations have a period equal to the orbital period (Comstock and Bills 2003; Van Hoolst et al. 2008). This libration increases the angular separation of the long axis from the direction to Jupiter (e.g. Tiscareno et al. 2009), and leads to a larger tidal dissipation (see e.g. Wisdom 2004, and Beuthe 2019 for Enceladus). Additional libration periods exist due to the non-Keplerian characteristics of the orbits (Lainey et al. 2006; Rambaux et al. 2011). Latitudinal librations, which represent orientation changes due to the gravitational torque from Jupiter, are smaller due to the small obliquity (Coyette et al. 2024) and are not considered further here.

Existing data show that the libration of Ganymede is smaller than 0.1°, or about 4.5 km at the surface (Zubarev et al. 2015). JUICE will improve the precision on the libration by

about three orders of magnitude. 3GM can detect the physical libration in longitude at orbital period with an accuracy of 0.4 arcsec, or about 5 m on the equator (Cappuccio et al. 2020). From the laser altimetry data of GALA, the amplitude of libration can be determined with an accuracy of about 0.8 arcsec, or 10 m on the equator (Steinbrügge et al. 2019). Libration will also be determined from tracking surface landmarks on JANUS high-resolution images of Ganymede (ground sampling distance of about 7 m/pixel at GCO500). Monte Carlo simulations considering a variable number of images (50 to 150), selected according to the positions of the science targets that will certainly be mapped, show that libration will be detected with an accuracy of about 2 arcsec (25 m) (see Palumbo et al. 2024, this collection). Since the duration of the GCO500 phase is limited to about 130 days, libration components with longer periods are more difficult to determine.

Longitudinal librations can be used to probe the interior of moons, and have for example been used to show that Enceladus has a global subsurface ocean (Thomas et al. 2016, Van HoolstGaia Collaboration 2016). When deformation of the shell is governed by the rigidity of the shell, as is the case for Enceladus, the libration at orbital period increases with decreasing shell thickness as a result of the strong rotational decoupling between the shell and the solid interior beneath the ocean. Libration is then a good indicator of the thickness of the shell (Van Hoolst et al. 2008). For Ganymede and Callisto (and also Europa), the tidal response of the ice shell is, however, mainly determined by the subsurface ocean, and its shape conforms to that of the response of the liquid layer beneath (Goldreich and Mitchell 2010; Van Hoolst et al. 2013; Beuthe 2018). As a result, the amplitude of libration at the orbital period is strongly reduced by deformation. The amplitude of libration of both Ganymede and Callisto is about 10 meters at the equator (Van Hoolst et al. 2013), at the limit of detectability by 3GM and GALA. Since it moreover only weakly depends on the interior structure, the diurnal libration amplitude alone cannot be used to constrain the interior.

Librations due to the non-Keplerian character of the orbital motion can inform on the interior if their period is close to a libration eigenperiod (Rambaux et al. 2011), which are between 63 days and 0.9 yrs for Ganymede, and between 0.74 yr and 3.3 yr for Callisto (Van Hoolst et al. 2013). For Ganymede, three orbital perturbations with a period in the range 460 days to 490 days and a forcing amplitude of the order of several hundred meter as measured at the equator (Lainey et al. 2006) seem most promising. A libration at about 50 days can also be resonantly amplified (Rambaux et al. 2011) but its forcing amplitude is an order of magnitude smaller than the librations at periods just below 500 days. The combination of the total libration measured by 3GM, and the libration of the ice shell measured by GALA and JANUS might in principle further allow improving the internal structure of Ganymede. Callisto does not have orbital perturbations with periods close to the libration eigenperiods (Lainey et al. 2006). Therefore, libration is expected to remain below the detection level on Callisto.

Besides periodic variations in the rotation rate, it has been suggested that torques on the tidal bulges of satellites can cause the ice shell to spin at a slightly nonsynchronous rate (e.g. Greenberg and Weidenschilling 1984). Also ocean currents may drive rotation of the ice shell at a rate slightly below or above synchronous (Ashkenazy et al. 2023; Hay et al. 2023; Kang 2024), and observation of the effect can inform on flow in the ocean. For Europa, the differential rotation with respect to the synchronous rotation rate could exceed 30 m/yr (Ashkenazy et al. 2023). A similar rate on Ganymede could be observable by JUICE. Nevertheless, it might be difficult to identify and disentangle long-period librations and a long-term secular drift as the duration of the GCO500 and GCO200 campaigns together, where the most accurate data will be acquired, is only 4 months (see Sect. 6).

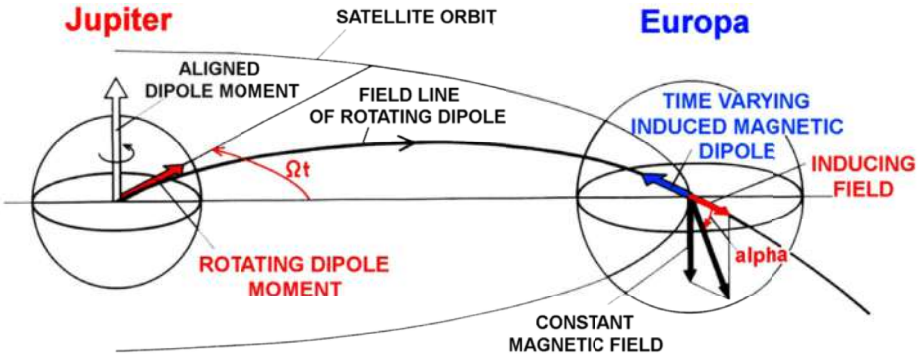

Fig. 5 Principle of induction at Jupiter's moon Europa after Neubauer (1998) (Saur et al. 2010)

2.2 Electromagnetic Interaction

2.2.1 Electromagnetic Induction

The electromagnetic induction technique is based on the idea that time-variable magnetic fields generate time-variable electric fields based on Faraday's law of induction. In electrically conductive media such as saline oceans, these electric fields drive electric currents and thus cause secondary magnetic fields. Observations of these secondary magnetic fields can be used to detect electrically conductive internal layers and hence to provide constraints on saline ocean characteristics (see Fig. 5 and Khurana et al. 1998, 2002, Kivelson et al. 2002a,b, Neubauer 1998; Zimmer et al. 2000, Saur et al. 2010, 2015).

The main inducing field at the Galilean moons is due to Jupiter's magnetic field (Fig. 5). Jupiter's field is non-axisymmetric and can be characterized to first order as a dipole magnetic field tilted by 9.8 degrees with respect to Jupiter's spin axis. Jupiter's moons orbit with Keplerian velocities near the equatorial spin plane of Jupiter with only very small inclination. The Keplerian periods are on the order of days while Jupiter's sidereal spin period is 9.93 hrs. In the rest frame of a moon rotating synchronously with its orbital motion, Jupiter's dipole magnetic field is seen as time variable. The largest amplitude-inducing component has a period equal to the Jupiter synodic rotation period, which varies from 11.23 hrs for Europa to 10.18 hrs for Callisto (Fig. 6). Lower amplitude inducing fields additionally occur at the orbital periods of the moons due to their non-zero eccentricity and inclination, at multiples of the synodic periods and at the solar rotation period (Seufert et al. 2011, Fig. 6).

Based on Galileo spacecraft magnetic field measurements, the induction response at Jupiter's moons could only be determined at Jupiter's synodic period. JUICE's J-MAG will be able to measure the induction response at the orbital period of the three moons and at other periods for Ganymede during the GCO phase. Measurements of the induction response at multiple inducing periods will allow to uniquely resolve the thickness, depth and salinity of the icy moons' oceans (Khurana et al. 2002; Seufert et al. 2011; Vance et al. 2021).

A basic problem in using the induction technique for a quantitative analysis of subsurface ocean properties are other non-ocean related sources of magnetic field perturbations (Fig. 7). These perturbations can stem from various sources:

1. The interaction of Jupiter's magnetospheric plasma with the atmospheres and ionospheres of the moons can generate magnetic field perturbations at Europa of about 10 nT when Europa is outside Jupiter's plasma sheet and perturbations of about 100 nT or

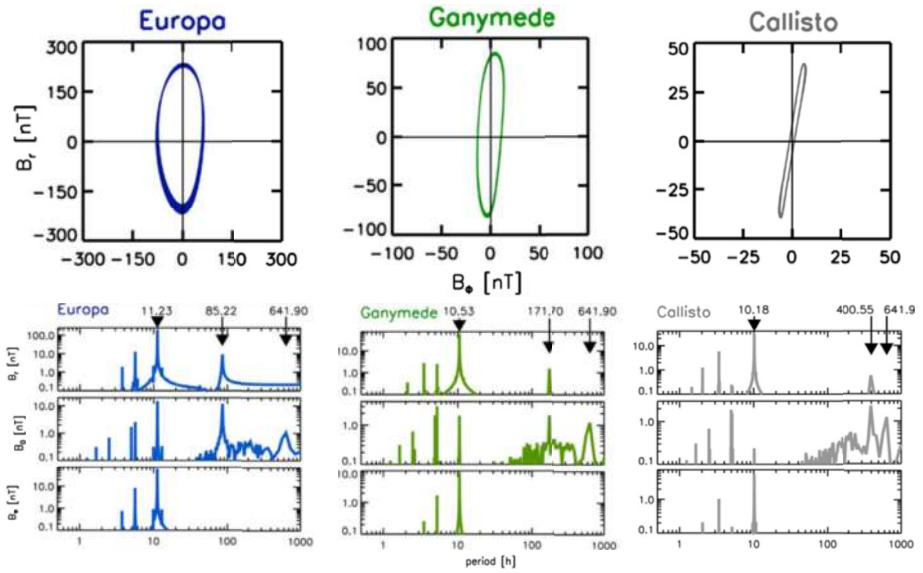

Fig. 6 Hodogram of time-varying magnetic field at Europa, Ganymede and Callisto (top) and modelled inducing frequencies and associated magnetic field amplitudes at the three moons with B_r in radial, B_ϕ in longitudinal and B_θ in latitudinal direction in Jupiter's system III coordinates (from Seufert et al. 2011). Arrows indicate the synodical period, the orbital period and the solar rotation period, respectively. Note that the scale of the magnetic field component varies from panel to panel. A similar frequency model can be also found in Vance et al. (2021) with an updated internal field model, but with an older current sheet model and without the inducing fields from Jupiter's breathing magnetopause

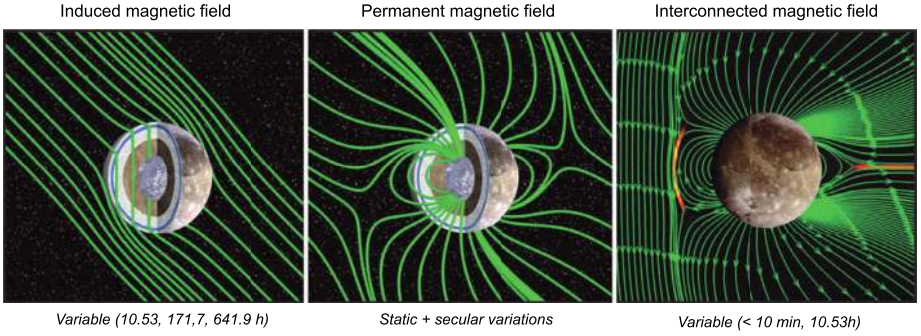

Fig. 7 Illustration of the various components of Ganymede's magnetic field: the time-varying induced field associated with the oceanic response at different forcing periods (left), the internally generated magnetic field (middle), and the total magnetic field interconnected with Jupiter's one, resulting in a miniature magnetosphere and rapidly varying plasma interactions (right) [Image credits: X. Jia (University of Michigan) and M. Kivelson (UCLA)]

more inside the current sheet (e.g., Schilling et al. 2007). At Ganymede the plasma interactions can drive perturbations of around 50 nT outside the plasma sheet (Kivelson et al. 2002a,b) and inside the plasma sheet of around 100 nT (Duling et al. 2014). At Callisto the plasma generated fields lie in the range of a few nT to about 10 nT, outside and inside the plasma sheet respectively (Zimmer et al. 2000; Liuzzo et al. 2018).

2. An internal dynamo magnetic field exists only within Ganymede and generates magnetic fields of about 720 nT near Ganymede's equator (Kivelson et al. 1996, 2002a, 2002b).
3. Induction in the ionospheres of the moons due to time-variable external fields are expected to generate very small magnetic field perturbations of about 1 nT at Europa and 0.05 nT at Ganymede, but might be very significant at Callisto with values of 30-40 nT, i.e. on the same order as the induced field in Callisto's possible ocean (Hartkorn and Saur 2017). The reason for the differences is that ionospheric Pedersen and Hall conductivities are inversely proportional to the magnetic field strength as the magnetic field inhibits the mobility of the ions and electrons. Since Callisto is the furthest away from Jupiter, Jupiter's magnetospheric field around Callisto is much smaller compared to that at Europa. At Ganymede the internal magnetic field causes large magnetic field amplitudes in its ionosphere causing low conductivities (see Table 2 in Hartkorn and Saur 2017).

These various sources of fields need to be quantified and separated from the future measurements to obtain the induction signatures from the oceans only, which are at maximum as large as the inducing fields shown in Fig. 6. Data from five main instruments will be combined with numerical modelling to achieve that goal. Those instruments are besides the magnetometer J-MAG, PEP, RPWI, 3GM, and UVS. To quantify the plasma interaction, which is essential to correctly retrieve the induction signatures, in-situ ion and electron measurements with PEP are crucial and need to be combined with numerical modeling in order to remove their effects from observed field measurements with J-MAG. For quantifying induction effects in the ionospheres of the moons, it is also crucial to have a detailed knowledge of the ionospheric electron and ion densities and their spatial structure. These can be obtained by radio occultations (3GM) and in-situ electron and ion measurements (PEP), and observations of the plasma waves (RPWI) and their upper-hybrid frequency. Both RIME and PRIDE can further contribute to measuring the Total Electron Content. Details on the plasma interaction aspects are provided in Masters et al. (2024, this collection).

An internal dynamo field is expected to be time-stationary over the mission duration of JUICE around Ganymede, while the induction fields are time-variable on time scales on the order of 10 hrs (see also Fig. 6). Along a trajectory during a single flyby it is impossible to separate temporal and spatial variations, however telescope images such as those with UVS and MAJIS will be able to monitor Ganymede's auroral ovals, which are maps of the open-closed field-line boundary on Ganymede (McGrath et al. 2013; Greathouse et al. 2022). The JUICE observations will provide a high resolution global map that will largely extend the Juno-UVS observations during the two flybys of Ganymede by Juno (Greathouse et al. 2022). The locations of modeled open-closed field line boundaries and observed locations of the auroral bands during Juno's Ganymede flyby agree within 1 degree latitude on the downstream, where the aurora was primarily observed, and within 4 degree on the upstream side (Duling et al. 2022). Observations of the time-variability structure of the ovals are thus an additionally important component for induction studies (Fig. 8 and Saur et al. 2015).

2.2.2 Electromagnetic Constraints on the Hydrosphere Structure

Since the electromagnetic induction response of a subsurface ocean at any frequency is determined by three parameters (the thickness of the ice crust and the thickness and conductivity of the ocean), induction responses are required at multiple frequencies to determine these parameters. As the response function is a complex quantity (two scalar numbers for each frequency), responses at a minimum of two frequencies are needed to determine all three of the physical parameters of an ocean. However, the naturally available frequencies

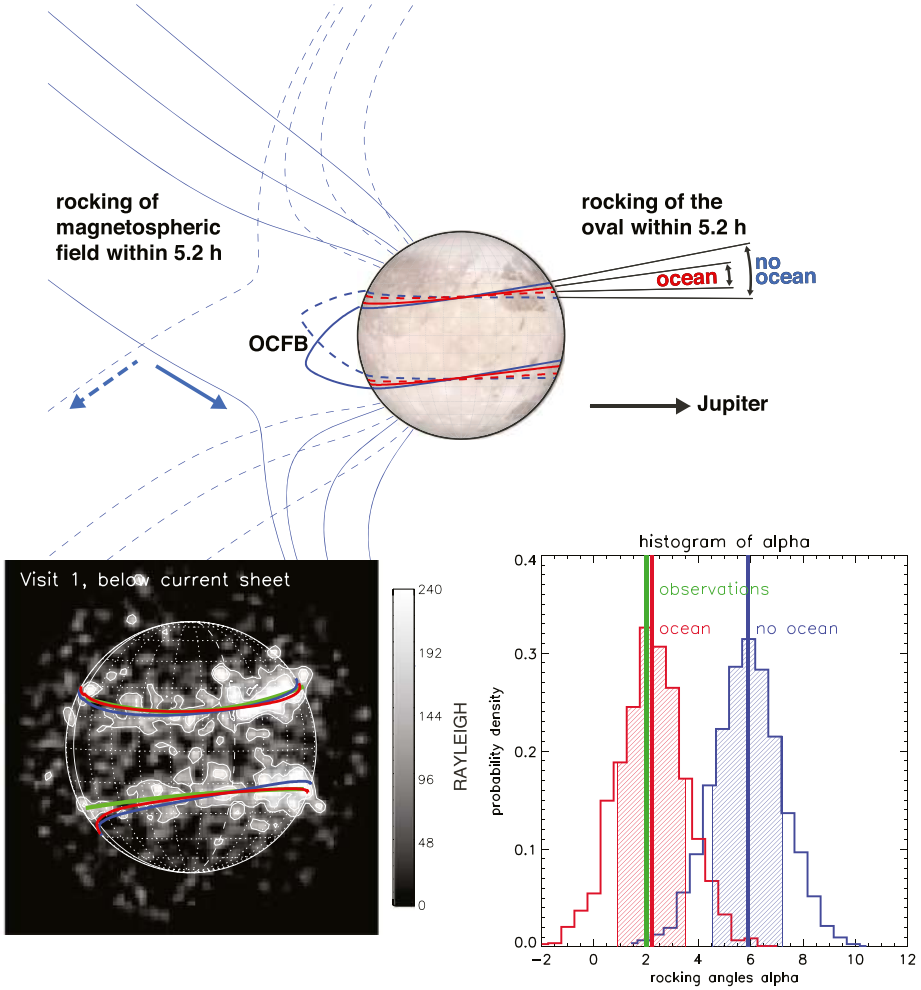

Fig. 8 Effects of the induction response from Ganymede's ocean resulting in the reduction of the amplitude of the rocking of the auroral ovals (top), auroral brightness as observed with the Hubble Space Telescope compared to the expected rocking amplitude for model with (red) or without an ocean (blue) (bottom left), and distribution function of modeled rocking angles with or without ocean (bottom right). The ovals are located where the open-closed field line boundary (OCFB) intersects Ganymede's surface (adapted from Saur et al. 2015)

(at the synodic rotation period of Jupiter, the orbital period of the moon and the second harmonic of the orbital period of the moon) are not separated in frequency by a large range, and therefore in practice, all three frequencies are needed to derive the physical parameters of the oceans (Khurana et al. 2009). In particular, the thickness of the ice shell is obtained from the response of the ocean at the larger-amplitude higher frequencies (synodic rotation period of Jupiter or its second harmonic) whereas the ocean's electrical conductivity and its thickness are obtained from the response of the ocean at lower frequencies (the orbital period of the moon, for example). Figure 9 shows the oceanic response at the three main frequencies for a range of ocean conductivities and thicknesses for the three moons based on the model

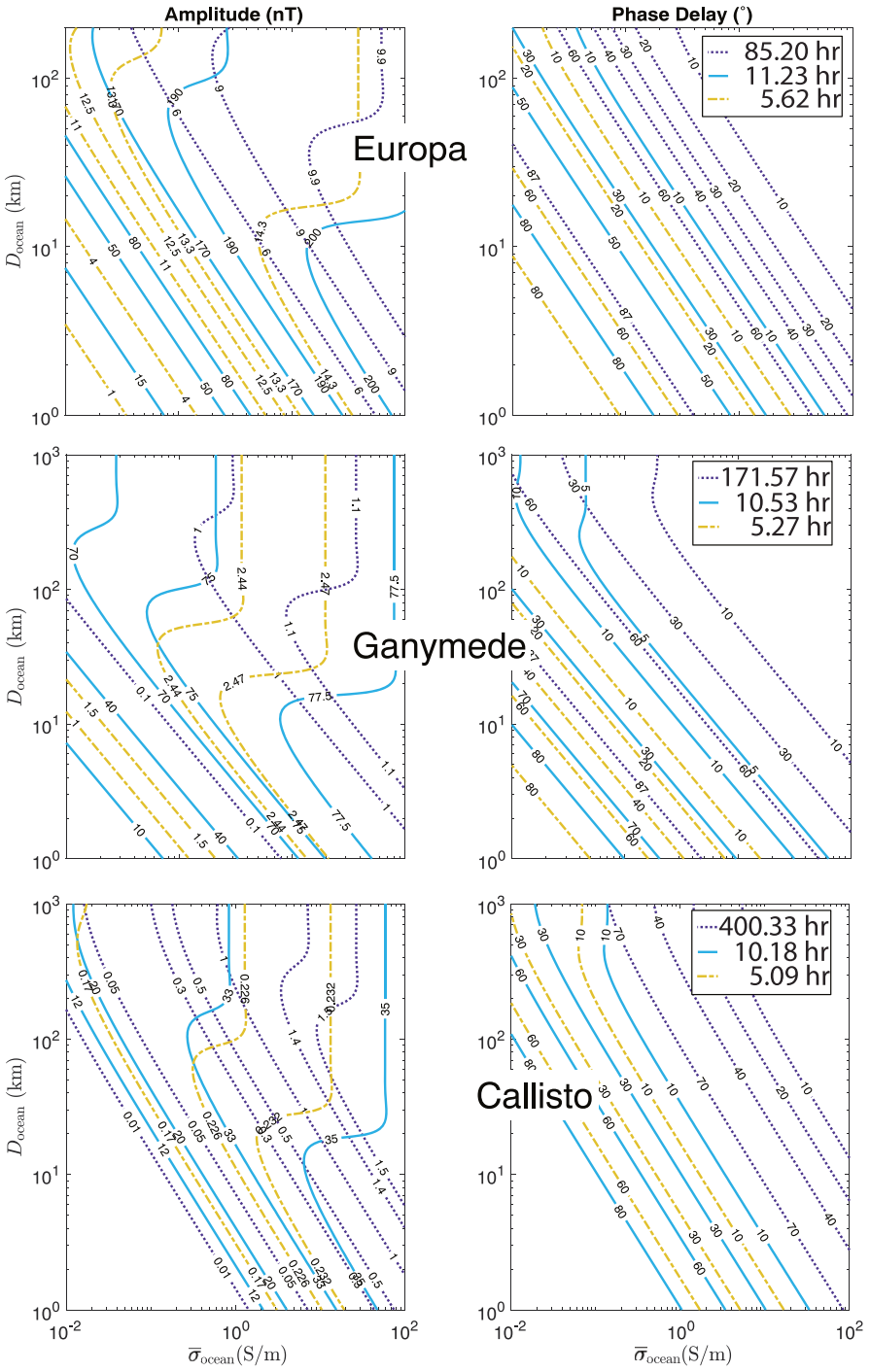

Fig. 9 Contours of the maximum induced field By components (in nT) and phase delays (in °) at the strongest inducing periods – orbital (dotted), Jupiter synodic (solid), and second synodic harmonic (dot-dash) for Europa, Ganymede and Callisto (adapted from Vance et al. 2021)

of Vance et al. (2021). In the lower left region of the contour plots (low ocean conductivity and small ocean thickness), the response curves at the three frequencies are parallel to each other and therefore the ocean conductivities and thickness cannot be determined uniquely. However, for a large range of ocean thicknesses and conductivities, the response curves at the two frequencies intersect each other where these parameters can be determined uniquely.

Two additional factors complicate the retrieval of ocean conductivities. First, as the conductivity of an ocean depends on local temperature, increasing temperatures with depth implied by adiabatic convection would increase the ocean conductivity with depth. Vance et al. (2018) show that this effect alone could increase the conductivity in the bottom layers of Europa, Ganymede and Callisto oceans by 20%, 40% and 30% compared to their top layers. Second, stratification in the ocean arising from melting or freezing at the ice-ocean interface or dissolution and precipitation of salt compounds would alter electrical conductivity of the ocean with depth (Vance et al. 2021). In the Earth's Black Sea, the bottom isothermal layer, 300-400 m thick, is 3% more saline than the overlying layers because of geothermal heating from below (Vance and Goodman 2009). Such effects must be taken into account in future models to predict more accurately the induction response, and the possible retrieval of the electrical conductivity from the observed multi-frequency response. At Europa, due to the very limited number of flybys, such multi-frequency inversion is not possible, but JUICE will provide additional data about the electromagnetic field and particle environment that will complement the Europa Clipper coverage and help to determine the multi-frequency response. For Callisto, JUICE observations combined with the potential additional flybys performed by Clipper will increase the possibility to constrain the multi-frequency response. However, Ganymede will remain the best candidate for JUICE to detect the multi-frequency oceanic response and to determine to its ocean thickness and to provide information on the electrical conductivity in the ocean.

Moreover, due to the high accuracy of magnetic field measurements during the GCO campaign, JUICE might be able to detect electromagnetic signatures due to fluid flows associated with tidal deformations (e.g. Tyler 2008) and to large scale oceanic circulation driven by internal heating (e.g. Amit et al. 2020; Soderlund et al. 2020; Kvorka and Cadek 2022; Vance et al. 2021; Jansen et al. 2023; Ashkenazy et al. 2023; Kang 2024). Because the moons are located in the background magnetic field of Jupiter, any advected parcel in their conducting oceans would be subject to the $\mathbf{v} \times \mathbf{B}$ Lorentz force and generate a motionally induced electromagnetic field. Tyler (2008) considered flows generated by the obliquity tidal force in Europa and estimated the flow speeds to be of the order of 8 cm/s. Since the tidal velocity due to obliquity tides scales as the ΩR times obliquity (Chen et al. 2014), it is expected to be of the order of a cm/s in Ganymede's ocean and about 4 cm/s in Callisto's ocean (obliquities of 0.03° and 0.2° for Ganymede and Callisto taken from Baland et al. 2012). Considering that the background field of Jupiter near Europa is 500 nT, Tyler (2011b) estimated that the induced magnetic field generated would be of order of 1 nT. The flows generated by thermally-driven oceanic circulation might be stronger (of the order of 3, 6, and 0.5 m/s in Europa, Ganymede and Callisto, respectively, Vance et al. 2021). The upper bounds on the motionally generated magnetic induction fields are then estimated to be of the order of 10-20 nT at Europa, as high as 330 nT at Ganymede (due to its strong internal magnetic field) and 1 nT in Callisto. These studies suggest that it might be possible to obtain information on the internal motions of Ganymede's ocean by studying the form and strength of the generated electromagnetic fields. However, energy constraints for equilibrium ocean dynamics show that expected flow velocities are at most a few cm/s for Europa (Jansen et al. 2023). For similarly low velocities at Ganymede, the induced field strength would be of the order of 10 nT, still more than an order of magnitude above the J-MAG accuracy, but limiting the possibility of JUICE to constrain the motions in the ocean. For flow speeds of the

order of a cm/s for Europa and Callisto, the induced magnetic field would be at the limit of detectability for Europa and below it for Callisto.

2.3 Mapping the 3D Structure of the Ice Shell

The largest topographic and gravitational signatures of Ganymede, Callisto and Europa are expected to be related to the long-term fluid response to the rotation and tidal forces caused by Jupiter. Over geologic time, the moons should approach a state of hydrostatic equilibrium at their longest wavelengths, which for the case of a tidally locked moon corresponds to a triaxial ellipsoid with the longest axis directed towards Jupiter and the shortest axis directed along the rotational axis. The amplitude of this degree-two distortion (polar flattening and elongation towards Jupiter) depends on the amplitude of the forcing, and hence on the distance to Jupiter. As a consequence, the long-term distortion remains very small at Callisto (estimated at 100-200 m, below the detection level of the Galileo data, Anderson et al. 2001), whereas it can exceed 2 km in the case of Europa and Ganymede (Nimmo et al. 2007; Zubarev et al. 2015). The degree-two shape and gravity field are therefore dominated by the hydrostatic distortion on Europa and Ganymede, whereas on Callisto, any largescale topography fluctuations of the order of hundred of meters can have a similar gravity signature making the determination of the hydrostatic reference state of Callisto more challenging. The relation between the degree-two shape, hydrostatic equilibrium, and the deep interior structure is further developed in Sect. 3.1 below. Here we focus on the deviations from the reference degree-two hydrodratic state, for which we currently only have observational constraints for Ganymede, and on what they can tell us about the hydrosphere structure.

The most recent gravity model of Ganymede, including both Galileo and JUNO datasets, has been developed up to spherical harmonic degree 5, which in principle can resolve features with sizes of 1600 km (Gomez Casajus et al. 2022). Though this model is based on a limited number of flybys, non-hydrostatic gravity anomalies with amplitudes of just over 20 mGal have been detected where the data coverage is best, confirming previous analysis of Galileo data (Anderson et al. 2004; Palguta et al. 2006, 2009). For comparison, these non-hydrostatic gravity anomalies are about 5 times larger than those detected on the similarly sized moon Titan, whose most recent gravity model has a similar resolution to Ganymede (Durante et al. 2019). These gravity anomalies could reflect external processes that shaped the surface, internal processes that could be occurring within the ice shell, or processes occurring within the underlying layers. Four possible origins for these gravity anomalies that will be discussed below are: uncompensated topography at the surface of the ice shell, surface topography combined with a compensating isostatic root at an ice-ocean interface, lateral variations in density associated with a convecting ice shell, and relief along the deeper ice-silicate interface.

The interface between the ice shell and the ocean is related to a phase change between liquid water and ice, and since the ice at this boundary is near the melting temperature, it would have a considerably lower viscosity than colder ice closer to the surface. Any relief that might have existed at this interface would have viscously relaxed over time, leaving the base of the ice shell close to a hydrostatic surface (e.g., Stevenson 2000; Lefèvre et al. 2014; Akiba et al. 2022; Kihoulou et al. 2022). The upper portion of the ice shell, however, being considerably more rigid, could have supported the loads associated with surface topography over geologic time. Support of the surface topography would require the existence of sufficient elastic stresses within the ice shell, whose magnitude would depend upon the equivalent elastic thickness of the shell, the amount of elastic deflection, and the wavelength of the load. The plausibility of such a scenario would need to be evaluated once

better constraints on these parameters are made available. For this scenario, only relief along the surface would give rise to non-hydrostatic gravity anomalies. By assuming a density of 1000 kg m^{-3} for the surface, we determine that the observed gravity could be accounted for by about $\pm$ 400 m of surface relief (see techniques summarized in Wieczorek 2015). This is comparable to the non-hydrostatic relief observed for Titan (Durante et al. 2019), suggesting that surface relief on Ganymede could conceivably be the main source of its observed gravity anomalies.

It is alternatively possible that the long-wavelength surface topography of Ganymede could have a compensating root at the ice-ocean interface that would balance the radial forces acting on the shell, bringing the shell into a state of isostatic equilibrium. Since the relief along this interface is predicted to viscously relax over short time scales, such relief would have to be maintained dynamically by large-scale mass exchange with the underlying ocean (e.g., Cadek et al. 2017, 2019, Kihoulou et al. 2019). Melting of ice and freezing of water would occur where the radial flow at the base of the ice shell was directed downwards and upwards, respectively, and a dynamic steady state would be achieved where the relief along these interfaces was constant with time. The treatment of isostatic equilibrium requires some care because of the small size of the moon and the low density of its ice shell. Prescriptions that minimize the elastic or viscous stresses in the shell give results that are close to the "equal weights" model of Airy isostasy, but these can differ significantly from models that impose equal pressures or equal mass constraints (e.g., Cadek et al. 2017, 2019, Beuthe 2021a; 2021b). The gravity anomaly associated with an ice shell that is in isostatic equilibrium depends primarily on the thickness of the ice shell and its density. If the ice is in isostatic equilibrium, the mean ice shell thickness can be estimated from the gravity-to-topography relationship as it has been done for Enceladus (e.g. BeutheGaia Collaboration 2016), providing an estimate independent from tidal deformation and magnetic induction. Since the gravity anomaly associated with the relief along the surface and base of the ice shell are opposite in sign, the observed anomaly will be substantially lower than that predicted for uncompensated surface topography alone. In particular, if the ice shell is in isostatic equilibrium, the ratio of gravity to topography at the wavelengths investigated by JUICE should be 3 - 10 times lower than for the case of uncompensated surface topography (e.g., Akiba et al. 2022). The non-hydrostatic long-wavelength gravity of Ganymede could hence be accounted for by relief that was several kilometers in amplitude. This prediction will be easily tested by JUICE laser altimeter measurements.

Another possibility is that the observed gravity anomalies are a result of lateral variations in density of the ice shell. Such variations could be a result of temperature, porosity variations, or lateral variations in the abundance of silicates or salts incorporated into the ice. If the density anomalies vary only laterally and are constant with depth, the observed gravity anomalies would require an amplitude of about 3 kg m^{-3} over a total thickness of 150 km. If the ice shell was thinner, the density anomalies would be larger, but still moderate. Convection in the ice shell should give rise to lateral temperature variations of about 10 K, corresponding to density anomalies of 0.7 kg m^{-3} (Palguta et al. 2006). Though these density anomalies could account for only about one-fourth of the amplitude of the observed gravity anomalies, lateral variations in the abundance of non-ice materials (e.g. salt, silicate dust) within the ice shell could easily generate larger density variations. Moreover, lateral variations in porosity in the upper part of the ice shell may significantly contribute to the long-wavelength topography and gravity anomalies, as it has been proposed for Enceladus (Besserer et al. 2013) and the Moon (Besserer et al. 2014). In fact, it has been suggested that the amplitude of the gravity anomalies on Ganymede might be correlated with its dark and bright terranes, with the darker older terrane being denser than the younger bright terrane

(Palguta et al. 2006, 2009), which might be associated with variations of porosity, composition, temperature or a combination thereof. Detailed gravity and topography mapping combined with subsurface radar sounding by JUICE will provide key information to determine the main origin of the gravity anomalies and their implications of the ice shell structure and composition.

Combined analysis with other instruments will be essential to decipher the different contribution to the gravity anomalies. Subsurface radar sounding with RIME and micro-wave observations with SWI will constrain the near-surface porosity and identify potential variations in crustal composition, while localized admittance analyses will provide information on the depth of the porous regolith and on potential shallow density mass anomalies. By analyzing the RIME radar echoes and attenuation losses, the subsurface layering, composition, temperature, and porosity of a given subsurface target can be inferred. RIME is expected to operate with a vertical resolution of either 50 m or 142 m in ice depending on the selected bandwidth and with an along and across track resolution better than 6 km and 10 km, respectively. RIME can perform both exploratory observations and focused hypothesis tests within icy surface materials for a wide range of composition, thermal, and structural variations. RIME will mainly operate on the anti-Jovian hemisphere of its targets to avoid possible inference of the strong radio emissions of Jupiter (Goldstein and Goertz 1983; Cecconi et al. 2012) with the radar acquisitions. Correlation with gravity anomalies will therefore be mostly possible in this hemisphere protected from Jupiter's radio emission. They can be complemented by passive radar measurements at the near side of the moon (see below). Jupiter's spectral emissions range from several kHz up to about 40 MHz. Part of this frequency range overlaps with the RIME frequency band, with a central frequency of 9 MHz and a selectable bandwidth of either 1 MHz or 2.8 MHz, and with the wider frequency range of RPWI (80 kHz - 45 MHz). The Jovian Decametric radiation (DAM) in the proximity of the moons can be very intense and in the order of 40 to 50 dB above galactic noise (Cecconi et al. 2012). Since the Jovian emission locations can be predicted in advance (Louis et al. 2019; Cecconi et al. 2021), the Jovian DAM could be exploited as a radar signal of opportunity to probe the moons interior (Romero-Wolf et al. 2015, HartoghGaia Collaboration 2016; Kumamoto et al. 2017; Schroeder et al. 2016; Carrer et al. 2020; Gerekos et al. 2019; Roberts et al. 2021; Gassot et al. 2022). This technique is referred to as passive radar sounding. It makes use of the correlation of the recorded incoming signal from Jupiter with its reflections from the surface and subsurface of a given target icy moon to locate the target features and their respective depths. The possibility to detect subsurface features by passive acquisition mainly depends on: (i) the Jovian flux density value, (ii) the radar bandwidth, (iii) the integration time, (iv) the surface roughness, (v) the attenuation in the ice and (vi) the orbit height. Although the radar measurements will also be affected by the total electron content (TEC) of the icy moons' ionospheres, which results in a delay corresponding to a distance of the order of a kilometer, there is no ionospheric delay on the differences between the time reception of echoes coming from the surface and these from the subsurface. A correction for the ionosphere is only needed to correct the distortion of the signal and can be done by ionospheric measurements by 3GM and PEP and by RIME and RPWI observations. Passive radar acquisitions will be performed by both RIME and RPWI during specific acquisition sequences and will be used to probe the sub-Jovian hemisphere of the moons, which provide additional opportunities to compare with gravity and topography anomalies in order to better constrain the 3D structure of the ice shell. The observations in the wide frequency range by RPWI will also complement GALA observations of the roughness of the surface.

Further constraints on the upper cm to m of the subsurface will be obtained by the Submillimetre Wave Instrument on JUICE (Hartogh et al. 2024, this collection). Compared to

the MicroWave Radiometer (MWR) on Juno (Janssen et al. 2017), SWI will observe the Galilean moons on substantially shorter wavelengths (0.5 and 0.25 mm) and will provide a higher horizontal and vertical spatial resolution. Numerical simulations of the radiative transfer of polarized thermal radiation in the submillimeter spectral bands in lossy ice with bubbles showed that some combinations of the model parameters (air-bubble size, single scattering albedo, thermal skin depth) can be effectively constrained from the microwave radiometry data (Ilyushin and Hartogh 2020). The MicroWave Radiometer data obtained during the Juno flybys of Ganymede and Europa provided insights into the ice temperature and structure potentially down to 24 km depths (Brown et al. 2023). They suggest that multiple reflections of the colder sky background at sub-surface interfaces (e.g., fractures) explain depressed brightness temperatures observed in brighter terrain types. A thin silicate or salt contaminant surface layer could explain the microwave reflectivity in the dark regions with little to no contribution from sub-surface fractures. SWI on JUICE will provide higher resolution and better coverage than what was achieved by Juno, allowing the identification of the subsurface structure at the origin of such reflections, although only on much shallower probing depths.

Lastly, it is also possible that part of the gravity anomalies of Ganymede come not from the ice shell itself, but from the underlying silicate layers (Palguta et al. 2006; Pauer et al. 2010; Dombard and Sessa 2019). If one were to remove the ice and water shell of Ganymede, one would be left with a terrestrial-like body similar in size to Earth's moon. The Moon was volcanically active for billions of years, and one might expect that volcanic activity occurring at the ice-silicate interface on Ganymede might have been even more prolonged given the higher amounts of tidal heating it experiences and the current existence of a core dynamo, which requires core convection and therefore a sufficiently large heat flow out of the core (Bland et al. 2008). Assuming that the ice-silicate interface is 900 km below the surface and that the difference in density between the silicate mantle and overlying high-pressure ice is 1500 kg m^{-3}, the relief along this interface would have an amplitude of about 3 km in order to explain the observed gravity anomalies in the model of Gomez Casajus et al. (2022). The amplitude of this relief is modest in comparison to that observed on the Moon, Mercury, and Mars (see Wieczorek 2015), demonstrating that long-wavelength deflection of the silicate interface could represent an important contribution of the observed gravity field of the body. Since the surface relief along the ice-silicate interface is unlikely to have an expression at the surface of Ganymede (especially if there is an intervening water ocean), detailed topography mapping by JUICE indicating that these gravity anomalies are uncorrelated with the surface topography would provide a pertinent test about the anomaly origin, as it has been proposed for seafloor gravity anomalies on Europa (Pauer et al. 2010; Dombard and Sessa 2019; Koh et al. 2022). However, as the ice/rock interface is much deeper than on Europa, the interpretation of the gravity anomalies will be more ambiguous. If a deep origin is confirmed this will put key constraints on the thermal state of the rocky interior.

Finally, we note that it is possible to estimate rheologic properties of the ice shell from measurements of lithospheric flexure associated with surface and internal loads (Watts 2001). Though such techniques often make use of both gravity and topography when applied to the terrestrial planets, surface topography alone can be used when the nature of the load is known a priori. Nimmo et al. (2002) and Nimmo and Pappalardo (2004) used stereo-derived topographic profiles of ridge-flank uplift features to estimate the effective elastic thickness of the shell to be 0.5-1.7 km at the time of rifting. It is possible to convert such an elastic thickness into an estimate of the heat flow by knowledge of the temperature where ice loses its elastic strength. Other methods that can be used to estimate the surface heat flow include modelling the wavelength of extensional features with an extensional

instability model (Dombard and McKinnon 2001), and modelling of a morphological transition that occurs in impact craters at about 26 km diameter on icy bodies (Bjonnes et al. 2022). Combined topography and gravity data will be essential to estimate the lithospheric flexure and possibly identify spatial variations in lithospheric properties. Regional analyses may reveal differences in lithospheric structure between old dark terrains and more recent bright terrains, which could provide crucial constraints on the thermo-mechanical evolution of Ganymede's ice shell and on possible changes in tectonic regime.

From numerical simulations of the 3GM measurements during the orbital phase at Ganymede, the static gravity field can be estimated up to degree and order 35-45, depending on the actual strength of the gravity field (Cappuccio et al. 2020; De Marchi et al. 2021). The high precision could be sufficient to distinguish between near-surface contributions from the hydrosphere and contributions from the deep interior (De Marchi et al. 2021). Numerical simulations indicate that 3GM can reconstruct the static gravity field of Callisto up to degree and order 7, depending on the actual strength of the field (Cappuccio et al. 2022). The topography of Ganymede will be determined with GALA at very high accuracy and very high degree and order during the GCO500. It is mostly the long-wavelength topography up to degree and order 35-45 that will be useful to compare with gravity data and to extract information on the subsurface density anomalies and interface deflection. For Callisto, the limited number of flybys will provide only a partial topography mapping with the GALA altimeter (Fig. 16). However, the combination of altimetric tracks with limb observations with JANUS and accurate occultations with UVS will provide complementary data, allowing a better representation of the long-wavelength topography, essential to interpret the gravity data and to infer the hydrosphere structure and to possibly identify deep mass anomalies.

2.4 Constraining the Ocean Dynamics and Ice-Ocean Exchanges

JUICE constraints on the salinity, density and ocean flow will help understanding the structure and dynamics of subsurface oceans. In addition, once the different sources of gravity anomalies will be identified, detailed analysis of 3GM and GALA data will provide information on the ice shell thickness variations, which can in principle be used to construct a heat flux map at the top of the ocean (Kvorka et al. 2018; Cadek et al. 2019). The preliminary maps for heat flux variations at the top of the ocean of Titan (Kvorka et al. 2018) and Enceladus (Hemingway and Mittal 2019; Cadek et al. 2019) are intriguing as they exhibit a significant zonally symmetric pattern with larger values beneath the high-latitude regions. While in the case of Enceladus, such a pattern might result from a strong heterogeneity of the seafloor heat flux (Choblet et al. 2017a), the case of Titan is more in line with an intrinsic feature of rotating thermal convection in the ocean. Depending on the convective forcing and on the influence of rotation, two main regimes are observed (Gastine et al. 2016): convection in itself sets in an isotropic pattern (non-rotating regime), but fast rotation can zonally (i.e. depending on latitudes) modulate the heat transfer (rapidly-rotating regime). Specific studies dedicated to convection in ocean worlds (Soderlund et al. 2014; Soderlund 2019; Amit et al. 2020; Kvorka and Cadek 2022; Bire et al. 2022) generally conclude that they lie either in the non-rotating regime or in a transitional regime where heat flux is larger at high latitudes (polar cooling regime). A potentially important aspect not accounted for in these studies is the pressure dependence of the melting point (cf. Labrosse et al. 2018), leading to colder temperatures beneath thicker ice regions, which may drive ocean currents (see Kihoulou et al. 2023). The exact role of composition on ocean dynamics is also a matter of debate (Ashkenazy and Tzipermanet 2021; Kang 2022; Jansen et al. 2023), requiring further study. The occurrence of double-diffusive convective phenomena in the framework of melting and freezing is also essentially an open question.

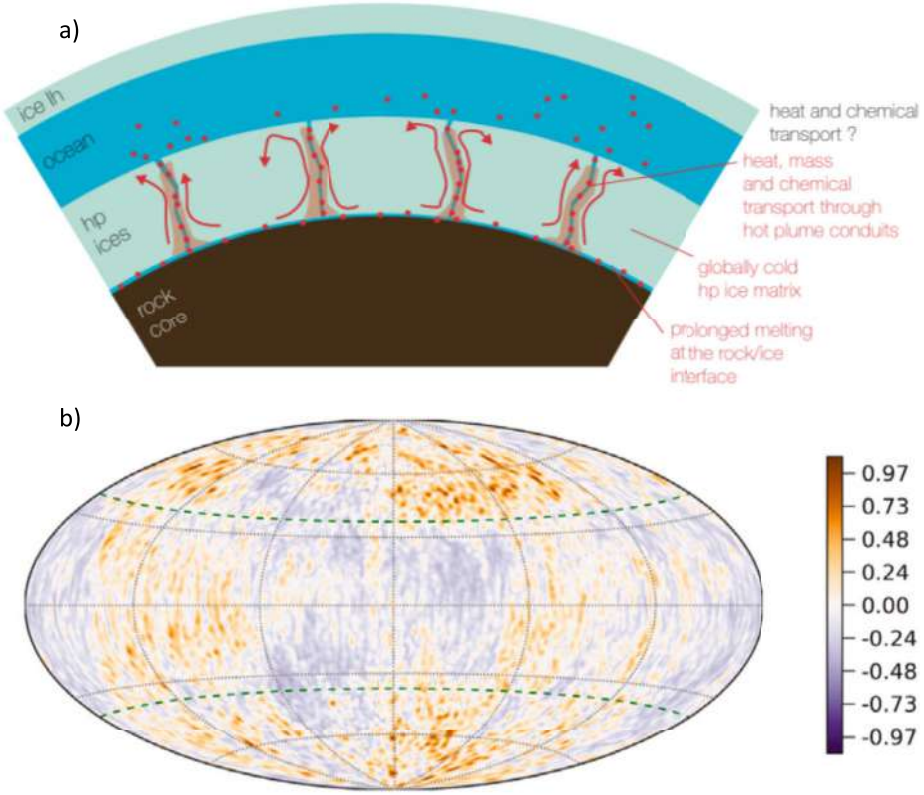

Fig. 10 a) Principle of melt transfer in the high-pressure ice mantle based on numerical simulations of Choblet et al. (2017b), resulting in efficient heat, mass and chemical transport through hot plume conduits; b) example of 3D ocean dynamics simulations showing the relative heat flux anomalies (no unit) at the top of Ganymede's ocean when heterogeneous heat flux is imposed at the bottom of the ocean (Terra-Nova et al. 2023)

As the ocean in Ganymede is trapped between two layers of water ice, an ice Ih layer at the top and a high-pressure ice layer at the bottom, the heat and mass transfer through these layers may have a significant influence on the ocean dynamics. Numerical simulations of the high-pressure mantle (Choblet et al. 2017b; Kalousová et al. 2018; Kalousová and Sotin 2020; Lebec et al. 2023; Fig. 10) showed that melting can occur in the high-pressure ice layer for a wide range of model parameters, especially at the top boundary with the deep ocean, and possibly also at the bottom boundary with the silicates. The melt transport through the high-pressure layer favors the heat and chemical transfer from the rocky core to the ocean, which can influence the ocean dynamics by creating heat flux anomalies at the seafloor (Terra-Nova et al. 2023, Fig. 10) and by injecting potentially salt-rich fluids which may induce stratification in the bottom part of the ocean. The existence of strong heat flux anomalies at the bottom may result in persistent preferred longitudes of intense outer boundary heat flux, which could result in significant ice shell thickness variations if the ice shell is in a conductive state, similar to what has been proposed for Titan (e.g. Kvorka et al. 2018). Large-scale ice shell thickness variations, revealed from topography-gravity analysis, as well as compositional variations may be used to better constrain the ocean dynamics and

efficiency of heat and chemical transport, which is essential to assess the habitability of Ganymede's internal ocean.

2.5 Synergies to Constrain the Hydrosphere Structure, Composition and Dynamics

Several JUICE instruments will contribute to the determination of the structure and composition of the hydrosphere of Ganymede and Callisto. The properties that will be determined include the average thicknesses of the outer ice shell, ocean and high-pressure ice mantle, the salt content of the ocean, the deflection of the ice/ocean interface and lateral variations in density. Although individual instruments can give information on these main parameters, the observational signals depend in a complicated way on several interior parameters that cannot be determined with confidence with any single instrument data set. A synergistic use of the instruments is therefore needed to avoid ambiguities in the interpretation. Ideally, a joint inversion of all data could provide the best constraints, but is challenging because of the large differences in data types, analysis tools, and modelling assumptions. A more straightforward and stepwise approach in which different interior parameters are estimated in sequence is likely to be more realistic.

The average thickness of the ice shell and possible lateral thickness variations are probably easiest to determine. The best estimate of the average thickness will be obtained at Ganymede from a joint analysis of the tidal response, based on gravitational monitoring with 3GM (Love number k_2) and on altimetric monitoring with GALA (Love number h_2), and of electromagnetic induction measurements (both magnetic and electric fields) by J-MAG and RPWI, supported by PEP, UVS and 3GM (see Petricca et al. 2023 for such a joint inversion method). At Callisto, only electromagnetic induction measurements and an estimate of the gravitational Love number k_2 will be possible due to the limited number of flybys and will be used to constrain the average thickness. Shape models determined by combining GALA, JANUS and UVS data together with 3GM gravity data may be used to infer large-scale variations in ice shell thickness. Although radar can determine an interface between ice and liquid water, the oceans on Ganymede and Callisto are expected to be much deeper (50-120 km) than the penetration depth of RIME ($< 10 - 15$ km), which prevents direct detection of the interface between the ice shell and the ocean by radar sounding. RIME will, however, provide key information on the structure of the upper ice shell, which will be essential to have better information on the underlying thermal structure. The two flybys of Europa will be insufficient to constrain time variations, however, RIME might in principle be able to detect Europa's ocean if the ice shell is shallower than the penetration depth. Further constraints on the shell thickness, in particular for Ganymede and to a lesser degree for Callisto, can be obtained from rotation (3GM, GALA, JANUS) and the combined use of gravity and topography data (3GM, GALA), which will also allow the identification of lateral variations in ice shell thickness and properties.

The thickness of the ocean can next be determined from electromagnetic sounding, especially by JUICE's ability to measure multiple frequencies. Diurnal tides are not sensitive to it, although moon-to-moon tides could constrain the ocean thickness if one of these tides is near resonant with a normal mode of the ocean. Once ice shell and ocean thicknesses are well known, information on the composition of the ocean can be derived from the electrical conductivity, to be determined by electromagnetic sounding. The density of the ocean will be constrained from gravimetric, altimetric, and rotational measurements. Since electromagnetic induction and tides are sensitive to variations in salinity and density with depth, respectively, measurements of those quantities hold in principle information on stratification of the ocean. Although a direct determination of salinity or density profiles will not be

possible, it might be possible to distinguish homogeneous from heterogeneous oceans by coupling the observations to chemical and physical models of the ocean and its dynamics. Once the shell and ocean thickness are determined, the visco-elastic response of the ice shell can be constrained from the amplitude and phase lag of the tidal response (k_2 and h_2) and the rotational dynamics. We nevertheless stress that a joint inversion of all geophysical data will be needed to get the best insight into the different properties of the satellite interior. The ice and ocean properties will be determined with much more confidence at Ganymede than at Callisto due to the orbital phase campaign. At Europa, JUICE measurements alone will most likely not be conclusive, but will complement and help the analysis of the much larger and more diverse Europa Clipper dataset.

In complement to the geophysical investigations, remote sensing instruments like MAJIS, SWI, and UVS and the in situ PEP instrument will provide information on the composition of the surface and exosphere, and potentially plumes in the case of Europa (see Sect. 4). This will help constraining the fraction of non-ice materials, their compositions, and lateral variations. By correlating with geological units and using data about possible subsurface radar reflectors and gravity-topography anomalies, a better determination of the exogenic or endogenic origin of non-ice surface components will be feasible (Gladstone et al. 2024, this collection, Poulet et al. 2024, this collection) and a link might be established with the composition of the ocean (see Sect. 4.2).

3 Deep Interior Structure and Evolution

3.1 Gravity and Shape Constraints on the Density Structure

Geophysical measurements acquired by the Galileo mission suggest a different degree of internal differentiation for Ganymede and Callisto (e.g., Sohl et al. 2002). The series of Galileo flybys around these icy moons (D'Amario et al. 1992) enabled gravity measurements of the degree-2 spherical harmonic coefficients J_2 and C_{22}. These coefficients are a measure of the triaxial ellipsoidal shape of the moons, mainly due to rotation and static tides, but could not be determined independently, essentially because most flybys except for the second flyby of Ganymede were equatorial. Two Ganymede encounters led to a preliminary estimation of the moon's quadrupole terms, by assuming the hydrostatic equilibrium constraint that J_2 is a factor 10/3 larger than C_{22} (Anderson et al. 1996). Assuming that the gravity field of the moons at large horizontal scales is dominated by a fluid response to average tidal and centrifugal forces, these degree-2 gravity coefficients can be used to determine the mean moment of inertia by means of the Radau approximation (e.g., Hubbard 1984; Van Hoolst et al. 2008), and thus provide constraints on the internal mass distribution of the moon. By using this approximation, the C_{22} coefficient determined by Galileo radio science investigations gives a MoI factor equal to 0.3105 ± 0.0028 for Ganymede. Such a value is well below the value for a homogeneous body (0.4) and therefore indicative of a complete differentiation into low-pressure ice, water, high-pressure ice, and rock layers surrounding a metallic core (Anderson et al. 1996). Additional Ganymede flybys led to obtain further gravity information and a refined mean density of 1942 ± 4.8 kg m^{-3} (Anderson et al. 2001). These measured geophysical quantities indicate the existence of a metallic core with a radius ranging between about 600 km, for a 100%wt Fe core, to about 900 km for a 100%wt FeS core, surrounded by a silicate mantle and a thick hydrosphere (e.g., Sohl et al. 2002). The detection of Ganymede's large intrinsic magnetic field with the magnetometers

onboard the Galileo spacecraft is also consistent with the presence of a molten iron core that could support an internal dynamo (Kivelson et al. 1996; Schubert et al. 1996).

Re-analysis of the Galileo data complemented with data acquired during a close flyby by JUNO (Gomez Casajus et al. 2022) indicate some deviation from the hydrostatic equilibrium, confirming the existence of deep mass anomalies in Ganymede previously highlighted by Palguta et al. (2006, 2009). This deviation from a perfectly hydrostatic state suggests that the MoI factor might be larger than the value initially reported by the Galileo team, indicating a smaller degree of differentiation. However, firm conclusions on the density structure cannot be drawn based on the existing data. Only with the improved gravity field of the JUICE mission will it be possible to quantify the effect of non-hydrostatic contributions to degree-2 and to provide unambiguous constraints on the internal mass distribution, both on its average profile and the lateral variations.

Gravity and magnetic data acquired during close encounters of the Galileo spacecraft with Callisto suggested a different differentiation state than for Ganymede. By processing Doppler measurements collected during five flybys, the quadrupole gravity coefficients were estimated assuming the hydrostatic relation $J_2 = (10/3)C_{22}$ and yield a MoI of Callisto of 0.3549 ± 0.0042 according to the Radau approximation (Anderson et al. 1998, 2001). This result suggests that Callisto is partially differentiated and has a significant degree of mixing between ice and denser rock-metal [Nagel et al. 2004; Kuskov and Kronrod 2005], and possibly organics [Neri et al. 2021]. A partial differentiation of Callisto's internal structure may be consistent with the highly cratered surface and the absence of tectonic activity and of any sign of an internal dynamo (Kivelson et al. 1999; Khurana et al. 1998). Nevertheless, any interpretation in terms of partial differentiation should be taken with caution since the MoI factor inferred from Galileo gravity data is poorly constrained. A higher degree of differentiation is not excluded since Callisto's actual moment of inertia might be up to 10% larger than the estimated value because of unconstrained non-hydrostatic effects (Gao and Stevenson 2013).

JUICE will determine the static quadrupole gravity field of Ganymede with an accuracy of 9×10^{-10} for J_2 and 3×10^{-10} for C_{22} (Cappuccio et al. 2020) from 3GM data taken during the orbital phase. The coefficients J_2 and C_{22} of Callisto can be estimated with an accuracy of 1.3×10^{-7} and 1.9×10^{-8}, respectively (Cappuccio et al. 2022). These very accurate data will allow to assess the deviation from the ratio of 10/3 for J_2/C_{22}, expected for hydrostatic equilibrium for slow rotators, with a precision of several orders of magnitude. GALA will determine very accurately the global shape of Ganymede, which will be able to quantify any deviation to the ellipsodial hydrostatic shape a, b and c, and to estimate any deviation from the degree-two value expected from gravity coefficients. For Callisto, due to the limited number of flybys and surface coverage (see Sect. 6), GALA alone will not be able to constrain accurately the global shape. Limb profile acquisition by JANUS and occultation data from UVS will be needed to complete the coverage and obtain an accurate global shape model. By combining the higher-degree gravity field with the higher-degree shape model, JUICE will further constrain the non-hydrostatic internal mass distribution (see Sect. 2.3), and will allow a more precise estimate of the moment of inertia.

3.2 Active Metallic Core

The Galileo magnetometer measurements revealed that Ganymede possesses a strong axial-dipole-dominant internal magnetic field, with a dipole moment $\sim$710 nT $\times R_G^3$, where R_G is the radius of Ganymede (Kivelson et al. 1996, 2002a, 2002b). For comparison, the dipole moment of planet Mercury is only $\sim$200 nT $\times R_M^3$, where R_M is the radius of Mercury (Anderson et al. 2012). The background Jovian magnetic field at Ganymede is around 110 nT

(Kivelson et al. 2002a,b). Thus, the internal magnetic field of Ganymede is about one order of magnitude larger than the background Jovian field when evaluated at the surface of Ganymede. Ganymede's internal magnetic field beyond the dipole component is not known. Only JUICE measurements will allow a clear description of both spatial and temporal variations of Ganymede's internally generated magnetic field (see Sect. 2.2), thus providing insights on both subsurface ocean and metallic core structure and dynamics.

A prerequisite for large-scale magnetic field generation is an electrically conducting fluid with complex flows (e.g. Kimura et al. 2009). Two possible layers of conducting fluids inside Ganymede are the subsurface ocean and the liquid iron-rich core. Magnetoconvection could modify an existing background field but is unlikely to amplify it significantly (Sarson et al. 1997). An extensive numerical dynamo survey showed that a magnetic Reynolds number larger than 50 is needed to maintain a self-sustaining dynamo (Christensen and Aubert 2006). The magnetic Reynolds number is defined as $R_m = \mu_0 \sigma_0 U L$, where μ_0 is the magnetic permeability of free-space, σ_0 is the electrical conductivity, U is the typical fluid velocity, L is the typical length-scale. The electrical conductivity of the subsurface ocean has been estimated to be on the order of 0.1-1 S/m (Saur et al. 2015; Vance et al. 2021). Running a dynamo in a 300 km thick subsurface ocean would require a fluid speed of 25 m/s even if the electrical conductivity is as high as 5 S/m. Such rapid flows seem rather unlikely. The several orders of magnitude higher electrical conductivity of iron under the core conditions of Ganymede make it much easier to satisfy the dynamo limit. Thus, dynamo action in the liquid iron core of Ganymede is the most likely source of Ganymede's internal magnetic field.

The dynamo interpretation of Ganymede's internal magnetic field offers an independent line of evidence that Ganymede is fully differentiated into a silicate mantle and an iron core in addition to the outer ice-ocean layers (Schubert et al. 1996). Moreover, a significant fraction of the iron core must be in a liquid state. Sufficiently strong convection needed for a dynamo can be generated by purely thermal buoyancy (for a completely liquid core) and/or compositional buoyancy. The latter is associated with the core crystallization, resulting in compositional convection. The iron snow regime in which iron crystallizes near the top of the core and then snows down is currently a popular candidate for powering Ganymede's core dynamo (Hauck et al. 2006; Rückriemen et al. 2015). In this scenario, the iron snow layer itself, which grows with time, is expected to be stably stratified due to the increasing sulfur content as a function of radius, while the remelt of iron is expected to drive compositional convection below the iron snow layer (Rückriemen et al. 2015). This is different from the Earth where, owing to higher pressure, iron crystallizes at the bottom of the outer liquid core, sinks toward the center and leads to the progressive growth of the solid inner core. Chemical buoyancy taking place just above the inner core boundary drives the present-day geodynamo. Thermal evolution calculations indicate that the iron-snow regime is a relatively recent state inside Ganymede's core with a timescale on the order of 500 Myrs (Hauck et al. 2006, Rückriemen et al. 2015). These models also suggest that there is no solid inner core today, because as soon as an inner core freezes out, i.e. when the snow layer comprises the entire core, no magnetic field can be generated in the iron snow regime. This may suggest either a late iron core formation or at least a slow cooling of the iron core (Bland et al. 2008; Rückriemen et al. 2018). Further studies are, however, needed to evaluate whether iron snow itself can generate or contribute to the generation of the magnetic field (see Huguet et al. 2023). Also our understanding of the effect of an increased tidal heating event in Ganymede's evolution on the evolution of its dynamo (e.g. Bland et al. 2008) would benefit from further investigations.

Gómez-Pérez and Wicht (2010) investigated the influence of an external magnetic field on planetary dynamos and found that an external field as weak as 2% of the undisturbed

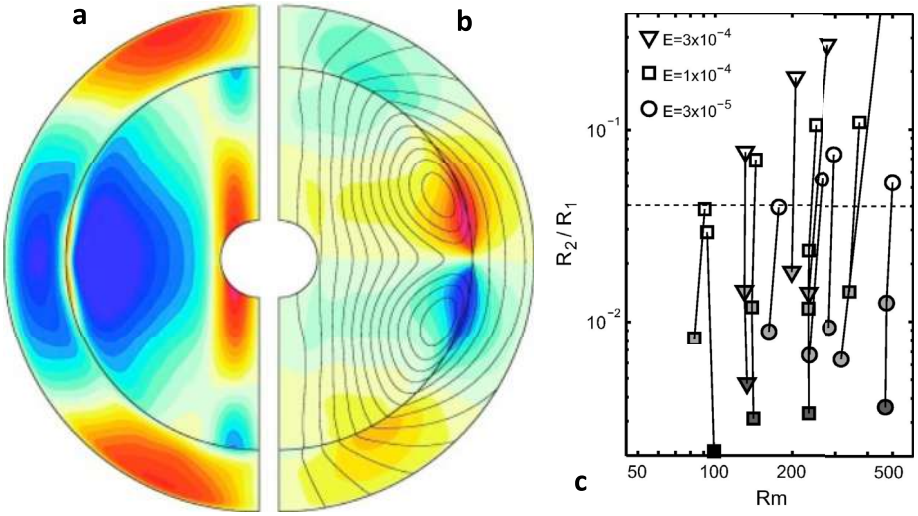

Fig. 11 Flow and magnetic field properties of a Ganymede dynamo simulation under the iron snow regime (a, b) and the quadrupole to dipole magnetic power ratio (R_2/R_1) in a suite of numerical dynamo simulations with and without a stably stratified iron snow layer (c). Panel a shows the zonal flow in color while panel b shows the toroidal magnetic field in color and the poloidal magnetic field lines. In panel c, the open symbols represent dynamo models without a stably stratified iron snow layer, light grey represent cases where the thickness of the iron snow layer is 10% of that of the underlying dynamo layer, mid-grey for 20%, and dark grey for 40% which applies to the case shown in panels a & b, and black for 80%. Figure is adapted from Christensen (2015)

dynamo field at the core surface could alter the behavior of the dynamo. However, the Jovian background field is only about 0.3% of Ganymede's present-day internal dipole field when downward continued to 0.3 Ganymede radii. Whether the Jovian magnetic field influenced the initial growth phase of Ganymede's dynamo is an open question. There are two critical unknowns here: the timing of the initiation of Ganymede's present-day dynamo and the history of the Jovian magnetic field.

Setting aside the influence of the external magnetic field, Christensen (2015) investigated iron snow dynamos for Ganymede with 3D numerical magnetohydrodynamic models. In addition to matching the observed dipole field strength and tilt angle, efforts were made to match the small quadrupole to dipole magnetic power ratio estimated for Ganymede. The dipole-quadrupole solution of Kivelson et al. (2002a,b) features a quadrupole to dipole magnetic power ratio of about 0.0025 at the surface of Ganymede. This value probably should be viewed as an upper limit given the trade-off with the induction effect. When viewed at the dynamo surface, this ratio becomes 0.02 - 0.04, which is significantly smaller than those of Mercury (0.3), Earth (0.14), and Jupiter (0.1), but is comparable to that of Saturn (0.02) (Anderson et al. 2012; Connerney et al. 2022; Cao et al. 2020).

In the dynamo models of Christensen (2015), only horizontal flows are allowed in the iron snow layer, which represents an end-member way to treat a stably stratified layer. In the fully convective region beneath the iron snow layer, both the magnetic field (Fig. 11b) and the zonal flow (Fig. 11a) resemble those of the geomagnetic field. Zonal flows comparable to those in the convective region also developed in the iron snow layer, which act to shear and filter the dynamo magnetic field. As a result of the filtering effect, the quadrupole to dipole power ratio at the core surface is significantly reduced. It can be seen from Fig. 11c

that this ratio at the core surface tends to be larger than or marginally comparable to 0.04 without the iron snow layer (open symbols). An iron snow layer that is 10% the thickness of the underlying dynamo layer (light grey) would be sufficient to reduce that value to below the observed upper limit.

Several other processes besides thermal and compositional core convection can in principle also power a dynamo. They have been studied in detail to explain the lunar dynamo (see Wieczorek et al. 2022, for a recent review), and might also be relevant for Ganymede. One such mechanism is mechanical forcing of the core by precession and libration. Both processes can lead to differential rotation between the liquid core and the solid mantle and could drive a dynamo (Le Bars et al. 2015). For the current moon, libration and precession are found to be too small to drive a dynamo. Since libration of the solid mantle of Ganymede is expected to be very small (Van Hoolst et al. 2013) and the inclination and obliquity of Ganymede is probably an order of magnitude smaller (Baland et al. 2012) than the inclination angle of the moon, it seems unlikely that libration and precession could currently generate a dynamo in Ganymede. Impacts can also change the rotation of the ice shell and excite motion in the core (e.g. Le Bars et al. 2011, for the moon), but decoupling of motion between the shell and solid interior by the subsurface ocean suggests that a large recent impact would be required.

The upcoming JUICE J-MAG measurements, in synergy with PEP and RPWI to account for plasma interactions, will allow us to separate the contributions of ocean induction from the internal magnetic field beyond the dipole. These measurements would enable us to constrain the quadrupole-to-dipole ratio and the octupole-to-dipole ratio for Ganymede, from which the thickness of the iron snow layer inside Ganymede could be estimated. If Ganymede has a solid inner core, it might be possible to constrain its presence and size by analysing the core field morphology as it has been done on Mercury (Wardinski et al. 2021). Moreover, JUICE J-MAG measurements would enable an estimate of the secular variation of Ganymede's internal magnetic field, which provides an additional measure to probe the fluid dynamics inside the core.

3.3 Differentiation Processes and Thermal Evolution

The difference in internal structure between Ganymede and Callisto, as inferred from Galileo data (see Sect. 3.1 and note the uncertainty on the moment of inertia for Callisto), may be a consequence of either the accretion environment or/and the subsequent thermal evolution, possibly due to a difference in tidal heating or the slight difference in silicate content. The mean density of Callisto is somewhat less than 6% below that of Ganymede. Part of that difference is due to compression. Ganymede and Callisto possibly experienced different accretion rates from solid blocks as they grew in the circumplanetary disk (Canup and Ward 2009; Estrada et al. 2009; Ronnet et al. 2018; Shibaike et al. 2019; Batygin and Morbidelli 2020). During this very early stage of the evolution of the moons, the accretional (impact) heating was the predominant heat source, possibly favoring ice melting in the outer layers (Monteux et al. 2014). High impact rates about 700 Myr after formation during the period of late heavy bombardment could further accelerate the differentiation process, possibly triggering a catastrophic ice-rock separation in the case of Ganymede while Callisto remained partly differentiated since both the impact rate and the impact velocity is larger on Ganymede than on Callisto (Barr and Canup 2010). Callisto may have preserved in the structure of its outer layer some information regarding this intense bombardment event, which may be revealed from crater statistics and morphology and from detailed characterization of its subsurface structure from radar sounding, altimetric and gravimetric measurements. As

mentioned previously, detailed gravity and shape measurements by JUICE will refine the determination of the MoI factor, thus providing more precise estimates of the mass distribution and the degree of differentiation.

During accretion and the very early stage of the moon evolution, heat from short-lived radioactive isotopes, mainly ^{26}Al and ^{60}Fe, can be important heat sources depending on the accretional timescale in addition to accretional (impact) heating. The growth and survival of moons in a circumplanetary disk is controlled by the balance between moon accretion and inward migration due to interactions with the disk (Canup and Ward 2002, 2009, Barr and Canup 2008; Shibaike et al. 2019; Batygin and Morbidelli 2020). The large icy moons of the giant planets formed on timescales possibly longer than 0.1 Myrs years at temperatures low enough to accrete ice. The longest timescales correspond to sufficiently slow accretion to prevent short-lived radionuclides and accretional heat from melting ice. In Callisto, this may have enabled the preservation of mixed ice-rock layers. For a later stage of evolution, decay heat of long-lived radioactive isotopes, e.g. ^{235}U, ^{238}U, ^{232}Th and ^{40}K, are essential heat sources for all large moons. Due to the moderate volatile behavior of potassium, ^{40}K may be relatively more important for moons of the outer solar system than for terrestrial planets in the inner Solar System.

Friction inside moons deformed by periodic tidal forces can also lead to significant production of heat, depending on the amplitude and frequency of tidal deformation. Under some circumstances depending on the orbital configuration, tidal heating can have a large impact on the thermal evolution of a moon and might have been substantially different between the moons during their history. In their current orbits, the tidal heating rate in Ganymede and Callisto is significantly smaller than the radiogenic heating rate, but eccentricity pumping by a Laplace-like resonance during the orbital evolution of Ganymede is expected to have led to phases with a significantly increased heating rate (Showman and Malhotra 1997; Bland et al. 2009). Since Callisto is not involved in a similar resonance, the absence of such a pumping on Callisto may be a reasonable explanation for the difference in evolution of both moons. In addition, the larger distance of Callisto compared to Ganymede also significantly reduces tidal heating. Ganymede's large mass likely caused it to be the most rapidly migrating object in the Jovian disk, suggesting that the Laplace resonance may have been assembled from the outside in (Peale and Lee 2002; Madeira et al. 2021) during moon formation. Alternatively, tidal evolution driven by dissipation in Io may have assembled the resonance at a later time from the inside out (e.g. Yoder and Peale 1981; Greenberg 1987). Independent of the timing, eccentricity perturbations during resonance assembly may have been responsible for heating Ganymede sufficiently to drive differentiation through tidal dissipation.

It is possible that the Galilean moons passed through one or more Laplace-like resonances before evolving into the current Laplace resonance, resulting in prolonged periods with enhanced eccentricity and tidal dissipation in Ganymede (Showman and Malhotra 1997; Bland et al. 2009). There is abundant surface evidence for wide-spread resurfacing and high heat fluxes associated with the emplacement of bright terrains, which may be the consequences of previous orbital resonances (e.g. Showman et al. 2004; Bland et al. 2009). Also Callisto may have passed through a 2:1 mean motion resonance with Ganymede (Downey et al. 2020; Lari et al. 2023). Tidal dissipation in Ganymede in the past may have been comparable to the estimated present-day dissipation inside Europa if the eccentricity was ten times larger than the current value (i.e. 10×0.0015). As shown by Showman and Malhotra (1997), the eccentricity may likely have exceeded 0.01 when Ganymede entered the resonance, the exact amplitude depending on the entrance path and the dissipation factor in Jupiter. Analysis of tectonic patterns and cryolvolcanic landforms on Ganymede may reveal ancient periods with higher tidal deformation and dissipation, which may be indicative of

when Ganymede entered the Laplace resonance (Showman and Malhotra 1997; Bland et al. 2009). Among the three Galilean moons involved in the Laplace resonance, Ganymede is the only one that may have kept records of the past evolution of the Laplace resonance, since the surfaces of Europa and Io are extremely young. If the entrance occurred during the first billion years, enhanced tidal heating may have had an impact on ice-rock separation, favoring ice melting and water-rock reactions. If it occurred later, tidal heating may have had a consequence on the organics-rock-metal evolution and their progressive separation leading to the formation of the metallic core.

Throughout the differentiation process, especially during the earlier stage, ice melting and associated water extraction controls the efficiency of heat and chemical transfer. In the case of Ganymede, the separation of rock and ice phases is expected to be rather fast and catastrophic (<0.5 Gyr, Kirk and Stevenson 1987), while for Callisto a more gradual ice-rock separation would be expected in order to explain the apparent low degree of differentiation of its interior (Nagel et al. 2004). O'Rourke and Stevenson (2014) showed than double-diffusive convection in a mixed ice-rock interior can delay internal melting and ice-rock separation, but cannot prevent it. This indicates that it may be difficult to prevent full ice-rock separation even in the case of Callisto. During the ice-rock separation, it is likely that melt-water is produced. Melt migration is an efficient way to transport heat and to favor chemical exchange. The composition of internal oceans have almost certainly been conditioned by leaching processes (Fig. 12). Therefore, the composition of the oceans and salt assemblages identified at the surface of these moons will be indicative of the past leaching processes. Especially, the ratio of Na/K/Ca/Mg assessed at the icy moon surface, especially in the most ancient terrains, may provide key constraints on these past leaching processes.

Ice-water-rock separation should leave the silicate interior mostly hydrated. This should then be followed by a progressive warming due to the decay heat of long-lived radioactive isotopes (and possibly enhanced by tidal heating) until the dehydration temperature is reached. Evolution models indicate that this dehydration phase may last several billion years depending on the available radiogenic sources (Castillo-Rogez and Lunine 2010; Kimura and Kuramoto 2012). For Callisto, it is possible that this dehydration temperature has never been reached even in the center. Density profiles assessed from the 3GM data will be crucial to constrain the density of Callisto's deep interior.

Once ice and rock is fully separated, which likely occurred during the first billion years on Ganymede (Fig. 12), radiogenic heating in the rock+metal phase is sufficient to raise the temperature to the Fe-FeS melting temperature (Spohn and Breuer 1998). However, it is still unclear how long it takes to reach the Fe-FeS melting temperature, as it strongly depends on the available heat sources and efficiency of heat transfer by solid-state convection and meltwater extraction. Contrary to terrestrial planets where metal-silicate separation has occurred in a very early stage as a consequence of accretion processes (Kleine et al. 2002; Brennan et al. 2022), the formation of a metallic core on Ganymede is likely delayed by several billions of year due to the different processes described above (Kirk and Stevenson 1987, see Fig. 12). If the metallic core formed in a runaway melting event, it might have induced a transient increase of heat flux, which might have left some geological signatures at the surface. From surface mapping, JUICE may reveal changes in tectonic patterns and/or enhanced crater relaxation indicative of such an event.

As the current magnetic field plays a role in the surface composition, with charged particles being more heavily precipitated in the polar region (Liuzzo et al. 2020; Duling et al. 2022), detailed analysis of the surface composition and correlation with surface ages may reveal past fluctuations in the boundary between open and closed field lines, thus providing indirect constraints of the past evolution of the magnetic field.

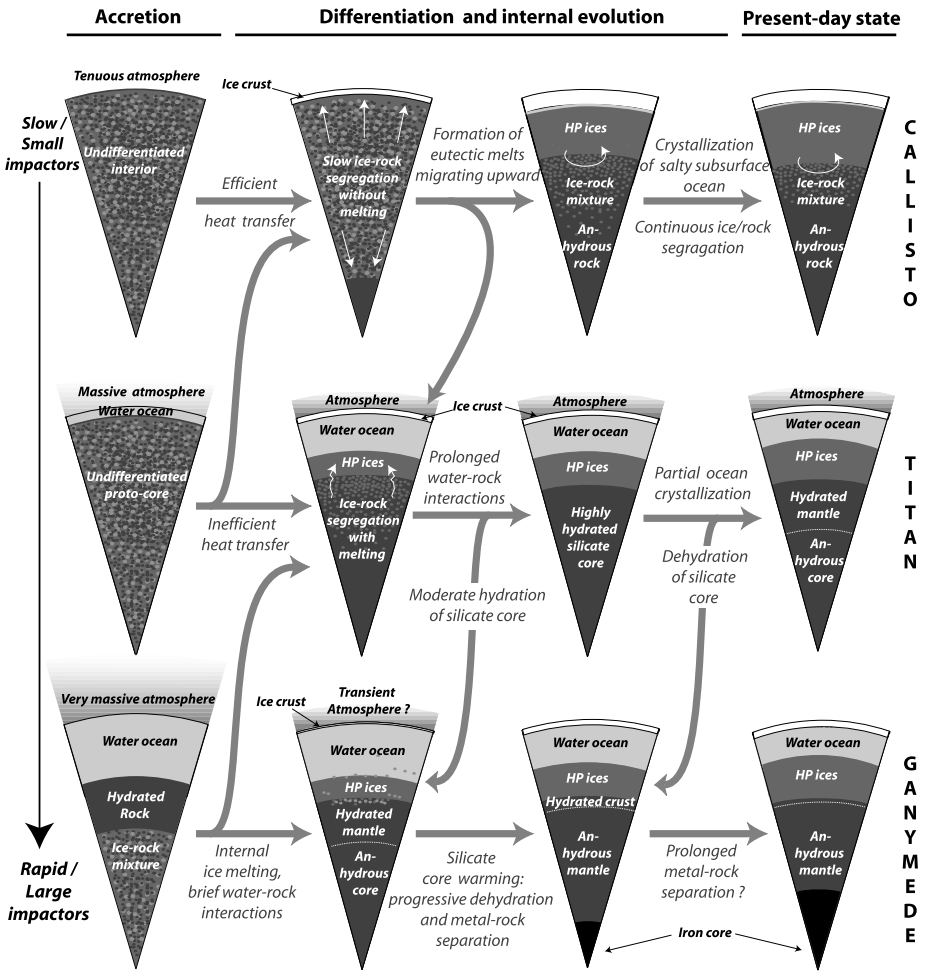

Fig. 12 Possible evolution scenarios for the interior of Callisto, Titan, and Ganymede assuming different initial states. Depending mostly on the efficiency of heat transfer in the interior, different bifurcations in the evolutionary path may have occurred explaining the present-day state of their interior. The interior structure shown here are just possible interior structures compatible with existing observational constraints. Existing data are, however, not sufficient to conclude with certainty about the differentiation state of these moons (from Journaux et al. 2022, adapted from Tobie et al. 2014)

3.4 Synergy to Characterize the Deep Interior Structure and Evolution

Better understanding of how Ganymede and Callisto attained their internal structure rests on synergistic information on the current state of the metallic core and rock and ice mantles, especially their size, thickness and density. In order to characterize the structure, size and density of the refractory cores of Ganymede and Callisto, the moment of inertia constrained from gravity measurements combined with shape and rotation data will be considered together with the geophysical constraints on the hydrosphere described in Sect. 2. Precise determination of the gravity field and shape of Ganymede and Callisto by 3GM and GALA (with the complement of JANUS and UVS for Callisto) will not only improve the moment

of inertia estimate but will also quantify the deviation from hydrostatic equilibrium, and may reveal deep mass anomalies and inform on any uncompensated topography anomaly of the rocky mantle. Although solutions for the moon's interior for a given moment of inertia are highly non-unique, an improved MOI restricts the amount of possible interior models compatible with it and hence provides indirect information on the density. These results will put constraints on the possible thermal evolution of the mantle and on its consequences for the past evolution of the hydrosphere. Comparison between the interior structure and geological record of Ganymede and Callisto will provide key information on the differentiation processes. Further insight will be obtained by comparing Ganymede and Callisto with the geophysical information on Europa, mainly to be obtained with the Europa Clipper (Roberts et al. 2023). Global and continuous electromagnetic field measurements at Ganymede by J-MAG, complemented by RPWI and PEP, will provide constraints on the dynamo model of the metallic core. This will lead to a further understanding of the composition and thermal state of the deep interior and will shed further light on the origin of the geodynamo and possibly on its age. It remains to be studied whether the electromagnetic measurements could also reveal the existence of magnetic anomalies in the rock mantle.

4 Surface Manifestation of Internal Processes

4.1 Tectonism and Volcanism

Tectonism and volcanism, as observed mainly on Europa and Ganymede, are geological processes that can strongly affect the evolution of the surface of icy moons and the material exchange with the subsurface ocean. Europa and Ganymede are characterized by different landforms that are due to different stress mechanisms and can vary in time and space depending on the mechanical properties of the icy lithosphere and the thermal history of the satellites. Various processes can result in stress accumulation in the coldest part of the icy shell, resulting in rupture either by extension or compression, although contractional deformation is less observed. These include stresses associated with ocean crystallization/melting, thermal stresses associated with lithosphere cooling, and stresses associated with tidal deformation and non-synchronous rotation. Volume changes due to ice/water phase changes are an important driving mechanism for tectonics and volcanism, both globally at the ice/ocean interface and locally. Thermal stresses and stress related to volume changes can be of the order of 1 MPa (e.g. Nimmo and Pappalardo 2004 and Rudolph et al. 2022 for Europa), while tidal stresses are much smaller, of the order of 0.01-0.1 MPa for Europa at present (e.g. Wahr et al. 2006; Harada and Kurita 2006), and potentially of the same level on Ganymede in the past (Steinbrügge et al. 2024).

The main stress source of tectonic activity likely varies in the history of the moons. For example, tidal stress is identified to be a key driver of tectonic activity on Europa, and possibly also was so on Ganymede in the past when the ice shell was thinner and the eccentricity larger. Even though tidal stresses are expected to play a key role in faulting dynamics, the stresses associated with tides are small ($<$0.1-1 bar) (e.g. Wahr et al. 2006; Harada and Kurita 2006) and insufficient to break ice. However, the periodic distortion due to tides can generate global pattern of stress that may control the distribution and strain of tectonic features located on the surface of the icy moons. Identification of specific fault patterns in ancient terrains on Ganymede may reveal the role of tides in the past. Therefore, tectonic and cryovolcanic features observed on icy moons provide insights in their past geological and orbital history.

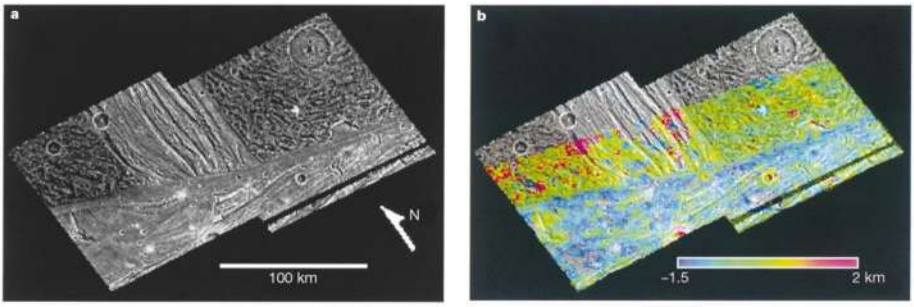

Fig. 13 Terrain units (a) and topography (b) at the intersection of Erech Sulcus and northern Sippar Sulcus, Ganymede, corresponding to a 75-km-wide band of grooved terrain extending between two blocks of older, dark terrain (adapted from Schenk et al. 2004, figure credit NASA/JPL/LPI)

The JUICE mission will be pivotal in performing an in depth analysis of such features thanks to the onboard suite of instruments. Specifically, the JANUS camera (Palumbo et al. 2024, this collection) will investigate tectonic features through a global and regional mapping in order to better understand the stresses acting on the moons. The combination of these data with RIME, GALA and 3GM investigations will allow a better determination of the lithosphere properties and their lateral variations. In addition, SWI will provide maps of the thermophysical properties of the first subsurface meters, such as changes in composition, and diverse scatterers (cracks, bubbles, changes in dielectric properties due to local enrichments in brines or salts, etc.). Changes in lithosphere thickness, as can for example be inferred from surface load flexure or crater relaxation, and in tectonic style may also provide constraints on the past evolution of the ice shell and its coupling with the underlying ocean.

On the two flybys of Europa, JANUS will focus on regional and local targets with a resolution of about 100 m/pixel and 10 m/pixel, respectively. It will map local tectonic features, such as ridges and bands. The spatial distribution and the geometrical properties determined from the mapping will be used to understand the mode of formation of tectonic structures, which in turn can help constraining the moon's geophysical state. For example, the different models proposed for the origin of Europa's ridges (Greeley et al. 2004) have different implications for the presence and distribution of liquid water at the time of ridge formation. Cryovolcanic features, such as lenticulae, chaos and low-lying smooth low-albedo structures, will also be mapped in different filters by JANUS and at a sufficiently precise resolution to study their distribution, morphometry and composition. Since such features may be the surface expression of the subsurface liquid reservoir (Fagents 2003; Quick et al. 2017; Lesage et al. 2020), their nature and formation mechanism can be assessed by combining data from JANUS with RIME subsurface sounding and MAJIS compositional mapping.

On Ganymede, regional- and high-resolution scale images of the Galileo SSI camera revealed that intense tectonism was the dominant process to create and shape Ganymede's bright terrain (Fig. 13), while cryovolcanism played a comparably minor role (Pappalardo et al. 2004). Thanks to the JANUS coverage, the spatial distribution as well as the azimuthal orientation of tectonic structures such as furrows and grooves systems will be analyzed at higher resolution and better spatial coverage. Quantitative comparisons of tectonic characteristics between regions of different ages will be used to infer the geodynamic setting of the tectonized regions and provide information on the dynamic and kinematic processes affecting the upper ice layer. Specifically, differences in tectonic characteristics between dark and bright terrains will be used to reconstruct Ganymede's tectonic history. Images acquired

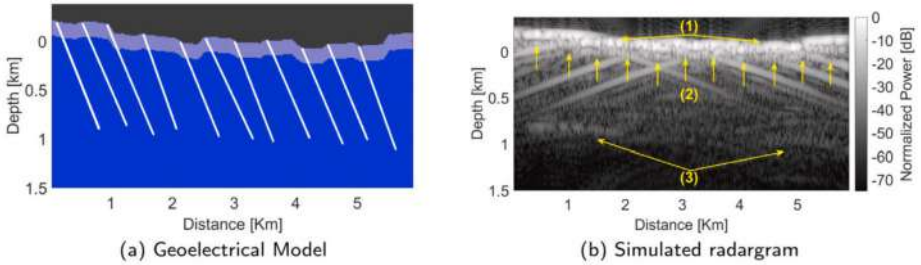

Fig. 14 Example of simulated radargrams of groove bright terrain models revealing the potential signature of crevassing, characterized by a non-specular return due to the rough surface profile associated with the grooves caused by faulting (arrow 1), by a diffused scattering extending up to 1 km below the surface (arrow 2) and a stronger reflection at depth linked to the orientation of the fractures (arrow 3) (Sbalchiero et al. 2023)

at high resolution (7-8 m pixel) during GCO500 (see Sect. 6) on targeted areas in various geological units will allow a detailed scaling analysis of fault systems (length, width, displacement) and their stratigraphy, which is difficult to unambiguously identify at lower resolution. Such measurements will be coupled with the topography obtained by JANUS stereo coverage, RIME and GALA in order to have a complete dataset capable to constrain the depth penetration of the tectonic systems and, hence, to provide information about the thickness and layering of the ice shell. Note that GALA will determine absolute altimetric values with a precision of about 5 m on areas with a width of on average 50 m along the track, corresponding to the laser spot size at the surface during GCO500. The DTM determined from JANUS stereo-pairs at GCO500 will also have a spatial resolution of the order of 50 m. Complementary data from MAJIS, UVS, and SWI will also provide constraints on the surface composition and physical properties of the icy regoliths, which may reveal further information on the mechanism controlling the formation of the different landforms and geological units.

In support of surface morphology and topography constrained by JANUS and GALA, RIME can detect the dielectric interface caused by the difference in composition between cryovolcanic lava, which is relatively pure ice, and older terrain with a higher fraction of dust due to impacts (see Thakur and Bruzzone 2021). RIME will be able to detect and differentiate different emplacement scenarios for bright terrains. Interpretation of radargrams will rely on high resolution DTMs provided by JANUS and GALA in selected regions of interest in order to carefully simulate surface clutter echoes due to surface topography (Nouvel et al. 2004; Berquin et al. 2015; Gassot et al. 2022; Tosi et al. 2023a).

The brittle-ductile transition in the ice-shell may be characterized by a change in the ice-crystal orientation fabric, which forms a structural interface. Alternatively, a set of tilt-block normal faults fracturing the brittle ice and extending in length up to the ductile layer represents a distributed subsurface scatterer. In this context, RIME can detect the depth to the brittle-ductile transition from echoes caused by changes in the crystal orientation or from diffused scattering caused by the block faults, as already demonstrated by RIME simulations of the grooved bright terrain on Ganymede, when considering fracturing of the brittle ice in the process of normal faulting (Sbalchiero et al. 2019, 2023, Heggy et al. 2017, Fig. 14). The temperature at the location of this mechanical transition can then be estimated and therefore the heat flux can also be better constrained.

Faulting may also result in a vertical offset between stratigraphically and compositionally similar horizons. If the offset is at the scale of the RIME wavelength (33 m), evidence of

faulting can be interpreted from RIME radar profiles as a discontinuity in otherwise continuous horizontal reflectors (Bruzzone et al. 2013). In case faulting causes fracturing in the ice (with fractures being filled by predominantly non-ice material, such as voids), it is also possible to extract information regarding the characteristics of the fractures, such as dip angle, geometry, thickness and composition (Sbalchiero et al. 2019). Other features that RIME can detect are: Europa's double ridges associated with shallow micro-cracks and deep thermal cracks, fractures of Europa's chaos terrains, and fractures associated with Ganymede's dark terrain furrow systems. Finally, RIME may detect near-surface liquid reservoirs in recent chaotic terrains and active ridges on Europa in case such active systems exist along the two tracks performed by JUICE (see Fig. 16). On Ganymede, the probability to detect surface reservoirs are very low, as significant tidal heating, required to melt the ice at shallow depth (< 10 km) is not expected at present (Steinbrügge et al. 2024). However, RIME might detect salt-rich subsurface layers, remnants of ancient near-surface cryovolcanic reservoirs, especially underneath ancient caldera as identified at Ganymede's surface by Galileo (Schilling et al. 2007, Fig. 19).

4.2 Surface Composition as an Insight to Interior Composition and Exchange Processes

On the three moons, a variety of non-ice materials has been identified, which includes hydrated mineral salts, hydrated sulfuric acid, phyllosilicate minerals, organic compounds, sulfur dioxide, and carbon dioxide (see Tosi et al. 2024, this collection for an extended review). Correlation of different compounds with main geological units and surface features will be essential to determine their endogenic origin and to constrain the exchange processes with the subsurface ocean. Global maps obtained from Galileo, ground-based telescopic observations (e.g. Ligier et al. 2016, 2019; King and Fletcher 2022) and JWST observations (Villanueva et al. 2023; Trumbo and Brown 2023; Bockelée-Morvan et al. 2024) already suggested some correlations between the distribution of some identified species and main geological units on Europa and Ganymede, but the spatial resolution remains too low to constrain the emplacement processes. Data collected by JANUS, MAJIS and UVS, especially at Ganymede, will provide a global coverage with unprecedented resolution and very high-resolution data over a set of features of interest. In particular, recent impact crater structures, cryovolcanic edifices, recent landslide structures in crater rims or in any topographic scarp, will be targeted in order to potentially identify materials freshly exposed to the surface. Even on the old and highly cratered surface of Callisto, large mass movements in crater walls (Chuang and Greeley 2000) may expose subsurface materials, providing key information on the composition of the ice shell, especially on the fraction of non-ice materials. Compositional layering observed on recently exposed topography scarps by JANUS and MAJIS combined with potential identification of subsurface reflectors by RIME will provide crucial data on the formation and evolution of the ice shell (Tosi et al. 2023a).

The identification of Na- and Mg-bearing salt species and their correlation with specific features or layers will provide constraints on the oceanic composition and on the efficiency of exchange between the ocean and the surface. Based on the infrared reflectance spectra acquired by the Near-Infrared Mapping Spectrometer on the Galileo mission (e.g., McCord et al. 1999; Carlson et al. 2009; Dalton and Pitman 2012) and more recently from ground-based telescopic observations (Hand and Brown 2013; Ligier et al. 2016, 2019; Trumbo et al. 2019, 2023, King et al. 2022; Tan et al. 2022), JWST observations (Villanueva et al. 2023; Trumbo and Brown 2023; Bockelée-Morvan et al. 2024) and Juno observations (Mura et al. 2020; Tosi et al. 2024), several salt species have been identified. However, the composition of identified salt compounds is still debated and their link with the ocean composition

is unclear. While non-ice materials on Europa and Ganymede have been initially interpreted as dominated by sulfate species (e.g. Zolotov and Kargel 2009; Carlson et al. 2009), more recent ground-based infrared observations (Ligier et al. 2016, Trumbo et al. 2019, 2022) indicate regions with the highest concentration of chlorinated salts in the chaotic terrain regions on Europa, suggesting a subsurface aqueous source dominated by chlorinated species. JWST observations also indicated that the Tara Regio on Europa where enrichment in chlorinated salts was observed is also characterized by a signature of CO_2 ice, suggesting an endogenic origin (Villanueva et al. 2023; Trumbo et al. 2022). Again, in absence of high-resolution spatial data, it is difficult to constrain the geological processes at the origin of these enrichments. Recent observations of Ganymede are also indicative of areas enriched in chlorinated and ammoniated species (Ligier et al. 2016; Tosi et al. 2024). It is, however, still unclear whether this chlorinated signature is representative of the ocean composition or is a consequence of fractional crystallization during the emplacement of upwelling cryomagmatic fluids which rapidly increase $Cl^-/SO_4{}^{2-}$ ratio (Kargel et al. 2000; Ligier et al. 2016; Vu et al. 2020). Inferring this ratio in the salt-rich layers observed at the surface will provide key constraints on the oceanic composition, on the oxidation state of the interior and the efficiency of water-rock interactions during the early evolution of the moon (Zolotov 2012). Identification of salt assemblages, carbon species, and other volatile species in different geological contexts on Ganymede and Europa (and possibly Callisto) with MAJIS and UVS, together with their distribution at both regional and local scales, will provide key constraints on their emplacement and hence on their potential link with the composition of the subsurface reservoirs and the internal ocean. The contribution of Io's material to the surface of Europa, Ganymede and Callisto will also be assessed by evaluating the large-scale variations in sulfuric compounds, which will help distinguish between endogenic and exogenic compounds. Even if Io's material flux is much smaller at Ganymede and Callisto than at Europa, the surface integrated its potential contribution on a much longer timescale, and so it may provide clues on material flux ejected by Io in the past.

4.3 Dust and Vapor Sources and Link with Subsurface Structure and Composition

Icy grains and vapor emitted from the surface by eruption, sublimation or impact processes, can provide crucial information about subsurface activity and composition if the ejected materials are associated with endogenic processes such as cryovolcanism, diapirism, and tectonism. Their variability and strength depend directly on the underlying geophysical source processes and can therefore contribute to the geophysical characterization of the moon's subsurface. In addition, various trace elements such as noble gases and isotopic ratios sampled in the moon exosphere are indicative of early solar system conditions and internal chemical processes. They may shed light on the conditions for the formation of the Galilean moons as well as on how their interior chemically evolved since their formation. In this article, we focus on the geophysical and geochemical implications of dust and vapor emission observed in the near-surface atmosphere. More information on the observation strategy for exosphere characterisation, including plume search at Europa, is provided in the articles dedicated to surface and exosphere sciences by Tosi et al. (2024, this collection) and Masters et al. (2024, this collection).

So far, of the three icy Galilean moons, plumes have been tentatively observed only on Europa. The observations appear to record several discrete, possibly unrelated, incidents of plume activity. Plumes might contain several thousand tons of water, and reach heights of a few hundred (~100-200) kilometers (Roth et al. 2014; Sparks et al. 2016, 2017; Jia et al. 2018; Arnold et al. 2019; Paganini et al. 2020; Huybrighs et al. 2020). First JWST observations did not confirm any plume activity at the time of their acquisition (Villanueva et al.

2023). The source processes responsible for plume activity on Europa remain unclear (e.g., Vorburger and Wurz 2021). As the probability of active plumes on Ganymede is very low and even less favorable on Callisto, no specific plume searches will be performed for these two moons. However, exospheric observations during limb scans by UVS and MAJIS may potentially reveal impact-induced plumes or composition anomalies associated with surface sublimation processes, as recently indicated by JWST observations (Bockelée-Morvan et al. 2024), which can provide indirect constraints on surface/subsurface composition and properties.

As demonstrated by Cassini from the multi-instrument characterization of plume activity on Enceladus (e.g. Hansen et al. 2006, 2017; Porco et al. 2014; Postberg et al. 2009, 2011; Waite et al. 2006, 2017), multiple lines of evidence and synergies between different instruments are needed to learn more about the plumes, their formation mechanisms, and the geophysical properties of their source reservoirs. JUICE, with its extensive instrumentation, is well equipped to study active processes on the Galilean moons, including any plumes that might exist, both remotely and in situ.

4.3.1 Chemical Composition of the Exosphere and Plumes

Several instruments can provide information on the chemical composition of the exosphere, potentially revealing spatial and temporal variations, possibly associated with plume activity. These chemical fingerprints and their variability may help elucidate if the material originates from the subsurface ocean or from a more local reservoir in the icy shell. However, identification of the chemical constituents is not always straightforward, and the data interpretation can be ambiguous. Measurements with different instruments can help to eliminate such ambiguities. On JUICE, several instruments, in particular UVS, the PEP Neutral Gas and Ion Mass (NIM) spectrometer and SWI, are capable of determining the chemical composition of the gas phase of the exosphere and of plumes (if any).

UVS will search for plumes remotely via observations of ultraviolet emissions of O (130.4 nm) and H (121.6 nm) resulting from the dissociative excitation of H_2O by impacting Jovian magnetospheric electrons and will perform additional searches using atmospheric transmission spectra obtained during stellar and solar occultation events, and during Jupiter transits. While it is expected that UV plume transmission spectra will be dominated by the absorption signature of H_2O around 150 - 180 nm, the UVS bandpass also encompasses absorption features of several constituent materials of the Enceladus plumes, which may reasonably be expected to exist within the ocean. Stellar occultation measurements of the plumes at Enceladus by Cassini UVIS (Esposito et al. 2004) have been used to constrain the abundances of minor species including CO, NH_3, C_2H_2, C_2H_4, CH_3OH and O_2 (Hansen et al. 2020), which JUICE UVS will also be capable of probing.

PEP, consisting of six individual sensors, will measure the neutral and charged (positive and negative) environments (including plumes) around the Galilean moons. NIM, PEP's neutral mass spectrometer, is capable of determining the chemical composition of a plume's gas phase in situ if the spacecraft encounters a plume. At a flyby altitude of 400 km, a local H_2O enrichment of up to four orders of magnitude are expected, assuming mass fluxes similar to those derived from Europa plume observations by Rhoden et al. (2015) (Winterhalder and Huybrighs 2022). Assuming a chemical composition of the plume similar to that measured in the Enceladus plume (Waite et al. 2017), further enhancements of NIM measurements for CH_4, NH_3, CO_2, Ar, and various hydrocarbons are also expected (e.g., Magee and Waite 2017), which could provide information on ocean geophysical conditions if the plume is indeed oceanic in nature. For Enceladus, the chemical composition of gases

and solid particles has been used to learn more about Enceladus' interior, for example by constraining the pH of the ocean (Glein et al. 2015) and the possible composition of the core (Glein and Waite 2020). In addition to neutral measurements, the Jovian Electrons and Ions (JEI) and the Jovian Plasma Dynamics and Composition (JDC), two of the four PEP ion sensors, will also observe an increase in signal when the spacecraft actually crosses a plume (Huybrighs et al. 2017), which provides limited information about the chemical abundances of various ions.

SWI will monitor the Galilean moons atmospheres about one hour per day even from large distances. A water plume with a total mass of <1 ton can be easily detected from distances of up to 3 million km. All water isotopic ratios and the ortho-to-para ratio of the main isotopologue can be detected from nearer distances, e.g. during GEO and the GCOs. Furthermore more than 70 molecules (including CHNOPS and gases bearing chemical energy), covered in the tuning ranges of SWI, could be identified, providing potentially insights on the exchange processes with the surface and subsurface in most active regions.

4.3.2 Characteristics and Location of Past and Present Plume Activity

Direct detection of plumes, if they exist, can provide information about the geophysical processes in the source region. Oceanic plumes are expected to be narrower than near-surface plumes and to reach greater heights (see, e.g., Vorburger and Wurz 2021). Plume scale heights provide valuable information about the temperature of the underlying reservoir and/or the release mechanism, while temporal variability also provides information about the geophysical state of the plume source (e.g., Roth et al. 2014). MAJIS and JANUS can detect dust plumes at high phase angles in the visible and near infrared spectral range by observing sunlight scattered by water ice particles (Tosi et al. 2024, this collection). However, due to a larger gravity on the Galilean moons compared to Enceladus, the vertical extension of any dust plume will be significantly reduced (Southworth et al. 2015) making optical detection more challenging than on Enceladus. Several JUICE instruments (PEP-JNA, UVS, RPWI, SWI) will be more sensitive to putative more extended gaseous plumes, providing information on gaseous plume structure and extension, temperature, composition, and speed of the gas molecules within the plumes (see Masters et al. 2024, this collection, and Hartogh et al. 2024, this collection, for more details). Combined information on the structure of the plume from both gas and solid phase could provide key constraints on the eruption processes, similarly to what has been achieved with Cassini at Enceladus (Ingersoll et al. 2016). Possible plume detection from distant observations with JANUS and UVS might also bring additional information on plume location and potential time variability, which again will help determining the eruption mechanisms at their origin.

The chance to detect direct plume activity is low. However, UVS, MAJIS and JANUS could identify regions of anomalous surface reflectance that may indicate a recent plume on Europa and possibly more ancient plume activity on Ganymede. The ultraviolet spectrum of water ice is dominated by a sharp spectral edge near 165 nm, but this feature is not seen in disk-averaged UV reflectance spectra of Europa and Ganymede obtained using the Hubble Space Telescope (Becker et al. 2018; Molyneux et al. 2020), and recent observations of Ganymede by Juno UVS show that it remains muted even in regions known to be icy, such as the bright polar caps (Molyneux et al. 2022). The lack of UV H_2O signature at Europa and Ganymede may be due to radiation-induced defects or impurities within the ice, or to the presence of a thin, UV-absorbing lag deposit that may be formed by sputtering of mixed ices (Teolis et al. 2017). If JUICE UVS detects localized regions with a strong 165 nm H_2O signature, this could be indicative of fresher ice from recent plume activity,

and may be used to identify likely source regions. Similarly, fresh ice is characterized by a strong Fresnel reflectance peak at 3.1 μm, which, in the case of Enceladus, is strongly correlated with the most active regions (Brown et al. 2006; Robidel et al. 2020), and have been used to identify a previously active region in the northern hemisphere (Robidel et al. 2020). Surface morphology as observed by JANUS and different physical properties of the regolith as observed by SWI may also be used to identify both fresh and ancient deposits. RIME can also detect subsurface reflectors, which combined with surface anomalies may reveal the existence of subsurface reservoirs, even when eruption is not active. The distribution of plume deposits (recent and ancient) and their possible correlations with some geological units, subsurface features identified by RIME and/or gravity anomalies by 3GM will provide essential constraints on the geodynamical context at their origin, and will help determine if their composition is representative of the oceanic composition.

5 Tidal Dissipation Constraints from Ephemerides

Since the orbital motion of the Galilean moons depends on the tidal dissipation in the moons and in Jupiter, the accurate determination of their ephemerides is an important complement to the more direct methods of probing the interior of the moons. Current Galilean moon ephemerides are based on Earth-based optical astrometric and photometric data, which go back to 1652 with eclipse timings of Jupiter (Lieske 1986). Most Earth-based data, including photographic and CCD measurements and observations of mutual eclipses and occultations, have an accuracy of the order of several 10 to 100 milli-arcseconds, which corresponds to a position accuracy of up to 300 km at Earth opposition (Lainey et al. 2004a,b, 2009). Thanks to the Gaia catalog (Gaia Collaboration 2016), the most precise astrometric measurements (several mas; 5 km at opposition) of the Galilean moons are now made by stellar occulations (Morgado et al. 2022). The quality and diversity of the tracking data that the JUICE mission will provide (Sect. 5.1), both during the flybys and the Ganymede orbital phase, will facilitate an improvement of several orders of magnitude in the Galilean moon ephemerides (Dirkx et al. 2017; Lari and Milani 2019; Cappuccio et al. 2020; Magnanini et al. 2024; Fayolle et al. 2022, see also Sect. 5.2). In addition, the data acquired by the mission will be an important contributor to the ephemeris of Jupiter itself (Sect. 5.3). Fully exploiting the data to achieve these highly accurate ephemerides will require several challenges to be overcome in terms of data processing, estimation methodology and dynamical modelling techniques. The combination of historical astrometric data with JUICE (and Europa Clipper) data is discussed by Fayolle et al. (2023a). Here, we focus on the contribution of the JUICE data types

5.1 JUICE Data

The main observables that will be used in the determination of moon ephemerides are two-way range and range-rate (Doppler) 3GM measurements between the spacecraft and the ground station antennas (Iess et al. 2024, this collection). By detecting the downlink radio signal by a network of radio astronomical telescopes (Duev et al. 2012), PRIDE will provide supplementary tracking data including VLBI observables of the lateral position (right ascension and declination) of the JUICE spacecraft and its multi-static range-rate (Doppler) estimates, recentered to the geocenter. See Dirkx et al. (2017) and Fayolle et al. (2023a,b) for a preliminary analysis of the contribution of PRIDE to Jovian system ephemerides, and Gurvits et al. (2023, this collection) for an overview of the PRIDE experiment.

The process of determining the spacecraft and moon dynamics in a flyby tour is typically performed in a decoupled process, with the spacecraft orbit being estimated on a per-flyby (arc) basis, and a correction to the moon state estimated during each arc (Antreasian et al. 2008). This moon state correction (or normal point) can then be used in a second step to determine the moon ephemeris. The exceptional tracking data quality and the unique mission profile of JUICE with a Ganymede orbital phase make an alternative approach appealing, which could, in principle, allow superior results to be obtained, both in the quality of the ephemerides and in the fidelity of the solution covariance. In this approach (e.g. Jacobson 2014, 2022), the dynamics of the spacecraft and moon(s) is estimated concurrently, with a multi-arc approach for the spacecraft and a single arc approach for the moons (Fayolle et al. 2022). A drawback is that the more stringent requirements on the dynamical modelling accuracy of the spacecraft must indirectly also be imposed on the moon dynamical model (Durante et al. 2019; Zannoni et al. 2020). In particular the coupling between orbital, rotational, and tidal dynamics of a moon will require additional developments to allow the formal error values presented in Sect. 5.2 to be realized (Lainey et al. 2004a; Dirkx et al. 2016). Ideally, the long-term data set of Earth-based astrometric and photometric data would be concurrently analyzed with the JUICE-based radiometric range, Doppler and angular position data, as well as JUICE-based astrometry. Any supplementary data sets, such as altimetric measurements by GALA (e.g. Villamil et al. 2021), would also need to be concurrently analyzed to maximally exploit the coupling. Although inclusion of GALA crossover measurements improves the spacecraft position only marginally (Villamil et al. 2021) because of the high accuracy of the 3GM Doppler measurements, it can be useful for orbit determination when the normal 8 h/day Doppler data (see Sect. 6.2.2) are not available, due to for example occultations.

Because the orbital dynamics of Io, Europa, or Ganymede is strongly coupled through the Laplace resonance, any uncertainty in their dynamics strongly influences the uncertainty in the dynamics of the other two moons. Although JUICE will produce a highly accurate data set for Ganymede during the orbit phase, it will only have two Europa flybys, very closely spaced in time, and there will be no direct tracking data of Io. As a consequence of this strong data imbalance, the orbit determination of the inner three Galilean moons is an ill-posed problem (Fayolle et al. 2022). Europa Clipper radio science data during the multiple flybys will be important in stabilizing the solution (Mazarico et al. 2023), but other JUICE data will also provide essential contributions. Io's orbital dynamics will be constrained by optical astrometric data of Io by both JUICE (JANUS) and Europa Clipper, similar to the ISS data of Saturnian moons acquired by Cassini, which has been invaluable for Saturnian system ephemerides (Lainey et al. 2017, 2020). Space probe imagery has many advantages over ground-based data. First of all, the moons are much closer to the observer, which allows for very precise measurement. Second, the moons are often resolved, which allows for a very accurate estimation of the astrometric position of the center of mass.

The data will further be complemented by UVS observations of stellar occultations by Io, and by Earth-based data of Io, including stellar occultations (Morgado et al. 2022), mutual events (Saquet et al. 2018), mutual approximations (apparent close encounters of two moons in the plane of the sky, Fayolle et al. 2021), and radar ranging (Brozović et al. 2020) before, during and after the JUICE mission. The UVS data is expected to provide a unique contribution to the moon system ephemerides because of the very precise UVS timing with a resolution of down to 1 ms, translating to a raw limb positioning measurement of the Galilean moons on the order of meters. A few hundred occultations of the Galilean moons are planned (e.g., two or more per flyby encounter phase), providing important constraints to shape models and ephemerides of Galilean moons (Abrahams et al. 2021). These observations are, however, optimized for exosphere and plume investigations with a 100 ms

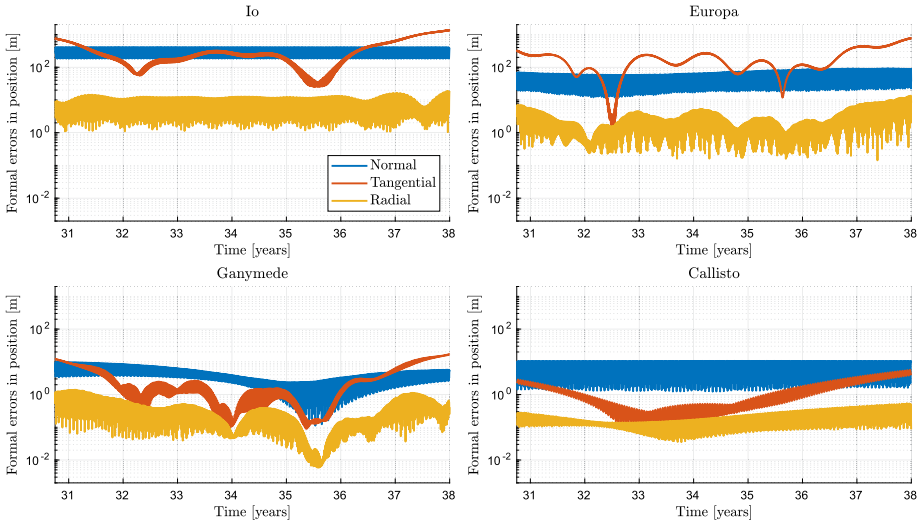

Fig. 15 Propagated formal errors in position for the four Galilean moons, derived from simulated 3GM measurements using the coupled model by Fayolle et al. (2022). The position components are expressed in the RTN (radial, tangential, normal) frame

time resolution. Either astrometric-focused occultation events can be planned in addition to the baseline set measurements, or more data volume could be allocated, to acquire 1 ms pixel-list atmospheric plus astrometric datasets combined. Events with low angular velocity between the star and the moon (<1 km/s) should be prioritized for obtaining highest precision, assuming that the star's UV signal provides sufficient signal quality (Velez et al. 2022). Incorporating the UVS stellar occultation into ephemerides estimation will require a translation from limb to center of figure which, considering the exceptional accuracy of the data, may present new challenges.

5.2 Moon Ephemerides

Figure 15 displays the formal uncertainties of the Galilean moon ephemerides obtained using a covariance analysis in a coupled approach for simulated 3GM range and range-rate measurements. Estimated parameters in addition to moon states include the arc-wise initial states of the JUICE spacecraft, gravitational parameters and gravity field coefficients of the Galilean moons, tidal dissipation parameters k_2/Q of the moons and of Jupiter (at each moon's frequency), as well as range observation biases and accelerometer calibrator factors. A conservative error budget was applied, assuming a noise level of 15 μm/s (60 s integration time) and 20 cm for Doppler and range observations, respectively (e.g. Magnanini 2021; Fayolle et al. 2022).

During the flybys and the orbital phase, the formal errors will be significantly reduced (Fig. 15). The two flybys of Europa in mid-2032 appear very distinctly for both Io and Europa. The lower uncertainty in Ganymede's position during the orbital phase in 2035 also causes the formal errors in Io's and Europa's positions to drop down in this period due to the Laplace resonance. The imbalance of the JUICE-only data set (Sect. 5.1) leads to different orders of magnitude of the uncertainties of the inner three moons and also explains the rapid rise of the propagated formal errors in the tangential direction once no observations

constrain the ephemerides anymore. Although this simulated covariance analysis predicts an unprecedented level of accuracy, down to a few centimeters for Ganymede's radial position during the orbital phase, dynamical modelling issues may yield larger errors and could even impede obtaining a global solution for the moons (Durante et al. 2019; Fayolle et al. 2022). Complementary data sets will not only be useful in stabilizing the solution, but may also be useful for identifying sources of mismodelling, and for driving the development of estimation models so as to be able to achieve a coupled solution.

5.3 Planetary Ephemerides

The planetary ephemeris for the Jupiter barycenter is at present mostly constrained by the radio tracking data obtained with the Juno mission and has an accuracy of about 10 meters, including corrections from the moon positions (Di Ruscio et al. 2020). JUICE is expected to improve that accuracy to the meter level but it will be important to take care of the consistency between the moon and the planetary ephemerides, for example by adopting an iterative approach as has been tested with Cassini (Di Ruscio et al. 2020). The combination of JUICE with Juno and Europa Clipper data, covering more than 15 years of tracking, will allow a better model of the Jupiter barycenter orbit to be obtained.

The Saturn barycenter orbit will also be more constrained thanks to the combination of these Jovian mission data and the Cassini radio tracking data as the Jupiter and Saturn orbits are strongly related by the resonance mechanisms. The global improvement of the orbits of Saturn and Jupiter will improve our knowledge of the distribution of mass in the outer solar system and may even inform on the existence of the hypothetical planet 9 (Fienga et al. 2020). Tests of alternative theories of General Relativity especially in the furthest regions of the solar system such as dark sector theories or dark matter detection will also benefit from it.

5.4 Parameter Estimation and Implications for Evolution

Work on ephemerides is synergistic with the geophysical instruments of JUICE since the ephemerides reconstruction is performed through a joint estimation of a set of parameters that characterize the dynamical model. These parameters include the masses of the planet and its moons, their static gravity field coefficients, rotational model parameters, and parameters (Love numbers) characterizing the time-variability of the gravity due to tidal interactions.

JUICE will not be able to improve the current knowledge of the gravity field of Jupiter, which is based on Juno data (Dirkx et al. 2016; Durante et al. 2020, 2022). However, the level of accuracy of the JUICE measurements will allow the tidal dissipation in both Jupiter and its moons to be characterized in greater detail, with important consequences on the study of the past evolution of the Laplace resonance and the habitability of the Galilean moons. It is the Laplace resonance that excites the eccentricity of the orbits of the moons, which in turn is responsible for the significant tidal heating that causes Io's volcanic activity and helps maintaining global oceans inside Europa and Ganymede. The origin and the evolution of the Laplace resonance is still an active subject of study. Depending on how and when the moons entered the resonance, it may have strong implications on the differentiation processes, the formation and evolution of internal oceans and their habitability (see Sect. 3.1).

Regarding the future of the Laplace resonance, Musotto et al. (2002) and Celletti et al. (2019) showed its stability for at least 10^5 years. Lari et al. (2020) analyzed the future evolution of the resonance over a timescale of 10^9 years and predicted that, after an initial

inward migration of Io, the moons will drift outward, eventually capturing also Callisto into resonance. Long-term predictions make, however, simplifying assumptions about the tidal interaction and are often based on the classical tidal theory that assumes a Jupiter tidal factor Q constant in time and with respect to the forcing frequency. Recent theoretical developments and measurements suggest that the tidal dissipation of Saturn is higher than previously assumed, and that it is not constant between the different moons, as predicted by the resonance locking tidal theory (Lainey et al. 2012; Fuller et al. 2016; Lainey et al. 2017, 2020). According to this theory, the moons' dynamics could enter in resonance with internal modes of Jupiter, such as inertial waves, increasing the dissipation. In this condition, the tidal migration is ultimately driven by the time evolution of the planet internal structure. The JUICE mission will improve the knowledge of the Jupiter tidal parameters, potentially detecting a frequency-dependent dissipation, ultimately better constraining the long-time evolution of the Laplace resonance.

The orbital effects of the dissipation in the moons interior and in Jupiter are strongly correlated (Lainey et al. 2009). The presence of the Ganymede orbital phase, during which JUICE will directly sample the gravity of Ganymede to high accuracy, will allow the dissipation inside Ganymede and the dissipation inside Jupiter at Ganymede's forcing frequency to be fully decorrelated. This is achieved by virtue of the fact that JUICE's dynamics with respect to Ganymede during the orbit phase is sensitive to Ganymede's k_2/Q only, while the ephemeris of Ganymede is sensitive to a combination of the two. A similar, but weaker, decorrelation may well be possible for the case of Europa, but only when combining the JUICE data with Europa Clipper data (Magnanini et al. 2024). For Callisto, it is unlikely that Callisto's k_2/Q will be directly determined from radio science during flybys. Moreover, the influence of Callisto's dissipation on its own orbital evolution is likely to be negligible due to the larger distance from Jupiter. Any measurement of orbital migration of Callisto could be attributed to strong dissipation inside Jupiter, due to for example resonance locking (Fuller et al. 2016). In addition, the JUICE observations of the tidal migration rates of Ganymede and Callisto could lend support to or disprove an hypothesis about the origin of Jupiter's obliquity of 3°.12 (Dbouk and Wisdom 2023). This model predicts either an upper limit on Ganymede's migration of 12.8 cm/yr or an upper limit on Callisto's migration of 15.7 cm/yr, rates that JUICE would be able to detect (see Fig. 15).

6 Operational Aspects and Observation Synergies

6.1 Mission Profile

Acquisition of scientific data and the transmission of it to Earth depends not only on the instruments but also on the characteristics of the spacecraft, on its trajectory, and on the mission design. The JUICE spacecraft is a three-axis stabilized platform powered by 85 m^2 solar arrays generating about 790 W at end-of-life, which puts constraints in terms of maximal power consumption during flybys and dedicated time for battery recovery, potentially impacting data acquisition. It is equipped with a fixed high-gain antenna and a steerable medium-gain antenna both operating in X and Ka band. The ESTRACK radio station allocated to the mission as baseline is Malargue, equipped with a Ka-uplink system, including a 500 W amplifier, necessary for the measurements of the moons' gravitational fields. Science data transmission occurs typically once per day, with the High Gain Antenna pointed toward Earth for about 8 hours. A detailed description of the JUICE spacecraft is provided in Erd et al. (2024, this collection).

Table 1 Main operational phases of the JUICE mission based on the trajectory scenario CREMA 5.1_150LB_23 (https://www.cosmos.esa.int/web/juice/crema-5.1_150lb_23_1)

Phase Name	Start date	End date
Jupiter Tour phase		
1- Approach and first ellipse	2031-01-19	2032-02-08
2- Energy reduction	2032-02-08	2032-06-25
3- Europa flybys	2032-06-25	2032-07-24
4- High-latitude	2032-07-24	2033-08-18
5- Low energy	2033-08-18	2034-12-19
Ganymede orbital phase		
Elliptical Orbit (GEOa)	2034-12-19	2035-01-17
Circular Orbit at 5100 km (GCO5000)	2035-01-17	2035-04-16
Elliptical Orbit (GEOb)	2035-04-16	2035-05-13
Transient Circular Orbit (TGCO)	2035-05-13	2035-05-21
Circular Orbit at 490 km (GCO500)	2035-05-21	2035-09-29

The trajectory of the nominal mission can be decomposed into two main phases. The spacecraft will first perform data acquisition in the Jupiter system, called "Jupiter tour phase", from Jupiter Orbit Insertion (July 2031) until December 2034, when the spacecraft will be inserted in orbit around Ganymede, thus becoming the first ever orbiter of a moon of another planet than Earth. During the Jupiter tour phase, geophysical investigations of the three moons, Europa, Ganymede and Callisto will be performed only during close flybys (Table 3). The Jupiter tour phase begins with a reduction of the orbit eccentricity around Jupiter, and includes the second to fifth flybys of Ganymede. The two Europa flybys of the mission follow in July 2032. Then a series of Callisto flybys is used as a 'ladder' to increase the orbit's inclination with respect to Jupiter's equatorial plane, before going back to low inclinations and preparing the insertion into Ganymede orbit in late 2034. The Ganymede orbital phase lasts until the end of the nominal mission in September 2035. A detailed description of the mission design and trajectory are given in Witasse et al. (2024, this collection) and Boutonnet et al. (2024, this collection).

The Ganymede orbital phase is divided in four sub-phases defined by their variations of pericenter and apocenter altitudes: a first highly eccentric phase (with closest approach of about 200 km, GEOa) is followed after a few weeks by a three months long circular phase at 5100 km GCO5000), then another highly eccentric phase with about 500 km as the lowest altitude (GEOb) is flown for a few weeks before entering a circular phase at 490 km altitude (GCO500) for the last four months of the mission. Most of the geophysical investigations of Ganymede will be performed during the GCO500 phase, but a few opportunity will also be possible during GEOa and GEOb. Geophysical investigations will also strongly benefit from an additional circular mission phase with an altitude at 200 km, recently added to the mission scenario (Witasse et al. 2023, this collection, Boutonnet et al. 2024, this collection). It will improve the resolution of the gravity field and temporal and spatial coverage for altimetry, and will also lead to a better characterization of the intrinsic magnetic field and the induced electromagnetic field. A mission extension by several months will moreover permit to monitor tidal deformation when the eccentricity reaches maximal values. A detailed study of this additional mission phase still needs to be performed.

Table 2 Main science operations relevant for the geophysical investigations of JUICE during the different mission phases. Instruments between brackets provide supporting measurements. The main mission phases to achieve the objectives for Ganymede are indicated in boldface

Measurement objectives	Instruments	Moons	Mission phases	Operation requirements
Tidal deformations (Love numbers)	3GM (HAA), GALA (3GM)	Callisto, Ganymede	Flybys, GEOa, GEOb, **GCO500, GCO200**	Acquisition at different true anomalies
Rotation of the ice shell and the whole interior	3GM, GALA, JANUS	Ganymede	GCO500, GCO200	JANUS & GALA: Repeated control point observations at the surface
Gravity field	3GM (HAA)	Ganymede, Callisto	Flybys, GEOa, GEOb, **GCO500, GCO200**	Ground station availability; steerable Medium Gain Antenna during flybys and when GALA is operating; High Gain Antenna during downlink windows
Electromagnetic induction	J-MAG, RPWI (PEP, UVS, MAJIS)	Europa, Callisto, Ganymede	Flybys, GCO5000, GEOa, GEOb, **GCO500, GCO200**	near-continuous data acquisition
Magnetic field from the active metallic core	J-MAG (RPWI, PEP)	Ganymede	Flybys, GCO5000, GEOa, GEOb, **GCO500 GCO200**	near-continuous data acquisition
Surface topography: global and regional mapping	GALA (3GM), JANUS	Europa, Callisto, Ganymede	Flybys, GCO5000, GEOa, GEOb, **GCO500, GCO200**	GALA: data acquired for altitude below $\sim$ 3000 km, nadir pointing; JANUS: Acquisition of at least two images from the same area at two different viewing angles ($> 15^o$), off-nadir pointing required.
Subsurface sounding	RIME, RPWI (JANUS, GALA)	Ganymede, Callisto, Europa	Flybys, GEOa, GEOb, **GCO500, GCO200**	Below 1000 km, shielding from Jupiter's DAM required, except for passive radar mode
Surface and plume activity	MAJIS, JANUS, UVS, SWI, PEP, RIME, RPWI	Ganymede, Europa	Flybys, GCO5000, GEOa, GEOb, GCO500, GCO200	High-phase angle viewing for MAJIS and JANUS for plume detection; Distant monitoring with UVS
Moon ephemerides	3GM, PRIDE, UVS, JANUS	Europa, Ganymede, Callisto	Flybys, GCO5000, GEOa, GEOb, GCO500, GCO200	Radio tracking of JUICE via VLBI, stellar occultations and mutual event astrometry

6.2 Geophysical Investigations and Requirements

The measurements (described in Sects. 2 to 5) required to achieve synergistic campaigns of observations for geophysical investigations are listed in Table 2. Those measurements and their operational requirements are a main driver of the science operations during the flybys at closest approach ($< 2000 - 3000$ km), at the lowest altitude of the GEOa and GEOb phase,

and during the GCO500 phase. We describe below the main operational characteristics, first for the Jupiter tour phase and then for the Ganymede orbital phase. Specific synergies with remote sensing instruments for regions of interest are discussed in Sect. 6.2.3, and a general assessment of the operational challenges is given in Sect. 6.2.4.

6.2.1 Geophysical Investigation During the Jupiter Tour Phase

During the Jupiter tour, detailed geophysical investigations of the icy moons are performed during close moon flybys ($<$ 1600 km for Europa, $<$ 1400 km for Ganymede, $<$ 1100 km for Callisto; distances determined by the maximum altitude for which GALA can acquire stable range measurements, and which differs between the moons because of their different albedo, Fig. 16). 21 Callisto flybys, 12 Ganymede flybys and 2 Europa flybys are foreseen in the baseline trajectory. Among these different flybys, only 13 Callisto flybys, 4 Ganymede flybys and the 2 Europa flybys satisfy the altitude constraints for geophysical measurements (indicated in green in Table 3), with lowest altitudes of 200 km for Callisto and 400 km for Ganymede and Europa. The bulk of science operations for geophysics is typically performed a few tens of minutes before and after the times of closest approach of the spacecraft to the moon. However, even more distant parts of the flyby trajectories are important to provide essential support for geophysical data analysis and interpretation. For example, the DTM support from JANUS, essential for the interpretation of RIME data, as well as limb profiles complementary to GALA data for global shape determination will be partly acquired at distance greater than 1000 km.

Stereo DTM support requires at least two JANUS acquisitions with different viewing angles and at relatively close altitudes ($<$ 5000 km), which will be challenging to obtain as illustrated in Fig. 16. For Europa flybys, support from Europa Clipper observations will allow a more complete interpretation of the acquired radargram. For Ganymede, the interpretation of radar data acquired during these flybys will be possible once GCO500 data will be available. For Callisto, the situation is more problematic, as most of the flybys with a favorable configuration for geophysics occur on the nightside in the current mission scenario. Surface images in the corresponding areas will be acquired only with a moderate-to-low resolution ($>$ 1 km) (Tosi et al. 2024, this collection) making the clutter simulation not sufficiently accurate to unambiguously interpret the radargrams.

During flybys, a number of operational constraints and flight rules must be respected. Twelve hours after closest-approach, a wheel-off loading must take place to remove the angular momentum accumulated in the spacecraft reactions wheel. To ensure quiet measurements conditions, wheel off-loading will be avoided during the time period -12 h/$+6$ h around the closest approach time. The spacecraft attitude is negotiated for each flyby between the different instruments, and may include complex pointing operations of the spacecraft $+$Z axis (aligned with the boresight of the optical instruments) to be able to perform surface mosaic and limb observations of the moon. From approximately -1 h to $+1$ h around closest approach (the exact timing being refined based on the science planning, which takes notably into account the sub-spacecraft illumination conditions), the spacecraft is oriented in 'push-broom' mode (the solar panels aligned with the direction of motion), and the solar panel motion is stopped to reduce micro-vibration perturbations.

During the Jupiter Tour phase, the science planning relies on an overall segmentation of the trajectory, in which the different science objectives define the measurement priorities (and hence, the allocation of spacecraft resources). Resources permitting, typical operations for geophysical investigations unfold as follows:

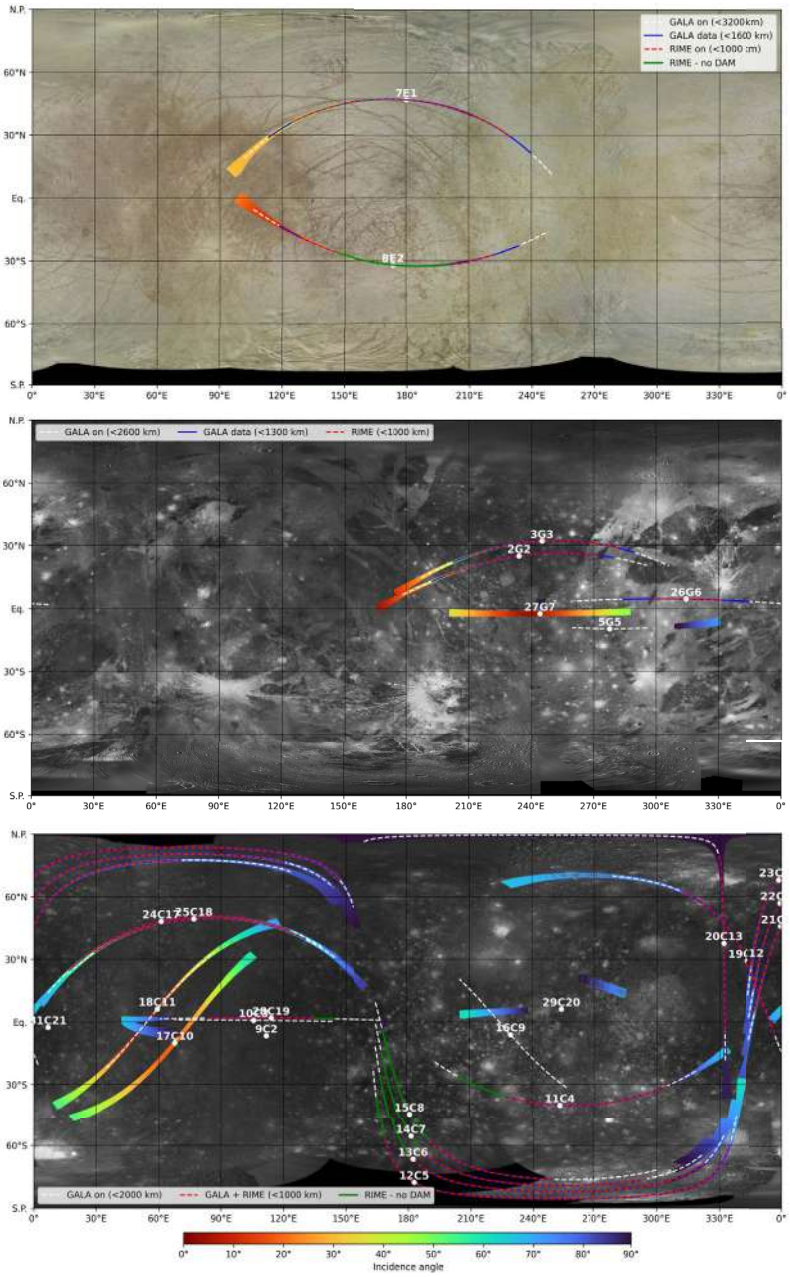

Fig. 16 JUICE flybys at Europa, Ganymede and Callisto indicating when GALA (dashed white (on), solid blue (data acquisition)) and RIME (green line and dashed red line) will operate. The red (green) arc corresponds to the period where RIME will (not) be perturbed by Jupiter's radio emission (DAM) as computed with the ExPRES tool (Louis et al. 2019; Cecconi et al. 2021). The colored regions represent the Field of View of JANUS below 5000 km for incidence angle lower than 90^o (dayside), they are limited to the closest approach phase when a pure nadir pointing is imposed. The white dot indicated the position of the closest approach (see Table 3). The presented flyby configuration is based on the trajectory scenario CREMA 5.1_150LB_23 (https://www.cosmos.esa.int/web/juice/crema-5.1_150lb_23_1)

Table 3 Flyby characteristics based on the trajectory scenario CREMA 5.1_150LB_23 (https://www.cosmos.esa.int/web/juice/crema-5.1_150lb_23_1)

ID	Time UTC	Altitude (km)	LON(°)	LAT(°)	Moon true anomaly (°)	Flyby characteristics
1G1	21-JUL-2031 07:14:23	400	239	2	109	No data acquisition
2G2	13-FEB-2032 23:04:50	400	234	25	116	partially dayside, radio source partially occulted
3G3	11-APR-2032 04:14:26	508	245	32	128	partially dayside, radio source almost not occulted
4G4	09-MAY-2032 18:34:32	5633	254	12	127	No geophysics
5G5	02-JUN-2032 21:30:34	2365	278	-10	277	Nightside, no radar
6C1	21-JUN-2032 00:37:42	3559	249	14	288	No geophysics
7E1	02-JUL-2032 16:22:25	400	180	47	82	partially dayside, radio source not occulted
8E2	16-JUL-2032 22:17:57	399	174	-32	97	partially dayside, radio source mostly occulted
9C2	29-JUL-2032 01:49:28	4437	112	-6	28	nightside, no geophysics
10C3	14-AUG-2032 18:13:55	1132	106	1	30	nightside, no radar
11C4	10-SEP-2032 19:24:45	200	253	-40	255	mostly nightside, radio sourcepartially occulted
12C5	27-SEP-2032 11:59:26	200	183	-78	253	nightside, high latitude, radio source partially occulted
13C6	14-OCT-2032 04:28:19	200	182	-67	254	nightside, high latitude, radio source partially occulted
14C7	30-OCT-2032 20:53:06	200	181	-56	252	nightside, high latitude, radio source partially occulted
15C8	16-NOV-2032 13:16:08	200	181	-44	254	nightside, high latitude radio source partially occulted
16C9	03-DEC-2032 05:36:32	1219	230	-6	252	nightside, no radar
17C10	24-FEB-2033 16:08:00	2071	68	-10	251	dayside, no geophysics
18C11	13-MAR-2033 08:31:08	1162	59	6	252	dayside, no radar
19C12	10-MAY-2033 16:08:57	313	343	29	67	partially dayside, radio source not occulted
20C13	04-JUN-2033 18:37:57	200	332	38	254	partially dayside, radio source not occulted
21C14	21-JUN-2033 11:01:19	200	360	45	248	partially dayside, radio source not occulted
22C15	08-JUL-2033 03:23:28	200	359	57	254	partially dayside, radio source not occulted
23C16	24-JUL-2033 19:45:47	200	359	68	252	mostly nighside, radio source not occulted
24C17	10-AUG-2033 12:13:44	200	61	48	249	dayside, radio source not occulted
25C18	01-NOV-2033 22:59:43	316	77	49	254	dayside, radio source not occulted
26G6	27-NOV-2033 06:22:15	867	314	4	204	nightside, radio source not occulted
27G7	14-JAN-2034 18:38:52	3172	244	-3	107	dayside, no geophysics
28C19	15-FEB-2034 00:07:43	643	114	2	356	nightside, radio source partially occulted
29C20	01-MAY-2034 22:25:05	3074	254	6	193	partially dayside, no geophysics
30G8	06-JUN-2034 06:53:16	3351	190	14	54	no geophysics
31C21	24-JUN-2034 05:14:44	6623	7	-2	265	nightside, no geophysics
32G9	12-JUL-2034 07:50:48	107541	241	-3	65	no geophysics
33G10	07-SEP-2034 18:03:38	63702	226	-8	85	no geophysics
34G11	29-SEP-2034 06:48:32	66237	232	-10	97	no geophysics
35G12	18-NOV-2034 21:58:51	31797	189	-26	129	no geophysics

- Main KaT transponder observations to acquire the moon's gravity data around CA use the MGA tracking Earth with a Ka/Ka link (additional X/X and X/Ka link may be required whenever the Sun-Earth-Spacecraft angle is $< 60^o$ to cancel noise due to the solar wind plasma).
- RIME measurements take place when the spacecraft is below 1000 km altitude, and preferentially when Jupiter radio emissions are not visible from the spacecraft (corresponding to ground track segments indicated in green on Fig. 16).
- GALA's scientific operations are scheduled below 1600 km altitude for Europa, below 1400 km for Ganymede and 1100 km for Callisto
- During the operation of RIME and GALA, the spacecraft is in Nadir with push-broom mode (as required by the remote sensing observations of the moon's surface), and the solar panels are fixed to avoid mechanical disturbances.
- Two additional KaT tracking blocks are added before and after the main tracking to refine the knowledge on the spacecraft position wrt moon. The three tracking blocks should be scheduled such that they are not being interrupted by any wheel off loading for trajectory reconstruction.
- Exospheric measurements are performed by UVS and MAJIS on the ingress and egress branch of the flyby during stellar occultations by the moon's limb and limb scans.
- The High Accuracy Accelerometer (HAA) is operated continuously to isolate all non-gravitational accelerations, such as propellant sloshing and spacecraft moving mechanisms (Iess et al. 2024, this collection).
- PEP, RWPI and MAG are operated continuously throughout the flyby to acquire the moon's induced (and intrinsic for Ganymede) magnetic fields and constrain the perturbations from the ambient plasma.

6.2.2 Geophysical Investigation During the Ganymede Orbital Phase

Geophysical operations will be performed during the entire Ganymede orbital phase, but the best geophysical data, apart from the data during pericenter approaches in the GEO phases (Fig. 17), will be obtained at low altitudes during the GCO500 phase and the additional GCO200 phase. Low altitude observations can also be performed during the two elliptical orbit phases, the first just after Ganymede orbit insertion and before GCO5000 and the second when transiting from GCO5000 to GCO500. JUICE will then reach altitudes lower than 1300 km and 1000 km, which will also allow scientific operations of GALA and RIME (Fig. 17). These two phases will provide very good opportunities to acquire altimetric and radar data, and also the possibility to observe the surface over several tracks with resolution much better than during GCO5000 and better illumination conditions than during GCO500.

Most of the geophysical acquisition will take place during GCO500 (Fig. 18) during which a continuous geophysical campaign will allow the accurate monitoring of tidal deformation, rotation and electromagnetic signals as well as obtaining radar acquisition and associated DTMs over regions of interest. Operations for geophysical investigation during this phase will be divided in 2 main windows for each 24-hour period.

1. A 16 hours window during which the spacecraft's optical instruments will be mostly pointing to Ganymede in a nadir configuration (Fig. 18a). During that time, the GALA laser operates continuously and will perform topography, surface roughness and albedo measurements as well as measurements of tidal deformation, and rotation state of the moon. These measurements can be complemented with 3GM measurements using the steerable MGA for dedicated targets. During these 16 h operation windows, dedicated campaigns, possibly requiring specific off-nadir pointing or specific instrument operation modes, could be scheduled for:

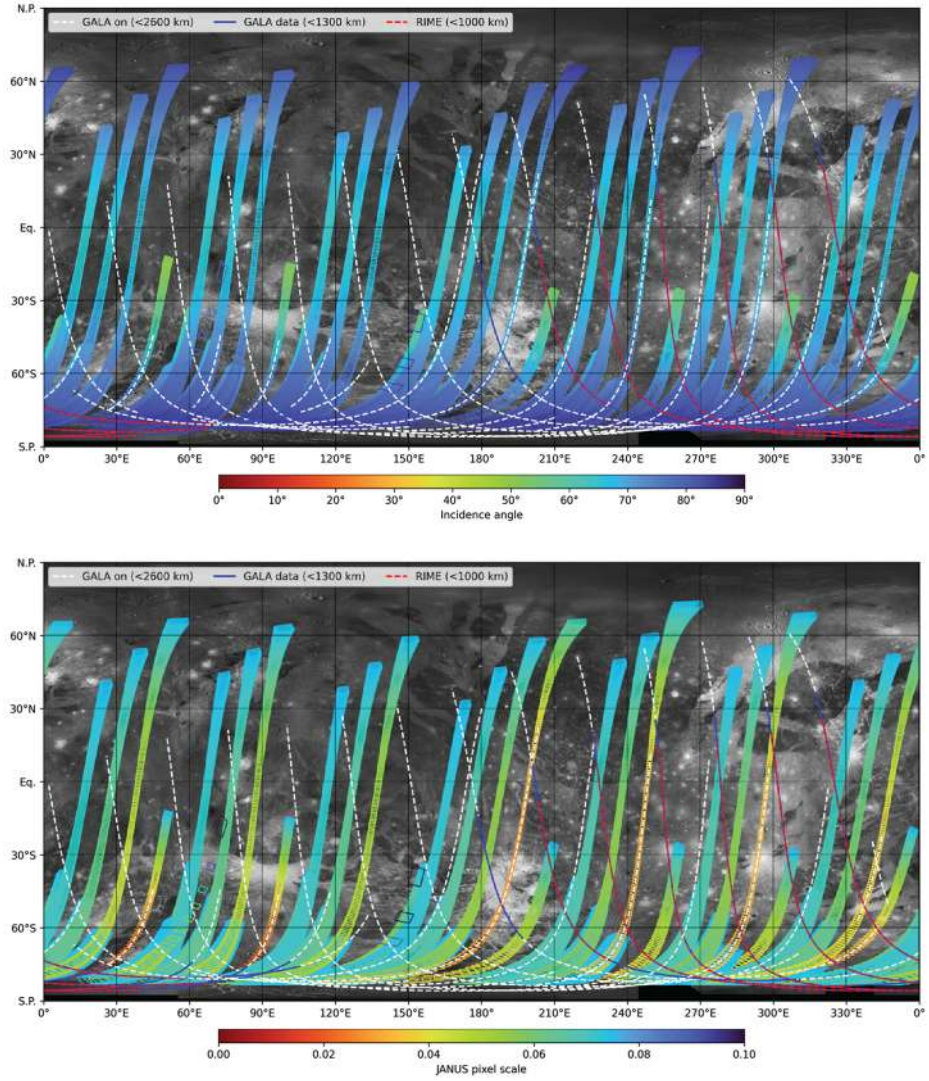

Fig. 17 Scientific data acquisition during GEOa and GEOb by GALA (< 1300 km, blue line), RIME (< 1000 km, red dashed line) and JANUS (< 5000 km). The altitude at which GALA will be activated (< 2600 km) is also indicated (white dashed line). The field of view (FoV) of JANUS is represented when the altitude is below 5000 km and on the dayside (incidence < 90°). This GEO configuration is based on the trajectory scenario CREMA 5.1_150LB_23 (https://www.cosmos.esa.int/web/juice/crema-5.1_150lb_23_1)

- Auroral oval observations by UVS and RPWI, in particular to measure the amplitude of the oscillation in the location of the auroral ovals, providing constraints on the subsurface ocean.
- Regions of interest characterization: most of the instruments, including RIME, will be operating to perform synergistic observations whenever JUICE is flying over an illuminated identified region of interest (Stephan et al. 2021). When JUICE will fly over the anti-Jovian region and is protected from Jovian radio emission, RIME will also

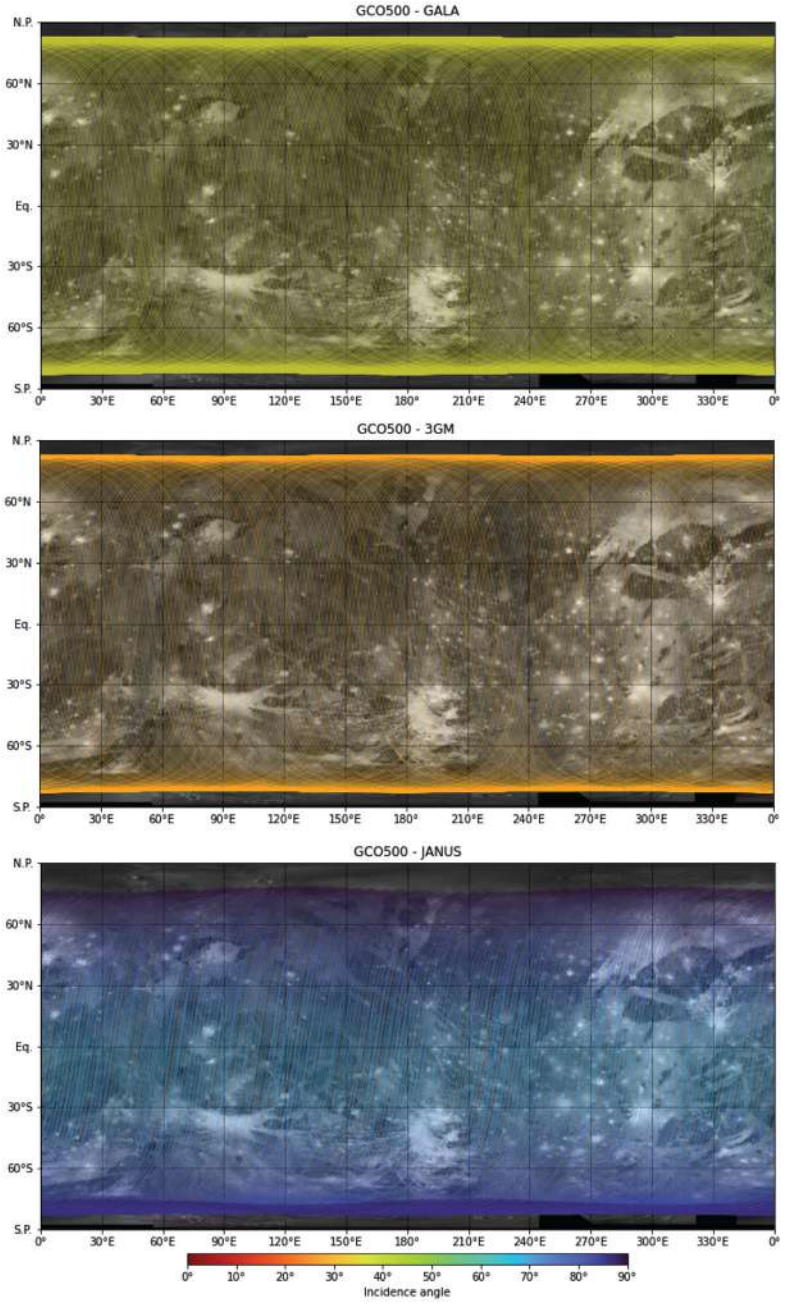

Fig. 18 Coverage during GCO500 for GALA and RIME when the spacecraft is pointing to Ganymede surface (top), for 3GM when the HGA is pointing to the Earth (middle) and for JANUS when the spacecraft is pointing to the surface on the dayside (bottom). GALA will acquire data during up to 16 h per day, 3GM with the High Gain Antenna during the remaining 8 h per day, RIME preferentially over region protected from Jupiter's radio emission, and JANUS during specific times within the 16 h period when the spacecraft flies over the dayside

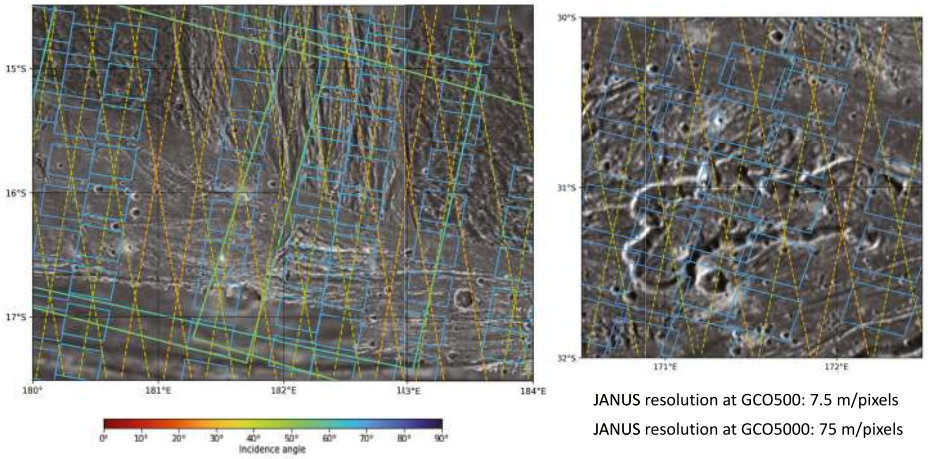

Fig. 19 Zoom on two selected features of interest: (right) the intersection between Erech Sulcus and the northern part of Sippar Sulcus (see also Fig. 13) and a caldera structure observed in Sippar Sulcus. The dashed yellow line corresponds to the ground track when GALA/RIME are operating and the orange one when 3GM-HGA is operating. The square, color coded with the incidence angle, corresponds to the Field of View of JANUS (large - GCO5000; small - GCO500)

operate to characterize the structure, composition and temperature of the subsurface. A digital elevation model of these areas, derived from the JANUS and GALA data, will support the interpretation of the data. This will require off-nadir pointing for JANUS in at least some regions of interests, along a selected set of orbit arcs.

- Additional anti-Jovian opportunities for RIME observations, and RIME and RPWI operations in passive mode when receiving Jupiter's radio sources.

2. An Earth link (HGA pointing to Earth) window of 8 hours: During this time the High Gain Antenna is pointing to Earth for data downlink and radio science range and range rate measurement with 3GM using the Ka band transponder and the High Accuracy Accelerometer. Opportunities for VLBI experiments with PRIDE using the HGA radio link can also be scheduled during these windows.

In-situ measurements by J-MAG and RPWI will be as continuous as possible to resolve separate components of the field (stationary dynamo field and time-varying field components, see Masters et al. 2024, this collection). The HAA is also continuously on to ensure a precise determination of the gravity field.

6.2.3 Typical Geophysical Investigations and Synergies with Remote-Sensing over Selected Regions of Interest

Figure 19 illustrates typical data acquisition over two selected regions of interest. At GCO5000, a single observation by JANUS, with a resolution of 77 m/pixel, will cover almost entirely the area showing the intersection between Erech Sulcus and the northern part of Sippar Sulcus, already observed by Galileo at lower resolution (143 m/pixel, Fig. 13). In principle, there will be no challenge to acquire a DTM covering entirely these regions of interest, but conflicts with other observational requirements may limit this capability. Moreover, the resolution of these DTMs, which can be from 3 to 10 times the image ground sample distance, depending on observations geometry and image quality (e.g. Kirk et al.

2016; Zubarev et al. 2015), may not be sufficient to correctly account for the clutter effect needed to interpret the radargrams (Gerekos et al. 2018; Sbalchiero et al. 2023; Tosi et al. 2023a). Mitigation strategies are being studied, based for example on the use of photoclinometry to derive the required DTMs. High-resolution images acquired during the GCO500 ($\sim$ 7.5 m/pixel) will provide much better DTMs that are sufficient to simulate clutter effects. But the coverage of such high-resolution DTMs will be much more limited as they require specific off-nadir pointings (with emission angle of at least 10-15°, and hence suspension of GALA and RIME data acquisition. As illustrated in Fig. 19 (left), a full coverage of the area at high-resolution by JANUS is not possible, so that specific regions of interest should be targeted. For smaller features, such as the caldera shown on Fig. 19 (right), an almost full coverage at high resolution might be possible; this, however, requires JANUS acquisition each time the spacecraft will pass over this region and no off-nadir pointings. A prioritization of features to be covered at high-resolution and a detailed analysis of the trade-off between altimetric measurements with GALA and acquisition of stereo-pairs with JANUS will need to be evaluated for each targeted area in order to optimize the topographic mapping. The downlink window (corresponding to the orange dashed line), which has been assumed in the current trajectory scenario to start at the beginning of the Malargue visibility window (determined when station topographic elevation $> 10°$), may also be shifted by a few hours. Such a flexibility may be useful to optimize the coverage on some areas of highest interest. A detailed observation plan still needs to be studied for the GCO500 phase.

6.2.4 Analysis of Operational Challenges for Geophysical Investigation

General and specific operational constraints must be considered at science and operations planning level to ensure that geophysical measurements can be performed at the required quality level. We analysed the operational challenges based on the detailed analysis of the simulated operations during the flyby 7E1 and of a week of simulated operations during the Ganymede GCO500 orbital phase.

High Power Demand Flybys are the only parts of the tour when all instruments plan to operate simultaneously and also the only times before Ganymede Orbit Insertion to acquire useful data of RIME and GALA. Power demand is therefore high around closest approach. At the same time, the solar arrays will no longer be in a power-optimized orientation since they are being fixed to ensure pointing stability (affected by microvibrations) for the remote sensing measurements and to limit obstruction of the field of view of the neutral Ion Mass spectrometer (PEP-NIM). The JUICE battery will provide additional power but its maximum allowed depth of discharge should remain below 70%. This may place constraints on the observations if the flyby is shortly after or during an occultation of the Sun by Jupiter. Mitigation strategies will thereto be developed during the JUICE cruise phase.

Data Downlink Capacity The large geocentric distance of JUICE limits the amount of data that can be sent to Earth. For high data intake periods of the tour, the data acquisition rate is larger than the downlink rate, and data will be stored at spacecraft level in the large solid state mass memory (ca 1 Tb). In addition, selective downlink strategies will be put in place to select a subset of high resolution data to be downloaded based on analysis of low resolution data. This functionality will for example be used by GALA during GCO500. We refer to the instrument articles of this collection for further details.

Spacecraft Pointing Specific orientations of the spacecraft are required for both science and spacecraft activities. A major constraint on the pointing of the science instruments is that the spacecraft must point the High Gain Antenna (mounted on the so-called −Xsc side of the spacecraft, see Erd et al. 2024, this collection) to Earth during about 8 hours per day for communication purposes. Payload mounted on the nadir deck (+Zsc), such as GALA and the remote sensing instruments, can therefore not observe during about 1/3rd of the time. Outside these communication windows, pointing requirements from different science instruments are often incompatible, especially during low altitude phases where both remote sensing and geophysics instruments will be operating. For example, RIME and GALA both have very limited off-nadir pointing tolerance, related to the need for having a sufficient signal to noise ratio and to limit the ambiguity in the RIME data interpretation due to off-nadir features. These nadir pointing requirements conflict with the pointing needed for exospheric observations by remote sensing instrument like UVS and MAJIS. They will need to point the +Zsc at the moon's limb, corresponding to tens of degrees away from nadir, far more than the maximum pointing tolerance of the GALA and RIME. Careful planning of the science operations is therefore needed to optimize the science results.

Strong requirements are also put on the performances of the spacecraft pointing to achieve several of the ambitious science objectives of the mission. Pointing error performances are a combination of guidance error performances, which are primarily due to performances of the ground navigation, and control error performances, mainly related to thermo-elastic distortions, microvibrations and gyrostellar estimator performances. Of particular importance for geophysics is that a pointing uncertainty results in errors on the position of the GALA laser spot on the surface. This will limit the quality of the cross-over observables and therefore of the estimate of the tidal amplitude of Ganymede. Measurements of the moon's rotation state by the JANUS camera during the Ganymede phase also impose very stringent requirements on the pointing performances. During the tour, an Enhanced Attitude Guidance through Limb Extraction (EAGLE) system will be used during the moon flybys to improve the absolute guidance error from a predicted navigation error through real time optical measurements during flybys. Its use relies on the underlying condition that the navigation camera can see the limb within its field of view, which will not be the case during GCO500 and where navigation entirely relies on radio signal tracking. During this latter phase, 3GM data will be essential in reducing guidance uncertainties and allowing accurate geophysical measurements to be obtained.

Tracking from Earth Radio Stations During flybys, radio science measurements will be performed with the Medium Gain Antenna (MGA), since the High Gain Antenna is not steerable and its Earth pointing is not compatible with moon observations by the remote- sensing instruments. The fast evolving geometry during a flyby may imply that the MGA boom and dish angular rates are not sufficient to keep continuous tracking of Earth. In addition, in some flyby cases, the boom reaches its maximum elongation and needs to be repositioned, leading to an MGA outage. In some positions of the MGA, the Earth link is also blinded by the spacecraft (body and solar panels). Finally, it should be avoided that the MGA beam illuminates RIME and RPWI. As a result, radio science gravity measurements will have to be shortened in some cases.

Gravity measurements by JUICE rely on Ka/Ka links and therefore require visibility and availability of a ground station equipped with Ka uplink during the flyby. Currently only the Malargue station (in Argentina) is equipped with the necessary equipment for radio-science. A second ESTRACK station is likely to be similarly equipped when JUICE will be in the Jupiter system.

During flybys, the gravity signal is maximum during closest approach, but additional tracking before and after closest approach is needed to unambiguously estimate the gravity field of the central body because it allows the full reconstruction of the spacecraft trajectory. Since the coherence of the spacecraft trajectory is not maintained when interrupted by a wheel off loading maneuver, the science planning should ensure a continuous uninterrupted tracking as much as possible.

Perturbations by the Jovian Radio Emissions The characterization of the subsurface will be addressed primarily by RIME. Since the central frequency of RIME is within the Jovian radio emission spectral range, Jovian emissions may interfere with RIME observations when the radar will operate in active mode. On the other hand, passive radar measurement can also be performed by using the Jovian radiation as a signal, either with RIME (in passive mode) or the RPWI radio antenna. For each flyby, an analysis is performed using the Exoplanetary and Planetary Radio Emission Simulator (ExPRES, Louis et al. 2019; Cecconi et al. 2021) code to model the temporal occurrence of the occultations of the Jovian radio sources as seen from the spacecraft for a range of frequencies (in particular 1 - 40 MHz). The simulations can be used to optimize the schedule of active and/or passive radar measurements. As illustrated in Fig. 16 for the current mission scenario, the occultations of the Jovian radiation (green line) occur only during a limited time period near the closest approach, and only for a limited number of flybys. This is particularly critical in the case of Callisto where this condition is met only for 5 flybys and over only a small portion of the low-altitude ground track.

Instrument Interferences Interference measurements during ground testing revealed some disturbances between different instruments or instrument modes and between instruments and spacecraft sub-units. A first set of in-flights tests have been conducted during the commissioning phase of the mission and the data analyses are still on-going. For geophysics, RIME is most affected by interferences. Radio frequency interference signals were detected on RIME data, which have been identified as harmonics from the spacecraft power converter PCDU (Power Control and Distribution Unit). MAJIS also identified interferences with RIME on its infra-red channel with a significant increase of the noise, likely due to radiated coupling between RIME and the IR thermal braid. The assessment of the impact on RIME performances and the development of adequate mitigation strategies will be pursued during the cruise phase of the mission. This will also be a key factor that the science planning will have to deal with in order to maximize the science return of this ambitious mission.

Calibrations In-flight calibration campaigns are important for geophysical measurements. They are especially needed for ensuring the correct monitoring of the magnetic field signals from the subsurface ocean and the core of Ganymede. This requires that the magnetic field of the spacecraft at the scalar sensor is accurately known to enable calibration of the two fluxgate sensors (Dougherty et al. 2024, this collection). This is done through spacecraft roll manoeuvres when the local magnetic field around JUICE is larger than 100 nT. This condition can only be met close to JUICE perijove crossings. The calibration campaign should ideally be scheduled at the beginning, in the middle and at the end of the tour phase (before Ganymede orbit insertion).

Precise gravity measurements to determine the tidal Love number k_2 also require in-flight calibration of the High Accuracy Accelerometer (Iess et al. 2024, this collection). At the start of GCO500 additional calibrations are needed to precisely determine the alignment direction of the GALA transmitter by performing off-nadir pointing measurements (Hussmann et al. 2024, this collection).

7 Summary

JUICE will be the first spacecraft to orbit an icy moon, the largest natural satellite of our solar system Ganymede, and will therefore be able to investigate Ganymede's interior in much more detail than could be done before from a few flybys. The comprehensive suite of instruments of JUICE is furthermore optimized for probing the interior from close orbit. The orbital phase at about 500 km altitude will be the prime phase for the interior investigations. After the successful launch, the spacecraft has been assessed to have sufficient resources for an even closer phase at 200 km altitude (Boutonnet et al. 2024, this collection). This lowest altitude phase will be very beneficial for geophysics since it will allow a significantly better determination of the gravity field and the electromagnetic field. In particular the higher-degree gravity field and the small induced electromagnetic field components will be much better determined from a lower altitude. The GCO200 phase is for the moment short (30 days) in the nominal mission, but could potentially last much longer if the available resources allow for a mission extension beyond October 2035. A quantitative assessment of the expected improvements in scientific results of the addition of the nearly-circular orbital phase at 200 km altitude will be performed during JUICE's cruise to Jupiter.

The radio science instrument 3GM and the laser altimeter GALA will determine detailed maps of the gravity and topography field and will measure the tides and rotation characteristics. The magnetometer J-MAG and RPWI will measure the induced electromagnetic field generated in the subsurface ocean. Taken together the data from these instruments allow the determination of the average thicknesses of the outer ice shell, ocean and high-pressure ice mantle, the salt content of the ocean, and lateral variations in shell thickness and density, if present. They may inform on the flow dynamics in the ocean and the heat flux through the hydrosphere, providing key constraints on the habitability of the subsurface ocean. Radar sounding by RIME and RPWI (only in passive mode) will provide detailed images of the structure and composition of the ice shell. As described in the previous sections, the interior tomography of Ganymede can only be fully achieved through a synergistic use of the data of these instruments because of the non-unique relation between the observable quantities and the interior. The combination of the complementary information on the interior provided by the different instrument data sets is therefore essential for reaching JUICE's objectives on the hydrosphere structure and dynamics. The interpretation of the data of these instruments often also relies on data gathered by the five other JUICE instruments: the remote sensing instruments JANUS, MAJIS, UVS, and SWI, and the in situ instrument PEP, as detailed above. JANUS and UVS will furthermore provide independent and complementary data on the rotation, shape, topography, and induced electromagnetic field of Ganymede and Callisto.

The same set of instruments will also gather information on the deeper interior. Deviations of the mass distribution and shape from their expected values for a satellite in hydrostatic equilibrium will be assessed with high precision and the mean moment of inertia, the basic constraint on the internal differentiation and radial density profile, will be significantly improved for both Ganymede and Callisto. The morphology and variation of the internal magnetic field generated in the core will be determined from which it will be possible to identify the process driving the dynamo field and to learn about the structure and dynamics of the metallic core, including maybe the possible presence and size of a solid inner core. By precisely tracking the JUICE spacecraft, the ephemerides of the Galilean moons will be improved by several orders of magnitude, which will allow us to accurately estimate the tidal dissipation in the Galilean moons and in Jupiter. This will not only provide an additional constraint on the moons' interior, but will also set constraints on the past and future evolution of the Laplace resonance.

Internal processes will also be studied and constrained through their effects on and links with the surface. By observing various geological structures with JANUS and combining these data with those of RIME, GALA and 3GM, the structure of the upper ice shell will be mapped. The composition of the surface, from MAJIS, UVS, SWI and JANUS data, in particular over recent structures that may contain materials freshly exposed to the surface, will provide insight on the composition of the subsurface and internal ocean and on the evolution of the ice shell. If plumes exist, by studying icy grains and vapor ejected from the surface, further information on the subsurface activity and composition will be obtained.

Through a synergistic approach based on a complementary set of instruments, JUICE will provide unprecedented insight into Ganymede's interior, from the metallic core where the magnetic field is generated, to the subsurface ocean and ice shell. Although Ganymede is the prime focus of the interior objectives of the mission, JUICE will also unravel the interior of Callisto. It will unambiguously determine whether Callisto has a subsurface ocean and will clarify the different evolution of Callisto compared to Ganymede. On Europa, the local structure of the ice shell beneath the two JUICE flyby trajectories will be investigated and the subsurface ocean might be directly detected by radar sounding. JUICE will also substantially improve our understanding of the orbital evolution of all the Galilean moons, which has important bearings on the evolution of the subsurface oceans and their habitability.

Acknowledgements We thank Francis Nimmo and an anonymous referee for their thorough reviews that have helped to improve the paper. T. Van Hoolst (since 2015) and G. Tobie (since 2017) are chairing the JUICE Working Group on the 'Internal structure, subsurface and geophysics of giant icy moons'. T. Van Hoolst acknowledges support from the Belgian PRODEX program managed by the European Space Agency in collaboration with the Belgian Federal Science Policy Office. French authors acknowledge the support from CNES in the preparation of the ESA JUICE. The Italian participation in the JUICE mission is funded by the Italian Space Agency (ASI). In particular, this work has been developed under the ASI-INAF agreement n. 2023-6-HH.0.

Declarations

Competing Interests The authors declare that they have no competing financial or non-financial interests to declare that are relevant to the content of this article.

References

A G, Wahr J, Zhong S (2014) The effects of laterally varying icy shell structure on the tidal response of Ganymede and Europa. J Geophys Res, Planets 119:659–678. https://doi.org/10.1002/2013JE004570

Abrahams JN, Nimmo F, Becker TM, Gladstone GR, Retherford KD, Steinbrügge G, Mazarico E (2021) Improved determination of Europa's long-wavelength topography using stellar occultations. Earth Space Sci 8(7):e2020EA001586

Akiba R, Ermakov AI, Militzer B (2022) Probing the icy shell structure of ocean worlds with gravity-topography admittance. Planet Sci J 3:53. https://doi.org/10.3847/PSJ/ac4d2b

Amit H, Choblet G, Tobie G, Terra-Nova F, Cadek O, Bouffard M (2020) Cooling patterns in rotating thin spherical shells. Application to Titan's subsurface ocean. Icarus 338:113509

Anderson JD, Lau EL, Sjogren WL, Schubert G, Moore WB (1996) Gravitational constraints on the internal structure of Ganymede. Nature 384:541
Anderson JD, Schubert G, Jacobson RA, Lau EL, Moore WB, Sjogren WL (1998) Distribution of rock, metals, and ices in Callisto. Science 280(5369):1573–1576. https://doi.org/10.1126/SCIENCE.280.5369.1573
Anderson JD, Jacobson RA, McElrath TP, Moore WB, Schubert G, Thomas PC (2001) Shape, mean radius, gravity field, and interior structure of Callisto. Icarus 153:157–161
Anderson JD, Schubert G, Jacobson RA, Lau EL, Moore WB, Palguta JL (2004) Discovery of mass anomalies on Ganymede. Science 305:989. https://doi.org/10.1126/science.1099050
Anderson BJ, Johnson CL, Korth H, Winslow RM, Borovsky JE, Purucker ME, Slavin JA, Solomon SC, Zuber MT, McNutt RL Jr (2012) Low-degree structure in Mercury's planetary magnetic field. J Geophys Res 117:E00L12. https://doi.org/10.1029/2012JE004159
Antreasian PG, Ardalan SM, Beswick RM, Criddle KE, Ionasescu R, Jacobson RA, Jones JB, Mackenzie RA, Parcher DW, Pelletier FJ, Roth DC, Thompson PF, Vaughan AT (2008) Orbit determination processes for the navigation of the Cassini-Huygens mission. In: SpaceOps 2008 Conference, pp 1–18
Arnold H, Liuzzo L, Simon S (2019) Magnetic signatures of a plume at Europa during the Galileo E26 flyby. Geophys Res Lett 46:1149–1157
Ashkenazy Y, Tzipermanet E (2021) Dynamic Europa ocean shows transient Taylor columns and convection driven by ice melting and salinity. Nat Commun 12:6376
Ashkenazy Y, Tziperman E, Nimmo F (2023) Non-synchronous rotation on Europa driven by ocean currents. AGU Adv 4:e2022AV000849. https://doi.org/10.1029/2022AV000849
Aygün B, Cadek O (2023) Impact of the core deformation on the tidal heating and flow in Enceladus' subsurface ocean. J Geophys Res, Planets 128(11):e2023JE007907
Baland RM, Yseboodt M, Van Hoolst T (2012) Obliquity of the Galilean satellites: the influence of a global internal liquid layer. Icarus 220:435. https://doi.org/10.1016/j.icarus.2012.05.020
Baland RM, Tobie G, Lefèvre A, Van Hoolst T (2014) Titan's internal structure inferred from its gravity field, shape, and rotation state. Icarus 237:29. https://doi.org/10.1016/j.icarus.2014.04.007
Baland RM, Yseboodt M, Rivoldini A, Van Hoolst T (2017) Obliquity of Mercury: influence of the precession of the pericenter and of tides. Icarus 291:136–159. https://doi.org/10.1016/j.icarus.2017.03.020
Barabash S et al (2024) Title to be determined. Space Sci Rev 220
Barr AC, Canup RM (2008) Constraints on gas giant satellite formation from the interior states of partially differentiated satellites. Icarus 198:163–177
Barr AC, Canup RM (2010) Origin of the Ganymede-Callisto dichotomy by impacts during the late heavy bombardment. Nat Geosci 3:164–167
Batygin K, Morbidelli A (2020) Formation of giant planet satellites. Astrophys J 894:143. https://doi.org/10.3847/1538-4357/ab8937
Becker TM, Retherford KD, Roth L, Hendrix AR, McGrath MA, Saur J (2018) The far-UV albedo of Europa from HST observations. J Geophys Res, Planets 123:1327–1342
Berquin Y, Herique A, Kofman W, Heggy E (2015) Computing low-frequency radar surface echoes for planetary radar using Huygens-Fresnel's principle. Radio Sci 50:1097–1109
Besserer J, Nimmo F, Roberts JH, Pappalardo RT (2013) Convection-driven compaction as a possible origin of Enceladus's long wavelength topography. J Geophys Res, Planets 118:908–915. https://doi.org/10.1002/jgre.20079
Besserer J, Nimmo F, Wieczorek MA, Weber RC, Kiefer WS, McGovern PJ, Andrews-Hanna JC, Smith DE, Zuber MT (2014) GRAIL gravity constraints on the vertical and lateral density structure of the lunar crust. Geophys Res Lett 41:5771–5777. https://doi.org/10.1002/2014GL060240
Beuthe M (2016) Crustal control of dissipative ocean tides in Enceladus and other icy moons. Icarus 280:278–299. https://doi.org/10.1016/j.icarus.2016.08.009
Beuthe M (2018) Enceladus's crust as a non-uniform thin shell: I. Tidal deformations. Icarus 302:145–174. https://doi.org/10.1016/j.icarus.2017.11.009
Beuthe M (2019) Enceladus's crust as a non-uniform thin shell: II tidal dissipation. Icarus 332:66–91
Beuthe M (2021a) Isostasy with Love - I: elastic equilibrium. Geophys J Int 225:2157
Beuthe M (2021b) Isostasy with love: II Airy compensation arising from viscoelastic relaxation. Geophys J Int 227:693–716. https://doi.org/10.1093/gji/ggab241
Bills BG (2005) Free and forced obliquities of the Galilean satellites of Jupiter. Icarus 175:233. https://doi.org/10.1016/j.icarus.2004.10.028
Bire S, Kang W, Ramadhan A, Campin JM, Marshall J (2022) Exploring ocean circulation on icy moons heated from below. J Geophys Res, Planets 127(3):e2021JE007025
Bjonnes E, Johnson BC, Silber EA, Singer KN, Evans AJ (2022) Ice Shell Structure of Ganymede and Callisto Based on Impact Crater Morphology. JGR Planets 127. https://doi.org/10.1029/2021JE007028
Bland MT, Showman AP, Tobie G (2008) The production of Ganymede's magnetic field. Icarus 198:384–399

Bland MT, Showman AP, Tobie G (2009) The orbital-thermal evolution and global expansion of Ganymede. Icarus 200:207–221
Bockelée-Morvan D, Lellouch E, Poch O, Quirico E, Cazaux S, de Pater I et al (2024) Composition and thermal properties of Ganymede's surface from JWST/NIRSpec and MIRI observations. Astron Astrophys 681:A27
Boutonnet A, Langevin Y, Erd C (2024) Designing the JUICE trajectory. Space Sci Rev 220
Brennan MC, Fischer RA, Nimmo F, O'Brien DP (2022) Timing of Martian core formation from models of Hf-W evolution coupled with N-body simulations. Geochim Cosmochim Acta 316:295–308
Brown RH et al (2006) Composition and physical properties of Enceladus' surface. Science 311:1425–1428
Brown S, Zhang Z, Bolton S, Bonnefoy LE, Ermakov A, Feng J, Hartogh P, Levin S, Misra S, Siegler M et al (2023) Microwave observations of Ganymede's sub-surface ice: I. Ice temperature and structure. J Geophys Res, Planets 128:e2022JE007609
Brozović M, Nolan MC, Magri C, Folkner WM, Jacobson RA, Harcke LJ, McMichael JG, Richardson JE, Harmon JK, Taylor PA et al (2020) Arecibo radar astrometry of the Galilean satellites from 1999 to 2016. Astron J 159(4):149
Bruzzone L, Plaut JJ, Alberti G, Blankenship DD, Bovolo F, Campbell BA, Seu R (2013) RIME: radar for icy moon exploration. In: 2013 IEEE international geoscience and remote sensing symposium-IGARSS. IEEE, Los Alamitos, pp 3907–3910
Bruzzone L et al (2024) Title to be determined. Space Sci Rev 220
Cadek O, Behounkova M, Tobie G, Choblet G (2017) Viscoelastic relaxation of Enceladus's ice shell. Icarus 291:31. https://doi.org/10.1016/j.icarus.2017.03.011
Cadek O, Soudek O, Behounkova M (2019) Is Airy isostasy applicable to icy moons? Geophys Res Lett 46:14299. https://doi.org/10.1029/2019GL085903
Canup RM, Ward WR (2002) Formation of Galilean satellites: conditions of accretion. Astron J 124:3404–3423
Canup RM, Ward WR (2009) Origin of Europa and the Galilean satellites. In: Pappalardo RT, McKinnon WB, Khurana KK (eds) Europa. With the assistance of René Dotson. University of Arizona Press, Tucson, p 59. The University of Arizona space science series ISBN 9780816528448
Cao H, Dougherty MK, Hunt GJ, Provan G, Cowley SWH, Bunce EJ, Kellock S, Stevenson DJ (2020) The landscape of Saturn's internal magnetic field from the Cassini grand finale. Icarus 344:113541
Cappuccio P, Hickey A, Durante D, Di Benedetto M, Iess L, De Marchi F, Plainaki C, Milillo A, Mura A (2020) Ganymede's gravity, tides and rotational state from JUICE's 3GM experiment simulation. Planet Space Sci 187:104902
Cappuccio P et al (2022) Callisto and Europa gravity measurements from JUICE 3GM experiment simulation. Planet Sci J 3(8):199
Carlson RW, Calvin WM, Dalton JB, Hansen GB, Hudson RL, Johnson RE, McCord TB, Moore MH (2009) Europa's surface composition. In: Europa. University of Arizona Press, Tucson, pp 283–327
Carrer L, Schroeder DM, Romero-Wolf A, Ries PA, Bruzzone L (2020) Analysis of temporal and structural characteristics of Jovian radio emissions for passive radar sounding of Jupiter's icy moons. IEEE Trans Geosci Remote Sens 59(5):3857–3874
Castillo-Rogez JC, Lunine JI (2010) Evolution of Titan's rocky core constrained by Cassini observations. Geophys Res Lett 37:L20205. https://doi.org/10.1029/2010GL044398
Cecconi B, Hess S, Hérique A, Santovito MR, Santos-Costa D, Zarka P, Kofman W (2012) Natural radio emission of Jupiter as interferences for radar investigations of the icy satellites of Jupiter. Planet Space Sci 61(1):32–45
Cecconi B, Louis CK, Crego CM, Vallat C (2021) Jovian auroral radio source occultation modelling and application to the JUICE science mission planning. Planet Space Sci 209:105344
Celletti A, Paita F, Pucacco G (2019) The dynamics of Laplace-like resonances. Chaos, Interdiscip J Nonlinear Sci 29(3):033111
Chen EMA, Nimmo F, Glatzmaier GA (2014) Tidal heating in icy satellite oceans. Icarus 229:11–30. https://doi.org/10.1016/j.icarus.2013.10.024
Choblet G, Tobie G, Sotin C, Behounkova M, Cadek O, Postberg F, Soudek O (2017a) Powering prolonged hydrothermal activity inside Enceladus. Nat Astron 12:841–847. https://doi.org/10.1038/s41550-017-0289-8
Choblet G, Tobie G, Sotin C, Kalousová K, Grasset O (2017b) Heat transport in the high-pressure ice mantle of large icy moons. Icarus 285:252–262
Christensen UR (2015) Iron snow dynamo models for Ganymede. Icarus 247:248–259
Christensen UR, Aubert J (2006) Scaling properties of convection-driven dynamos in rotating spherical shells and applications to planetary magnetic fields. Geophys J Int 166:97–114
Chuang FC, Greeley R (2000) Large mass movements on Callisto. J Geophys Res 105(E8):20227–20244

Comstock RL, Bills BG (2003) A Solar System survey of forced librations in longitude. J Geophys Res 108(E9):5100. https://doi.org/10.1029/2003JE00210
Connerney JEP, Timmins S, Oliversen RJ, Espley JR, Joergensen JL, Kotsiaros S et al (2022) A new model of Jupiter's magnetic field at the completion of Juno's prime mission. J Geophys Res, Planets 127:e2021JE007055
Copernicus N (1543) De revolutionibus orbium coelestium
Coyette A, Baland R-M, Van Hoolst T (2024) Revisiting the Cassini states of synchronous satellites with an angular momentum approach. In: Proceedings of the International Astronomical Union, vol S382. in press
Dalton JB, Pitman KM (2012) Low temperature optical constants of some hydrated sulfates relevant to planetary surfaces. J Geophys Res 117:E09001
D'Amario LA, Bright LE, Wolf AA (1992) Galileo trajectory design. Space Sci Rev 60(1):23–78. https://doi.org/10.1007/BF00216849
Dbouk R, Wisdom J (2023) The origin of Jupiter's obliquity. Planet Sci J 4:188. https://doi.org/10.3847/PSJ/acf9f8
De Marchi F, Di Achille G, Mitri G, Cappuccio P, Di Stefano I, Di Benedetto M, Iess L (2021) Observability of Ganymede's gravity anomalies related to surface features by the 3GM experiment onboard ESA's JUpiter ICy moons Explorer (JUICE) mission. Icarus 354:114003
De Marchi F et al (2022) Frequency-dependent Ganymede's tidal Love number k2 detection by JUICE's 3GM experiment and implications for the subsurface ocean thickness.". Icarus 386:115150
Di Ruscio A, Fienga A, Durante D, Iess L, Laskar J, Gastineau M (2020) Analysis of Cassini radio tracking data for the construction of INPOP19a: a new estimate of the Kuiper Belt mass. Astron Astrophys 640:A7
Dirkx D, Lainey V, Gurvits L, Visser P (2016) Dynamical modelling of the Galilean moons for the JUICE mission. Planet Space Sci 134:82–95
Dirkx D, Gurvits LI, Lainey V, Lari G, Milani A, Cimò G, Bocanegra Bahamon T, Visser P (2017) On the contribution of PRIDE-JUICE to Jovian system ephemerides. Planet Space Sci 147:14–27
Dombard AJ, McKinnon WB (2001) Formation of grooved terrain on Ganymede: extensional instability mediated by cold, superplastic creep. Icarus 154:321. https://doi.org/10.1006/icar.2001.6728
Dombard AJ, Sessa AM (2019) Gravity measurements are key in addressing the habitability of a subsurface ocean in Jupiter's Moon Europa. Icarus 325:31. https://doi.org/10.1016/j.icarus.2019.02.025
Dougherty MC et al (2024) J-MAG. Space Sci Rev 220
Downey BG, Nimmo F, Matsuyama I (2020) Inclination damping on Callisto. Mon Not R Astron Soc 499:40–51
Duev DA, Calv'és GM, Pogrebenko SV, Gurvits LI, Cimo G, Bahamon TB (2012) Spacecraft VLBI and Doppler tracking: algorithms and implementation. Astron Astrophys 541:A43
Duling S, Saur J, Wicht J (2014) Consistent boundary conditions at nonconducting surfaces of planetary bodies: Applications in a new Ganymede MHD model. J Geophys Res Space Phys 119
Duling S, Saur J, Clark G, Allegrini F, Greathouse T, Gladstone R et al (2022) Ganymede MHD model: magnetospheric context for Juno's PJ34 flyby. Geophys Res Lett 49(24):e2022GL101688. https://doi.org/10.1029/2022GL101688
Durante D, Hemingway D, Racioppa P, Iess L, Stevenson D (2019) Titan's gravity field and interior structure after Cassini. Icarus 326:123–132
Durante D, Parisi M, Serra D, Zannoni M, Notaro V, Racioppa P, Buccino DR, Lari G, Gomez Casajus L, Iess L, Folkner WM, Tommei G, Tortora P, Bolton SJ (2020) Jupiter's gravity field halfway through the Juno mission. Geophys Res Lett 47(4):1–8
Durante D, Guillot T, Iess L, Stevenson DJ, Mankovich CR, Markham S, Galanti E, Kaspi Y, Zannoni M, Gomez Casajus L, Lari G, Parisi M, Buccino DR, Park RS, Bolton SJ (2022) Juno spacecraft gravity measurements provide evidence for normal modes of Jupiter. Nat Commun 13(1):4632
Erd C et al (2024) The JUICE spacecraft system design. Space Sci Rev 220
Esposito LW, Barth CA, Colwell JE, Lawrence GM, McClintock WE, Stewart AIF, Keller HU, Korth A, Lauche H, Festou MC, Lane AL, Hansen CJ, Maki JN, West RA, Jahn H, Reulke R, Warlich K, Shemansky DE, Yung YL (2004) The Cassini ultraviolet imaging spectrograph investigation. Space Sci Rev 115:299–361
Estrada PR, Mosqueira I, Lissauer JJ, D'Angelo G, Cruikshank DP (2009) Formation of Jupiter and conditions for accretion of the Galilean satellites. In: Pappalardo RT, McKinnon WB, Khurana KK (eds) Europa. With the assistance of René Dotson. University of Arizona Press, Tucson. The University of Arizona space science series ISBN: 9780816528448
Fagents SA (2003) Considerations for effusive cryovolcanism on Europa: the post-Galileo perspective. J Geophys Res, Planets 108(E12)

Fayolle M, Dirkx D, Visser P, Lainey V (2021) Analytical framework for mutual approximations - derivation and application to Jovian satellites. Astron Astrophys 652:A93
Fayolle M, Dirkx D, Lainey V, Gurvits L, Visser P (2022) Decoupled and coupled moons' ephemerides estimation strategies application to the JUICE mission. Planet Space Sci 219:105531
Fayolle M, Lainey V, Dirkx D, Gurvits LI, Cimo G, Bolton SJ (2023a) Spacecraft VLBI tracking to enhance stellar occultations astrometry of planetary satellites. Astron Astrophys 676:L6. https://doi.org/10.1051/0004-6361/202347019
Fayolle M, Magnanini A, Lainey V, Dirkx D, Zannoni M, Tortora P (2023b) Combining astrometry and JUICE – Europa Clipper radioscience to improve the Galilean moons ephemerides. Astron Astrophys 677:A42. https://doi.org/10.1051/0004-6361/202347065
Fienga A, Di Ruscio A, Bernus L, Deram P, Durante D, Laskar J, Iess L (2020) New constraints on the location of P9 obtained with the INPOP19a planetary ephemeris. Astron Astrophys 640:A6
Fletcher LN, Cavalié T, Grassi D et al (2023) Jupiter science enabled by ESA's Jupiter Icy Moons Explorer. Space Sci Rev 219:53. https://doi.org/10.1007/s11214-023-00996-6
Fuller J, Luan J, Quataert E (2016) Resonance locking as the source of rapid tidal migration in the Jupiter and Saturn moon systems. Mon Not R Astron Soc 458:3867–3879. https://doi.org/10.1093/mnras/stw609
Gaia Collaboration et al (2016) The Gaia mission. Astron Astrophys 595:A1
Galilei G (1610) Sidereus Nuncius pp p16–28
Gao P, Stevenson DJ (2013) Nonhydrostatic effects and the determination of icy satellites' moment of inertia. Icarus 226:1185–1191. https://doi.org/10.1016/j.icarus.2013.07.034
Gassot O, Herique A, Kofman W, Cecconi B, Witasse O (2022) Performances of the Passive SAR Imaging of Jupiter's Icy Moons. EEE Trans Geosci Remote Sens 60:4601713. https://doi.org/10.1109/TGRS.2022.3172633
Gastine T, Wicht J, Aubert J (2016) Scaling regimes in spherical shell rotating convection. J Fluid Mech 808:690–732
Gerekos C, Tamponi A, Carrer L, Castelletti D, Santoni M, Bruzzone L (2018) A coherent multilayer simulator of radargrams acquired by radar sounder instruments. IEEE Trans Geosci Remote Sens 56(12):7388–7404
Gerekos C, Bruzzone L, Imai M (2019) A coherent method for simulating active and passive radar sounding of the Jovian icy moons. IEEE Trans Geosci Remote Sens 58(4):2250–2265
Gladstone R et al (2024) Title to be determined. Space Sci Rev 220
Glein CR, Waite JH (2020) The carbonate geochemistry of Enceladus' ocean. Geophys Res Lett 47:e2019GL085885
Glein CR, Baross JA, Waite JH Jr (2015) The pH of Enceladus' ocean. Geochim Cosmochim Acta 162:202–219
Goldreich PM, Mitchell JL (2010) Elastic ice shells of synchronous moons: implications for cracks on Europa and non-synchronous rotation of Titan. Icarus 209:631–638
Goldreich P, Peale S (1966) Spin-orbit coupling in the Solar System. Astron J 71(6):425–437
Goldstein ML, Goertz CK (1983) Phenomenology of magnetospheric radio emissions. In: Dessler AJ (ed) Physics of the Jovian magnetosphere, p 317
Gomez Casajus L, Ermakov AI, Zannoni M, Keane JT, Stevenson D, Buccino DR, Durante D, Parisi M, Park RS, Tortora P, Bolton SJ (2022) Gravity field of Ganymede after the Juno extended mission. Geophys Res Lett 49:e2022GL099475. https://doi.org/10.1029/2022GL099475
Gómez-Pérez N, Wicht J (2010) Behavior of planetary dynamos under the influence of external magnetic fields: application to Mercury and Ganymede. Icarus 209:53–62
Greathouse TK, Gladstone GR, Molyneux PM, Versteeg MH, Hue V, Kammer JA et al (2022) UVS observations of Ganymede's aurora during Juno orbits 34 and 35. Geophys Res Lett 49:e2022GL099794. https://doi.org/10.1029/2022GL099794
Greeley R, Chyba CF, Head JW, McCord TB, McKinnon WB, Pappalardo RT, Figueredo PH (2004) Geology of Europa. Jupit Planet Satell Magnetosphere 2:329
Greenberg R (1987) Galilean satellites: evolutionary paths in deep resonance. Icarus 70:334–347
Greenberg R, Weidenschilling SJ (1984) How fast do Galilean satellites spin? Icarus 58(2):186–196
Gurvits LI et al (2023) Planetary Radio Interferometry and Doppler Experiment (PRIDE) of the JUICE mission. Space Sci Rev 219:79. https://doi.org/10.1007/s11214-023-01026-1
Hand KP, Brown ME (2013) Keck II observations of hemispherical differences in H_2O_2 on Europa. Astrophys J Lett 766:L21. https://doi.org/10.1088/2041-8205/766/2/L21
Hansen CJ, Esposito L, Stewart AIF, Colwell J, Hendrix A, Pryor W, Shemansky D, West R (2006) Enceladus' water vapor plume. Science 311:1423–1425
Hansen CJ, Esposito LW, Aye K-M, Colwell JE, Hendrix AR, Portyankina G, Shemansky D (2017) Investigation of diurnal variability of water vapor in Enceladus' plume by the Cassini ultra- violet imaging spectrograph. Geophys Res Lett 44:672–677

Hansen CJ, Esposito LW, Colwell JE, Hendrix AR, Portyankina G, Stewart AIF, West RA (2020) The composition and structure of Enceladus' plume from the complete set of Cassini UVIS occultation observations. Icarus 344:113461. https://doi.org/10.1016/j.icarus.2019.113461
Harada Y, Kurita K (2006) The dependence of surface tidal stress on the internal structure of Europa: the possibility of cracking of the icy shell. Planet Space Sci 54(2):170–180
Hartkorn, Saur J (2017) Induction signals from Callisto's ionosphere and their implications on a possible subsurface ocean. J Geophys Res 122. https://doi.org/10.1002/2017JA024269
Hartogh P et al (2024) Title to be determined. Space Sci Rev 220
Hauck SA II, Aurnou JM, Dombard AJ (2006) Sulfur's impact on core evolution and magnetic field generation on Ganymede. J Geophys Res 111:E09008. https://doi.org/10.1029/2005JE002557
Hay HCFC, Trinh A, Matsuyama I (2020) Powering the Galilean satellites with moon-moon tides. Geophys Res Lett 47:e2020GL088317. https://doi.org/10.1029/2020GL088317
Hay H, Matsuyama I, Pappalardo RT (2022) The high-frequency tidal response of ocean worlds: application to Europa and Ganymede. J Geophys Res 127:e2021JE007064
Hay HCFC, Fenty I, Pappalardo RT, Nakayama Y (2023) Turbulent drag at the ice-ocean interface of Europa in simulations of rotating convection: implications for nonsynchronous rotation of the ice shell. J Geophys Res, Planets 128:e2022JE007648. https://doi.org/10.1029/2022JE007648
Heggy E, Scabbia G, Bruzzone L, Pappalardo RT (2017) Radar probing of Jovian icy moons: understanding subsurface water and structure detectability in the JUICE and Europa missions. Icarus 285:237–251
Hemingway DJ, Mittal T (2019) Enceladus's ice shell structure as a window on internal heat production. Icarus 332:111–131. https://doi.org/10.1016/j.icarus.2019.03.011
Hough SS (1895) The oscillations of a rotating ellipsoidal shell containing fluid. Philos Trans R Soc Lond A 186:469–506
Howell SM, Pappalardo RT (2020) NASA's Europa Clipper - a mission to a potentially habitable ocean world. Nat Commun 11:1311. https://doi.org/10.1038/s41467-020-15160-9
Hubbard WB (1984) Planetary interiors. Van Nostrand Reinhold, New York
Huguet L, Le Bars M, Deguen R (2023) A laboratory model for iron snow in planetary cores. Geophys Res Lett 50:e2023GL105697. https://doi.org/10.1029/2023GL105697
Hussmann H et al (2016) Constraints on dissipation in the deep interiors of Ganymede and Europa from tidal phase-lags. Celest Mech Dyn Astron 126(1):131–144. https://doi.org/10.1007/s10569-016-9721-0
Hussmann H, Lingenauber K, Stark A et al (2024) The Ganymede Laser Altimeter (GALA) on the Jupiter Icy Moons Explorer (JUICE) Mission. Space Sci Rev 220
Huybrighs HLF, Futaana Y, Barabash S, Wieser M, Wurz P, Krupp N et al (2017) On the in-situ detectability of Europa's water vapour plumes from a flyby mission. Icarus 289:270–280. https://doi.org/10.1016/j.icarus.2016.10.026
Huybrighs HLF, Roussos E, Blöcker A, Krupp N, Futaana Y, Barabash S, Hadid LZ, Holmberg MKG, Lomax O, Witasse O (2020) An active plume eruption on Europa during Galileo flyby E26 as indicated by energetic proton depletions. Geophys Res Lett 47:e2020GL087806
Iess L et al (2012) The tides of Titan. Science 337(6093):457–459
Iess L et al (2024) The 3GM investigation of ESA's JUICE mission: geodesy and geophysics of Jupiter and the Galilean Moons. Space Sci Rev 220
Ilyushin YA, Hartogh P (2020) Submillimeter wave instrument radiometry of the Jovian icy moons. Numerical simulation of the microwave thermal radiative transfer and Bayesian retrieval of the physical properties. Astron Astrophys 644:A24. https://doi.org/10.1051/0004-6361/201937220
Ingersoll AP, Ewald SP, Trumbo SK (2016) Time variability of the Enceladus plumes: orbital periods, decadal periods, and aperiodic change. Icarus 344:113345
Jacobson R (2014) The orbits of the Uranian satellites and rings, the gravity field of the Uranian system, and the orientation of the pole of Uranus. Astron J 148(5):76
Jacobson RA (2022) The orbits of the main Saturnian satellites, the Saturnian system gravity field, and the orientation of Saturn's pole. Astron J 164(5):199
Jansen MF, Kang W, Kite ES, Zeng Y (2023) Energetic constraints on ocean circulations of icy ocean worlds. Planet Sci J 4:117. https://doi.org/10.3847/PSJ/acda95
Janssen MA, Oswald JE, Brown ST, Gulkis S, Levin SM, Bolton SJ et al (2017) MWR: microwave radiometer for the Juno mission to Jupiter. Space Sci Rev 213(1):139–185. https://doi.org/10.1007/s11214-017-0349-5
Jara-Orué HM, Vermeersen BLA (2016) Tides on Jupiter's moon Ganymede and their relation to its internal structure. Geol Mijnb 95(2):191–201
Jeffreys H (1926) The rigidity of the Earth's central core. Geophys Suppl Mon Not R Astron Soc 1:371
Jia X, Kivelson MG, Khurana KK, Kurth WS (2018) Evidence of a plume on Europa from Galileo magnetic and plasma wave signatures. Nat Astron 2:459–464

Journaux B, Brown JM, Abramson EH, Vance S (2022) The Thermodynamics of Titan's Abysses: Equation of State of Water-Ammonia Solutions at Conditions of Titan's Hydrosphere. LPI Contributions 2632
Kalousová K, Sotin C (2020) Dynamics of Titan's high-pressure ice layer. Earth Planet Sci Lett 545:116416
Kalousová K, Sotin C, Choblet G, Tobie G, Grasset O (2018) Two-phase convection in Ganymede's high-pressure ice layer - implications for its geological evolution. Icarus 299:133–147
Kamata S, Kimura J, Matsumoto K, Nimmo F, Kuramoto K, Namiki N (2016) Tidal deformation of Ganymede: sensitivity of Love numbers on the interior structure. J Geophys Res 121:1362–1375. https://doi.org/10.1002/2016JE005071
Kang W (2022) Different ice-shell geometries on Europa and Enceladus due to their different sizes: impacts of ocean heat transport. Astrophys J 934(2):116
Kang W (2024) Nonsynchronous rotation of icy moon ice shells: the thermal wind perspective. Sci Adv 10(4):eadk2277
Kargel JS, Kaye JZ, Head JW, Marion GM, Sassen R, Crowley JK, Ballesteros, Prieto O, Grant SA, Hogenboom DL (2000) Europa's crust and ocean: origin, composition, and the prospects for life. Icarus 148:226–265. https://doi.org/10.1006/icar.2000.6471
Khurana KK et al (1998) Induced magnetic fields as evidence for subsurface oceans in Europa and Callisto. Nature 395:777–780
Khurana KK et al (2002) Searching for liquid water in Europa by using surface observatories. Astrobiology 2(1):93–103
Khurana KK, Kivelson MG, Hand KP, Russell CT (2009) Electromagnetic induction from Europa's ocean and deep interior. In: Europa. University of Arizona Press, Tucson, pp 571–586
Kihoulou et al (2019)
Kihoulou et al (2022)
Kihoulou M, Cadek O, Kvorka J, Kalousova K, Choblet G, Tobie G (2023) Topographic response to ocean heat flux anomaly on the icy moons of Jupiter and Saturn. Icarus 391:115337
Kimura J, Kuramoto K (2012) Formation of a conductive core, grooved terrains, and strongly differentiated interior of Ganymede due to dehydration of primordial hydrous rock with implication for the dichotomy from Callisto. In: EPSC Abstracts, vol 7. EPSC2012-560-2. European Planetary Science Congress 2012
Kimura J, Nakagawa T, Kurita K (2009) Size and compositional constraints of Ganymede's metallic core for driving an active dynamo. Icarus 202:216–224. https://doi.org/10.1016/j.icarus.2009.02.026
King O, Fletcher LN (2022) Global modeling of Ganymede's surface composition: near-IR mapping from VLT/SPHERE. Journal of Geophysical Research: Planets 127(12):e2022JE007323
King O, Fletcher LN, Ligier N (2022) Compositional mapping of Europa using MCMC modeling of near-IR VLT/SPHERE and Galileo/NIMS observations. Planet Sci J 3:72. https://doi.org/10.3847/PSJ/ac596d
Kirk RL, Stevenson DJ (1987) Thermal evolution of a differentiated Ganymede and implications for surface features. Icarus 69(1):91–134
Kirk RL, Howington-Kraus E, Hare TM, Jorda L (2016) The effect of illumination on stereo DTM quality: simulations in support of Europa exploration. In: ISPRS annals of the photogrammetry, remote sensing and spatial information sciences, volume III-4, XXIII ISPRS congress, Prague, Czech Republic, 12-19 July 2016, pp 12–19
Kivelson MG et al (1996) Discovery of Ganymede's magnetic field by the Galileo spacecraft. Nature 384:537–541
Kivelson MG, Khurana KK, Stevenson DJ, Bennett L, Joy S, Russell CT, Walker RJ, Zimmer C, Polanskey C (1999) Europa and Callisto: induced or intrinsic fields in a periodically varying plasma environment. J Geophys Res Space Phys 104(A3):4609–4625. https://doi.org/10.1029/1998JA900095
Kivelson MG et al (2002b) Galileo magnetometer measurements: a stronger case for a subsurface ocean at Europa. Science 289:1340–1343
Kivelson MG, Khurana KK, Volwerk M (2002a) The permanent and inductive magnetic moments of Ganymede. Icarus 157(2):507–522. https://doi.org/10.1006/icar.2002.6834
Kleine T, Münker C, Mezger K, Palme H (2002) Rapid accretion and early core formation on asteroids and the terrestrial planets from Hf-W chronometry. Nature 418:952–955
Koh ZW, Nimmo F, Lunine JI, Mazarico E, Dombard AJ (2022) Assessing the detectability of Europa's seafloor topography from Europa Clipper's gravity data. Planet Sci J 3(8):197
Kumamoto A, Kasaba Y, Tsuchiya F, Misawa H, Kita H, Puccio W, Kobayashi T (2017) Feasibility of the exploration of the subsurface structures of Jupiter's icy moons by interference of Jovian hectometric and decametric radiation. In: Fischer G, Mann G, Panchenko M, Zarka P (eds) Planetary radio emissions VIII, proceedings of the 8th international workshop held at seggauberg, Austria, October 25-27, 2016. Austrian Academy of Sciences Press, Vienna, pp 127–136
Kuskov OL, Kronrod VA (2005) Internal structure of Europa and Callisto. Icarus 177(2):550–569
Kvorka J, Cadek O (2022) A numerical model of convective heat transfer in Titan's subsurface ocean. Icarus 376:114853

Kvorka J, Cadek O, Tobie G, Choblet G (2018) Does Titan's long-wavelength topography contain information about subsurface ocean dynamics? Icarus 310:149–164. https://doi.org/10.1016/j.icarus.2017.12.010
Labrosse S, Morison A, Deguen R, Alboussiére T (2018) Rayleigh-Benard convection in a creeping solid with melting and freezing at either or both its horizontal boundaries. J Fluid Mech 846:5–36
Lainey V, Arlot J, Vienne A (2004a) New accurate ephemerides for the Galilean satellites of Jupiter - ii. Fitting the observations. Astron Astrophys 427(1):371–376
Lainey V, Duriez L, Vienne A (2004b) New accurate ephemerides for the Galilean satellites of Jupiter - I. Numerical integration of elaborated equations of motion. Astron Astrophys 420(3):1171–1183
Lainey V, Duriez L, Vienne A (2006) Synthetic representation of the Galilean satellites orbital motions from L1 ephemerides. Astron Astrophys 456:783–788. https://doi.org/10.1051/00004-6361:20064941
Lainey V, Arlot J-E, Karatekin O, Van Hoolst T (2009) Strong tidal dissipation in Io and Jupiter from astrometric observations. Nature 459(7249):957–959
Lainey V, Karatekin Ö, Desmars J, Charnoz S, Arlot J-E, Emelyanov N, Le Poncin-Lafitte C, Mathis S, Remus F, Tobie G et al (2012) Strong tidal dissipation in Saturn and constraints on Enceladus' thermal state from astrometry. Astrophys J 752(1):14
Lainey V, Jacobson RA, Tajeddine R, Cooper NJ, Murray C, Robert V, Tobie G, Guillot T, Mathis S, Remus F et al (2017) New constraints on Saturn's interior from Cassini astrometric data. Icarus 281:286–296
Lainey V, Casajus LG, Fuller J, Zannoni M, Tortora P, Cooper N, Murray C, Modenini D, Park RS, Robert V et al (2020) Resonance locking in giant planets indicated by the rapid orbital expansion of Titan. Nat Astron 4(11):1053–1058
Lari G, Milani A (2019) Chaotic orbit determination in the context of the JUICE mission. Planet Space Sci 176:104679
Lari G, Saillenfest M, Fenucci M (2020) Long-term evolution of the Galilean satellites: the capture of Callisto into resonance. Astron Astrophys 639:A40
Lari G, Saillenfest M, Grassi C (2023) Dynamical history of the Galilean satellites for a fast migration of Callisto. Mon Not R Astron Soc 518:2023–2035. https://doi.org/10.1093/mnras/stac3299
Le Bars M, Wieczorek MA, Karatekin Ö, Cébron D, Laneuville M (2011) An impact-driven dynamo for the early Moon. Nature 479:215–218. https://doi.org/10.1038/nature10565
Le Bars M, Cébron D, Le Gal P (2015) Flows driven by libration, precession, and tides. Annu Rev Fluid Mech 47:163–193. https://doi.org/10.1146/annurev-fluid-010814-014556
Lebec L, Labrosse S, Morison A, Tackley PJ (2023) Scaling of convection in high-pressure ice layers of large icy moons and implications for habitability. Icarus 396:115494
Lefèvre A, Tobie G, Choblet G, Cadek O (2014) Structure and dynamics of Titan's outer icy shell constrained from Cassini data. Icarus 237:16–28
Lesage E, Massol H, Schmidt F (2020) Cryomagma ascent on Europa. Icarus 335:113369
Lieske J (1986) A collection of Galilean satellite eclipse observations, 1652-1983. I. Astron Astrophys 154:61–76
Ligier N, Poulet F, Carter J, Brunetto R, Gourgeot F (2016) VLT/SINFONI observations of Europa: new insights into the surface composition. Astron J 151:163
Ligier N, Paranicas C, Carter J, Poulet F, Calvin WM, Nordheim TA, Snodgrass C, Ferellec L (2019) Surface composition and properties of Ganymede: updates from ground-based observations with the near-infrared imaging spectrometer SINFONI/VLT/ESO. Icarus 333:496–515. https://doi.org/10.1016/j.icarus.2019.06.013
Liuzzo L, Simon S, Feyerabend M (2018) Observability of Callisto's inductive signature during the JUpiter ICy moons Explorer mission. J Geophys Res Space Phys 123. https://doi.org/10.1029/2018JA025951
Liuzzo L, Poppe AR, Paranicas C, Nénon Q, Fatemi S, Simon S (2020) Variability in the energetic electron bombardment of Ganymede. J Geophys Res Space Phys 125(9):e2020JA028347
Louis CK, Hess SLG, Cecconi B, Zarka P, Lamy L, Aicardi S, Loh A (2019) ExPRES: an exoplanetary and planetary radio emissions simulator. Astron Astrophys 627:A30
Madeira G, Izidoro A, Giuliatti Winter SM (2021) Building the Galilean moons system via pebble accretion and migration: a primordial resonant chain. Mon Not R Astron Soc 504:1854–1872
Magee BA, Waite JH (2017) Neutral gas composition of Enceladus' plume - model parameter insights from Cassini-INMS. In: 48th Lunar and Planetary Science Conference, The Woodlands, Texas, 20-24 March 2017. LPI contribution, vol 1964. pp 2974
Magnanini A (2021) Estimation of the ephemerides and gravity fields of the Galilean moons through orbit determination of the JUICE mission. Aerotec Missili Spaz 100(3):195–206
Magnanini A, Zannoni M, Gomez Casajus L, Tortora P, Lainey V, Mazarico E, Park RS, Iess L (2024) Joint Analysis of JUICE and Europa Clipper Tracking Data to Study the Jovian System Ephemerides and Dissipative Parameters. Astron Astrophys. Accepted
Masters A, Modolo R, Roussos E et al (2024). Magnetosphere and plasma science with the Jupiter Icy Moons Explorer. Space Sci Rev 220

Mazarico E, Buccino D, Castillo-Rogez J, Dombard AJ, Genova A, Hussmann H, Kiefer WS, Lunine JI, McKinnon WB, Nimmo F et al (2023) The Europa clipper gravity and radio science investigation. Space Sci Rev 219:30. https://doi.org/10.1007/s11214-023-00972-0

McCarthy C, Castillo-Rogez JC (2013) Planetary ices attenuation properties. In: Gudipati MS, Castillo-Rogez J (eds) The science of Solar System ices. Astrophysics and Space Science Library, vol 356, pp 183–225. https://doi.org/10.1007/978-1-4614-3076-6_7

McCarthy C, Cooper RF (2016) Tidal dissipation in creeping ice and the thermal evolution of Europa. Earth Planet Sci Lett 443:185

McCord TB, Hansen GB, Matson DL, Jonhson TV, Crowley JK, Fanale FP, Carlson RW, Smythe WD, Martin PD, Hibbitts CA, Granahan JC, Ocampo A (1999) Hydrated salt minerals on Europa's surface from the Galileo Near-Infrared Mapping Spectrometer (NIMS) investigation. J Geophys Res, Solid Earth 104:11827–11852. https://doi.org/10.1029/1999JE900005

McGrath M et al (2013) Aurora on Ganymede. J Geophys Res Space Phys 118:2043–2054. https://doi.org/10.1002/jgra.50122

Métivier L, Konrad CP (2008) Body tides of a convecting, laterally heterogeneous, and aspherical Earth. J Geophys Res 113:B11405. https://doi.org/10.1029/2007JB005448

Mitri G, Meriggiola R, Hayes A, Lefevre A, Tobie G (2014) Shape, topography, gravity anomalies and tidal deformation of Titan. Icarus 236:169–177

Molyneux PM, Nichols JD, Becker TM, Raut U, Retherford KD (2020) Ganymede's far-ultraviolet reflectance: constraining impurities in the surface ice. J Geophys Res, Planets 125(9):e2020JE006476

Molyneux PM, Greathouse TK, Gladstone GR, Versteeg MH, Hue V, Kammer J et al (2022) Ganymede's UV reflectance from Juno-UVS data. Geophys Res Lett 49:e2022GL099532

Monteux J, Tobie G, Choblet G, Le Feuvre M (2014) Can large icy moons accrete undifferentiated? Icarus 237:377–387

Moore WB, Schubert G (2000) The tidal response of Europa. Icarus 147:317–319

Moore WB, Schubert G (2003) The tidal response of Ganymede and Callisto with and without liquid water oceans. Icarus 166:223–226

Morgado B, Gomes-J únior A, Braga-Ribas F, Vieira-Martins R, Desmars J, Lainey V, D'aversa E, Dunham D, Moore J, Baillié K et al (2022) Milliarc-second astrometry for the gGalilean moons using stellar occultations. Astron J 163(5):240

Mura A, Adriani A, Sordini R, Sindoni G, Plainaki C, Tosi F, Filacchione G, Bolton S, Zambon F, Hansen CJ, Ciarniello M, Brooks S, Piccioni G, Grassi D, Altieri F, Migliorini A, Moriconi ML, Noschese R, Cicchetti A (2020) Infrared Observations of Ganymede from the Jovian InfraRed Auroral Mapper on Juno. J Geophys Res, Planets, 125:e06508. https://doi.org/10.1029/2020JE006508

Murray CD, Dermott SF (1999) Solar System dynamics. Cambridge University Press, Cambridge

Musotto S, Varadi F, Moore W, Schubert G (2002) Numerical simulations of the orbits of the Galilean satellites. Icarus 159(2):500–504

Nagel K, Breuer D, Spohn T (2004) A model for the interior structure, evolution, and differentiation of Callisto. Icarus 169:402–412

Neri A, Guyot F, Reynard B, Sotin C (2021) A carbonaceous chondrite and cometary origin for icy moons of Jupiter and Saturn. Earth Planet Sci Lett 530:115920

Neubauer (1998) The sub-Alfvénic interaction of the Galilean satellites with the Jovian magnetosphere. J Geophys Res 103(E9):19843–19866

Nimmo F, Pappalardo RT (2004) Furrow flexure and ancient heat flux on Ganymede. Geophys Res Lett 31:L19701. https://doi.org/10.1029/2004GL020763

Nimmo F, Pappalardo RT, Giese B (2002) Effective elastic thickness and heat flux estimates on Ganymede. Geophys Res Lett 29:62. https://doi.org/10.1029/2001GL013976

Nimmo F, Thomas PC, Pappalardo RT, Moore WB (2007) The global shape of Europa: constraints on lateral shell thickness variations. Icarus 191:183–192. https://doi.org/10.1016/j.icarus.2007.04.021

Nouvel J-F, Herique A, Kofman W, Safaeinili A (2004) Radar signal simulation: surface modeling with the facet method. Radio Sci 39:RS1013. https://doi.org/10.1029/2003RS002903

O'Rourke J, Stevenson DJ (2014) Stability of ice/rock mixtures with application to a partially differentiated Titan. Icarus 227:67–77

Paganini L, Villanueva GL, Roth L et al (2020) A measurement of water vapour amid a largely quiescent environment on Europa. Nat Astron 4:266–272

Palguta J, Anderson JD, Schubert G, Moore WB (2006) Mass anomalies on Ganymede. Icarus 180:428. https://doi.org/10.1016/j.icarus.2005.08.020

Palguta J, Schubert G, Zhang K, Anderson JD (2009) Constraints on the location, magnitude, and dimensions of Ganymede's mass anomalies. Icarus 201:615. https://doi.org/10.1016/j.icarus.2009.02.004

Palumbo et al (2024) Title to be determined. Space Sci Rev 220

Pappalardo RT, Collins GC, Head JW, Helfenstein P, McCord TB, Moore JM, Spencer JR (2004) Geology of Ganymede. In: Bagenal F, Dowling TE, McKinnon WB (eds) Jupiter. The planet, satellites and magnetosphere. Cambridge University Press, Cambridge, p 363–396
Pauer M, Musiol S, Breuer D (2010) Gravity signals on Europa from silicate shell density variations. J Geophys Res, Planets 115. https://doi.org/10.1029/2010JE003595
Peale SJ (1969) Generalized Cassini's laws. Astron J 74:483–489
Peale SJ, Lee MH (2002) A primordial origin of the Laplace relation among the Galilean satellites. Science 298:593–597
Petricca F, Genova A, Castillo-Rogez JC, Styczinski MJ, Cochrane CJ, Vance SD (2023) Characterization of icy moon hydrospheres through joint inversion of gravity and magnetic field measurements. Geophys Res Lett 50:e2023GL104016. https://doi.org/10.1029/2023GL104016
Porco C, DiNino D, Nimmo F (2014) How the geysers, tidal stresses, and thermal emission across the south polar terrain of Enceladus are related. Astrophys J 148:45
Postberg F, Kempf S, Schmidt J, Brilliantov N, Beinsen A, Abel B, Buck U, Srama R (2009) Sodium salts in E-ring ice grains from an ocean below the surface of Enceladus. Nature 459:1098–1101
Postberg F, Schmidt J, Hillier J, Kempf S, Srama R (2011) A salt-water reservoir as the source of a compositionally stratified plume on Enceladus. Nature 474:620–622
Poulet F, Piccioni G, Langevin Y et al (2024) Moons and Jupiter Imaging Spectrometer (MAJIS) on Jupiter Icy Moons Explorer (JUICE). Space Sci Rev 220:27. https://doi.org/10.1007/s11214-024-01057-2
Quick LC, Glaze LS, Baloga SM (2017) Cryovolcanic emplacement of domes on Europa. Icarus 284:477–488
Rambaux N, Van Hoolst T, Karatekin Ö (2011) Librational response of Europa, Ganymede, and Callisto with an ocean for a non-Keplerian orbit. Astron Astrophys 527:A118. https://doi.org/10.1051/0004-6361/201015304
Rhoden AR, Hurford TA, Roth L, Retherford K (2015) Linking Europa's plume activity to tides, tectonics, and liquid water. Icarus 253:169–178
Roberts TM, Romero-Wolf A, Bruzzone L, Carrer L, Peters S, Schroeder DM (2021) Conditioning Jovian Burst Signals for Passive Sounding Applications. IEEE Trans Geosci Remote Sens
Roberts JH, McKinnon WB, Elder CM, Tobie G et al (2023) Integrated interior science with Europa Clipper. Space Sci Rev 219:46. https://doi.org/10.1007/s11214-023-00990-y
Robidel R, Le Mouélic S, Tobie G, Massé M, Seignovert B, Sotin C, Rodriguez S (2020) Photometrically-corrected global infrared mosaics of Enceladus: new implications for its spectral diversity and geological activity. Icarus 349:113848
Romero-Wolf A, Vance S, Maiwald F, Heggy E, Ries P, Liewer K (2015) A passive probe for subsurface oceans and liquid water in Jupiter's icy moons. Icarus 248:463–477
Ronnet T, Mousis O, Vernazza P, Lunine JI, Crida A (2018) Saturn's formation and early evolution at the origin of Jupiter's massive moons. Astron J 155:224
Roth L, Saur J, Retherford KD, Strobel DF, Feldman PD, McGrath MA, Nimmo F (2014) Transient water vapor at Europa's south pole. Science 343:171–174
Rovira-Navarro M, Matsuyama I, Hay HCFC (2023) Thin-shell tidal dynamics of ocean worlds. Planet Sci J 4:23. https://doi.org/10.3847/PSJ/acae9a
Rückriemen T, Breuer D, Spohn T (2015) The Fe snow regime in Ganymede's core: a deep-seated dynamo below a stable snow zone. J Geophys Res, Planets 120:1095–1118
Rückriemen T, Breuer D, Spohn T (2018) Top-down freezing in a Fe-FeS core and Ganymede's present-day magnetic field. Icarus 307:172–196
Rudolph ML, Manga M, Walker M, Rhoden AR (2022) Cooling crusts create concomitant cryovolcanic cracks. Geophysical Research Letters 49(5):e2021GL094421
Saquet E, Emelyanov N, Robert V, Arlot J, Anbazhagan P, Baillie K, Bardecker J, Berezhnoy A, Bretton M, Campos F et al (2018) The PHEMU15 catalogue and astrometric results of the Jupiter's Galilean satellite mutual occultation and eclipse observations made in 2014-2015. Mon Not R Astron Soc Lett 474(4):4730–4739
Sarson GR, Jones CA, Zhang K, Schubert G (1997) Magnetoconvcetion dynamos and the magnetic fields of Ganymede and Io. Science 276:1106–1108
Saur J et al (2010) Induced magnetic fields in Solar System bodies. Space Sci Rev 152:391–421. https://doi.org/10.1007/s11214-009-9581-y
Saur J et al (2015) The search for a subsurface ocean in Ganymede with Hubble Space Telescope observations of its auroral ovals. J Geophys Res Space Phys 120:1715–1737. https://doi.org/10.1002/2014JA020778
Sbalchiero E, Thakur S, Bruzzone L (2019) 3D radar sounder simulations of geological targets on Ganymede Jovian Moon. In: Image and signal processing for remote sensing XXV, vol 11155. International Society for Optics and Photonics, p 111551J

Sbalchiero E, Thakur S, Cortellazzi M, Bruzzone L (2023) Subsurface signatures of bright terrain formation models on Ganymede by 3D radar sounder simulations. Icarus 394:0019. https://doi.org/10.1016/j.icarus.2022.115351
Schenk PM, Chapman CR, Zahnle K, Moore JM (2004) Ages and interiors: the cratering record of the Galilean satellites. In: Bagenal F, Dowling TE, McKinnon WB (eds) Jupiter. The planet, satellites and magnetosphere. Cambridge University Press, Cambridge, p 427–456
Schilling et al (2007) Time-varying interaction of Europa with the Jovian magnetosphere: constraints on the conductivity of Europa's subsurface ocean. Icarus 192:41–55
Schroeder DM, Romero-Wolf A, Carrer L, Grima C, Campbell BA, Kofman W, Blankenship DD (2016) Assessing the potential for passive radio sounding of Europa and Ganymede with RIME and REASON. Planet Space Sci 134:52–60
Schubert G, Zhang K, Kivelson M, Anderson J (1996) The magnetic field and internal structure of Ganymede. Nature 384:544–545
Seufert et al (2011) Multi-frequency electromagnetic sounding of the Galilean moons. Icarus 214:477–494. https://doi.org/10.1016/j.icarus.2011.03.017
Shibaike Y, Ormel CW, Ida S, Okuzumi S, Sasaki T (2019) The Galilean satellites formed slowly from pebbles
Showman AP, Malhotra R (1997) Tidal evolution into the Laplace resonance and the resurfacing of Ganymede. Icarus 127:93–111
Showman AP, Mosqueira I, Head JW III (2004) On the resurfacing of Ganymede by liquid-water volcanism. Icarus 172(2):625–640
Soderlund KM (2019) Ocean dynamics of outer Solar System satellites. Geophys Res Lett 46:8700–8710. https://doi.org/10.1029/2018GL081880
Soderlund KM, Schmidt BE, Wicht J, Blankenship DD (2014) Ocean-driven heating of Europa's icy shell at low latitudes. Nat Geosci 7:16–19
Soderlund KM, Kalousova K, Buffo JJ, Glein CR, Goodman JC, Mitri G, Patterson GW, Postberg F, Rovira-Navarro M, Rückriemen T, Saur J, Schmidt BE, Spohn T, Sotin C, Tobie G, Van Hoolst T, Vance SD, Vermeersen LLD (2020) Ice-ocean exchange processes in the Jovian and Saturnian satellites. Space Sci Rev 216(5):1–57. https://doi.org/10.1007/s11214-020-00706-6
Sohl F, Spohn T, Breuer D, Nagel K (2002) Implications from Galileo observations of the interior structure and chemistry of the Galilean satellites. Icarus 157:104–119
Southworth BS, Kempf S, Schmidt J (2015) Modeling Europa's dust plumes. Geophys Res Lett 42:10541–10548
Sparks WB, Hand KP, McGrath MA, Bergeson E, Cracraft M, Deustea SE (2016) Probing for evidence of plumes on Europa with HST/STIS. Astrophys J 829:121
Sparks WB, Smith BE, McGrath MA, Hand KP, Spencer JR, Cracraft M, Deustea SE (2017) Active cryovolcanism on Europa. Astrophys J Lett 839:L18
Spohn T, Breuer D (1998) Interior structure and evolution of the Galilean satellites. Planetary systems: the long view. In: Celnikier LM, Van Tran Thanh J (eds) 9th Rencontres de Blois: held June 22-28, 1997, at Château de Blois, France, p 135. Editions Frontières
Steinbrügge G et al (2015) Measuring tidal deformations by laser altimetry. A performance model for the Ganymede laser altimeter. Planet Space Sci 117:184–191
Steinbrügge G, Steinke T, Thor R, Stark A, Hussmann H (2019) Measuring Ganymede's librations with laser altimetry. Geosci 9:320. https://doi.org/10.3390/geosciences9070320
Steinbrügge G, Hussmann H, Tobie G, Castillo-Rogez J, Lainey V, Stark A (2024) Tidal deformation and tidal evolution of Ganymede. In: Volwerk M, McGrath M, Jia X, Spohn T (eds) Ganymede. Cambridge University Press, Cambridge
Stephan K, Roatsch T, Tosi F, Matz K-D, Kersten E, Wagner R, Molyneux P, Palumbo P, Poulet F, Hussmann H, Barabash S, Bruzzone L, Dougherty M, Gladstone R, Gurvits LI, Hartogh P, Iess L, Wahlund J-E, Wurz P, Witasse O, Grasset O, Altobelli N, Carter J, Cavalié T, D'Aversa E, Della Corte V, Filacchione G, Galli A, Galluzzi V, Gwinner K, Hauber E, Jaumann R, Krohn K, Langevin Y, Lucchetti A, Migliorini A, Piccioni G, Solomonidou A, Stark A, Tobie G, Tubiana C, Vallat C, van Hoolst T (The Juice Swt Team) (2021) Regions of interest on Ganymede's and Callisto's surfaces as potential targets for ESA's JUICE mission. Planet Space Sci 208:105324. https://doi.org/10.1016/j.pss.2021.105324
Stevenson DJ (2000) Limits on the variation of thickness of Europa's ice shell Lunar and Planetary Science XXXI. Abstract 1506
Tan S, Sekine Y, Kuzuhara Y (2022) Spatially resolved observations of Europa's surface with subaru/IRCS at 1.0-1.8 μm: upper limits to the abundances of hydrated Cl-bearing salts. Planet Sci J 3:70
Teolis BD, Plainaki C, Cassidy TA, Raut U (2017) Water ice radiolytic O_2, H_2, and H_2O_2 yields for any projectile species, energy, or temperature: a model for icy astrophysical bodies. J Geophys Res, Planets 122:1996–2012

Terra-Nova F, Amit H, Choblet G, Tobie G, Bouffard M, Cadek O (2023) The influence of heterogeneous seafloor heat flux on the cooling patterns of Ganymede's and Titan's subsurface oceans. Icarus 389:115232

Thakur S, Bruzzone L (2021) An approach to the generation and analysis of databases of simulated radar sounder data for performance prediction and target interpretation. IEEE Trans Geosci Remote Sens 59(10):8269–8287

Thomas PC, Tajeddine R, Tiscareno MS et al (2016) Enceladus's measured physical libration requires a global subsurface ocean. Icarus 264:37–47

Tiscareno MS, Thomas PC, Burns JA (2009) The rotation of JANUS and epimetheus. Icarus 204:254–261

Tobie G, Lunine JI, Monteux J, Mousis O, Nimmo F (2014) The origin and evolution of Titan. In: Müller-Wodarg I, Griffith CA, Lellouch E, Cravens TE (eds) Titan. Cambridge University Press, Cambridge, p 29

Tosi F, Galluzzi V, Lucchetti A, Orosei R, Filacchione G, Zambon F, Cremonese G, Palumbo P, Piccioni G (2023a) Mutidisciplinary analysis of the Nippur Sulcus region on Ganymede. J Geophys Res, Planets 128(7):e2023JE007836. https://doi.org/10.1029/2023JE007836

Tosi F, Mura A, Cofano A, Zambon F, Glein CR, Ciarniello M, Lunine JI, Piccioni G, Plainaki C, Sordini R, Adriani A, Bolton SJ, Hansen CJ, Nordheim TA, Moirano A, Agostini L, Altieri F, Brooks SM, Cicchetti A, Dinelli BM, Grassi D, Migliorini A, Moriconi ML, Noschese R, Carica P, Sindoni G, Stefani S, Turrini D (2024) Salts and organics on Ganymede's surface observed by the JIRAM spectrometer onboard Juno. Nat Astron 8(1):82–93. https://doi.org/10.1038/s41550-023-02107-5

Tosi F, Roatsch T, Galli A, Hauber E, Lucchetti A, Molyneux P, Stephan K et al (2024) Characterization of the surfaces and near-surface atmospheres of Ganymede, Europa and Callisto by JUICE. Space Sci Rev 220

Trumbo SK, Brown ME (2023) The distribution of CO2 on Europa indicates an internal source of carbon. Science 381(6664):1308–1311

Trumbo SK, Brown ME, Hand KP (2019) Sodium chloride on the surface of Europa. Sci Adv 5:7123

Trumbo SK, Becker TM, Brown ME, Denman WTP, Molyneux P, Hendrix A, Retherford KD, Roth L, Alday J (2022) A new UV spectral feature on Europa: confirmation of NaCl in leading-hemisphere chaos terrain. Planet Sci J 3:27. https://doi.org/10.3847/PSJ/ac4580

Tyler R (2008) Strong ocean tidal flow and heating on moons of the outer planets. Nature 456:770–772

Tyler RH (2011a) Tidal dynamical considerations constrain the state of an ocean on Enceladus. Icarus 211:770–779. https://doi.org/10.1016/j.icarus.2010.10.007

Tyler RH (2011b) Magnetic remote sensing of Europa's ocean tides. Icarus 211:906–908. https://doi.org/10.1016/j.icarus.2010.10.011

Van Hoolst T, Rambaux N, Karatekin Ö, Dehant V, Rivoldini A (2008) The librations, shape, and icy shell of Europa. Icarus 195/1:386–399. https://doi.org/10.1016/j.icarus.2007.12.011

Van Hoolst T, Baland RM, Trinh A (2013) The effect of tides on the longitudinal librations of large synchronously rotating icy satellites. Icarus 226:299–315

Van Hoolst T, Baland RM, Trinh A, Yseboodt M, Nimmo F (2020) The librations, tides, and interior structure of Io. J Geophys Res, Planets 125:e2020JE006473. https://doi.org/10.1029/2020JE006473

Vance S, Goodman J (2009) Oceanography of an ice-covered moon. In: Pappalardo RT, McKinnon WB, Khurana KK (eds) Europa. University of Arizona Press, Tucson, pp 459–482

Vance S, Bouffard M, Choukroun M, Sotin C (2014) Ganymede's internal structure including thermodynamics of magnesium sulfate oceans in contact with ice. Planet Space Sci 96:62–70

Vance SD, Panning MP, Stähler S, Cammarano F, Bills BG, Tobie G et al (2018) Geophysical investigations of habitability in ice-covered ocean worlds. J Geophys Res, Planets 123:180–205. https://doi.org/10.1002/2017je005341

Vance SD, Styczinski MJ, Bills BG, Cochrane CJ, Soderlund KM, Gómez-Pérez N, Paty C (2021) Magnetic induction responses of Jupiter's ocean moons including effects from adiabatic convection. J Geophys Res, Planets 126:e2020JE006418. https://doi.org/10.1029/2020JE006418

Velez MA, Retherford KD, Hue V, Kammer JA, Gladstone GR, Davis MW, Greathouse TK, Becker TM, Molyneux PM, Brooks SM et al (2022) An ultraviolet stellar catalog for occultation measurements, planetary illumination modeling, and spectral sky map analyses. In: Space telescopes and instrumentation 2022: ultraviolet to Gamma ray 12181. SPIE, Bellingham, pp 791–796

Villamil S, Dirkx D, Stark A, Hussmann H (2021) Improvement of orbit determination using laser altimeter crossovers: JUICE mission case study. Acta Astronaut 182:587–598

Villanueva GL, Hammel HB, Milam SN, Faggi S, Kofman V, Roth L et al (2023) Endogenous CO_2 ice mixture on the surface of Europa and no detection of plume activity. Science 381(6664):1305–1308

Vincent D, Lambrechts J, Tyler RH, Karatekin O, Dehant V, Deleersnijder E (2022) A numerical study of the liquid motion in Titan's subsurface ocean. Icarus 388:115219

Volwerk M, McGrath M, Jia X, Spohn T (eds) (2024) Ganymede. Cambridge University Press, Cambridge

Vorburger A, Wurz P (2021) Modeling of possible plume mechanisms on Europa. J Geophys Res Space Phys 126:e2021JA029690
Vu TH, Choukroun M, Hodyss R, Johnson PV (2020) Probing Europa's subsurface ocean composition from surface salt minerals using in-situ techniques. Icarus 349:113746. https://doi.org/10.1016/j.icarus.2020.113746
Wahlund J-E et al (2024) The Radio and Plasma Wave Investigation (RPWI) for the Jupiter Icy Moons Explorer (JUICE). Space Sci Rev 220
Wahr JM et al (2006) Tides on Europa, and the thickness of Europa's icy shell. J Geophys Res, Planets 111.E12
Waite JH et al (2006) Cassini ion and Neutral Mass Spectrometer: Enceladus plume composition and structure. Science 311:1419–1422
Waite JH et al (2017) Cassini finds molecular hydrogen in the Enceladus plume: evidence for hydrothermal processes. Science 356:155–159
Wardinski I, Amit H, Langlais B, Thébault E (2021) The internal structure of Mercury's core inferred from magnetic observations. J Geophys Res, Planets 126:e2020JE006792. https://doi.org/10.1029/2020JE006792
Watts AB (2001) Isostasy and flexure of the lithosphere. Cambridge University Press, Cambridge
Wieczorek MA (2015) Gravity and topography of the terrestrial planets. In: Spohn T, Schubert G (eds) Treatise on geophysics (second edition). Elsevier-Pergamon, Oxford, pp 153–193. https://doi.org/10.1016/B978-0-444-53802-4.00169-X
Wieczorek MA, Weiss BP, Breuer D, Cébron D, Fuller M et al (2022) Lunar magnetism. Hal-03524536
Williams JG, Boggs DH, Yoder CF, Ratcliff JT, Dickey JO (2001) Lunar rotational dissipation in solid body and Molten core. J Geophys Res 106(E11):27933–27968
Winterhalder TO, Huybrighs HLF (2022) Assessing JUICE's ability of in situ plume detection in Europa's atmosphere. Planet Space Sci 210:105375
Wisdom J (2004) Spin-orbit secondary resonance dynamics of Enceladus. Astrophys J 128:484–491. https://doi.org/10.1086/421360
Witasse O et al (2024) The Jupiter Icy Moons Explorer (JUICE). Space Sci Rev 220
Yoder CF, Peale SJ (1981) The tides of Io. Icarus 47:1–35
Zannoni M, Hemingway DJ, Gomez Casajus L, Tortora P (2020) The gravity field and interior structure of Dione. Icarus 345
Zhong S, Qin C, Wahr J (2012) Can tidal tomography be used to unravel the long-wavelength structure of the lunar interior? Geophys Res Lett 39:L15201. https://doi.org/10.1029/2012GL052362
Zimmer et al (2000) Subsurface oceans on Europa and Callisto: constraints from Galileo magnetometer observations. Icarus 147:329–347
Zolotov MY (2012) Aqueous fluid composition in CI chondritic materials: chemical equilibrium assessments in closed systems. Icarus 220(2):713–729
Zolotov MY, Kargel J (2009) On the chemical composition of Europa's icy shell, ocean, and underlying rocks. In: Pappalardo RT, McKinnon WB, Khurana K (eds) Europa. University of Arizona Press, Tucson, pp 431–457
Zubarev A, Nadezhdina I, Oberst J, Hussmann H, Stark A (2015) New Ganymede control point network and global shape model. Planet Space Sci 117:246–249

Authors and Affiliations

Tim Van Hoolst[1,2] · Gabriel Tobie[3] · Claire Vallat[4] · Nicolas Altobelli[4] · Lorenzo Bruzzone[5] · Hao Cao[6] · Dominic Dirkx[7] · Antonio Genova[8] · Hauke Hussmann[9] · Luciano Iess[8] · Jun Kimura[10] · Krishan Khurana[11] · Alice Lucchetti[12] · Giuseppe Mitri[13,14] · William Moore[15,16] · Joachim Saur[17] · Alexander Stark[9] · Audrey Vorburger[18] · Mark Wieczorek[19] · Alessio Aboudan[12] · Jan Bergman[20] · Francesca Bovolo[21] · Doris Breuer[9] · Paolo Cappuccio[8] · Leonardo Carrer[5] · Baptiste Cecconi[22] · Gaël Choblet[3] · Fabrizio De Marchi[8] · Marie Fayolle[7] · Agnès Fienga[23] · Yoshifumi Futaana[24] · Ernst Hauber[9] · Wlodek Kofman[25,26] · Atsushi Kumamoto[27] · Valery Lainey[28] · Philippa Molyneux[29] ·

Olivier Mousis[30,31] · Jeff Plaut[32] · Walter Puccio[20] · Kurt Retherford[33] · Lorenz Roth[34] · Benoit Seignovert[3] · Gregor Steinbrügge[32] · Sanchari Thakur[5] · Paolo Tortora[35] · Federico Tosi[36] · Marco Zannoni[35] · Stas Barabash[20] · Michele Dougherty[37] · Randy Gladstone[33] · Leonid I. Gurvits[38,7] · Paul Hartogh[39] · Pasquale Palumbo[40] · Francois Poulet[41] · Jan-Erik Wahlund[20] · Olivier Grasset[3] · Olivier Witasse[42]

✉ T. Van Hoolst
tim.vanhoolst@oma.be

✉ G. Tobie
gabriel.tobie@univ-nantes.fr

1 Royal Observatory of Belgium, Ringlaan 3, Brussels, 1180, Belgium

2 Institute of Astronomy, KU Leuven, Celestijnenlaan 200D, Leuven, 3001, Belgium

3 Nantes Université, Univ Angers, Le Mans Université, CNRS, Laboratoire de Planétologie et Géosciences, UMR 6112, 2 rue de la Houssinière, Nantes, 44322, France

4 ESAC, European Space Agency (ESA), Camino Bajo del Castillo s/n Villafranca del Castillo, Villanueva de la Cañada (Madrid), 28692, Spain

5 Department of Information Engineering and Computer Science, University of Trento, Via Sommarive, 5, Povo, 38123, Italy

6 Department of Earth, Planetary, and Space Sciences, University of California, Los Angeles, 595 Charles E Young Dr East, Los Angeles, 90095, CA, USA

7 Faculty of Aerospace Engineering, Delft University of Technology, Kluyverweg 1, Delft, 2629 HS, The Netherlands

8 Department of Mechanical and Aerospace Engineering, Sapienza University of Rome, Rome, Italy

9 Deutsches Zentrum für Luft- und Raumfahrt (DLR), Berlin,Germany

10 Department of Earth and Space Science, Osaka University, 1-1, Machikaneyama-cho, Toyonaka, 5600043, Osaka, Japan

11 Earth, Planetary, and Space Sciences, UCLA, Los Angeles, USA

12 INAF, Astronomical observatory of Padova, Vic. Osservatorio 5, Padova, 35122, Italy

13 International Research School of Planetary Sciences, Viale Pindaro 42, Pescara, 65127, Italy

14 Dipartimento di Ingegneria e Geologia, Università d'Annunzio, Viale Pindaro 42, Pescara, 65127, Italy

15 Department of Atmospheric and Planetary Sciences, Hampton University, 100 William R. Harvey Way, Hampton, 23668, VA, USA

16 National Institute of Aerospace, 100 Exploration Way, Hampton, 23666, VA, USA

17 Institute of Geophysics and Meteorology, University of Cologne, Cologne, Germany

18 Space Research and Planetary Sciences, Physics Institute, University of Bern, Sidlerstrasse 5, Bern, 3012, Bern, Switzerland

19 Laboratoire Lagrange, Observatoire de la Côte d'Azur, Nice, France

20 Swedish Institute of Space Physics, Uppsala, 75121, Sweden

21 Center for Digital Society, Fondazione Bruno Kessler, Via Sommarive 18, Povo, 38123, Italy

22 LESIA, Observatoire de Paris, Paris, France

[23] Géoazur, Observatoire de la Côte d'Azur, 250 av. A. Einstein, Valbonne Sophia-Antipolis, France

[24] Swedish Institute of Space Physics, Bengt Hultqvists väg 1, Kiruna, SE98192, Sweden

[25] Univ. Grenoble Alpes, CNRS, CNES, IPAG, CS 40700, Grenoble, 38058, France

[26] Centrum Badan Kosmicznych, Polskiej Akademii Nauk (CBK PAN), Bartycka 18A, Warsaw, PL-00-716, Poland

[27] Tohoku University, Sendai, Japan

[28] IMCCE, Observatoire de Paris, Paris, France

[29] Space Science Division, Southwest Research Institute, 6220 Culebra Road, San Antonio, 78238, TX, USA

[30] Aix-Marseille Université, CNRS, CNES, Institut Origines, LAM, Marseille, France

[31] Institut Universitaire de France (IUF), Paris, France

[32] Jet Propulsion Laboratory, California Institute of Technology, 4800 Oak Grove Drive, Pasadena, 91011, CA, USA

[33] Southwest Research Institute, San Antonio, TX, USA

[34] Space and Plasma Physics, KTH Royal Institute of Technology, Teknikringen 31, Stockholm, 11 428, Sweden

[35] Dipartimento di Ingegneria Industriale, Università di Bologna, Via Fontanelle 40, Forlì, Italy

[36] Istituto Nazionale di AstroFisica - Istituto di Astrofisica e Planetologia Spaziali (INAF-IAPS), Via del Fosso del Cavaliere, 100, Rome, 00133, Italy

[37] Blackett Laboratory, Imperial College London, London, UK

[38] Joint Institute for VLBI ERIC, Oude Hoogeveensedijk 4, Dwingeloo, 7991 PD, The Netherlands

[39] Max-Planck-Institut für Sonnensystemforschung, Göttingen, 37077, Germany

[40] Istituto di Astrofisica e Planetologia Spaziali, Istituto Nazionale di Astrofisica, Via del Fosso del Cavaliere, 100, Roma, I-00133, Italy

[41] Institut d'Astrophysique Spatiale, CNRS/Université Paris-Saclay, Bâtiment 121, Orsay Cedex, 91405, France

[42] European Space Research and Technology Centre (ESTEC), European Space Agency (ESA), Keplerlaan 1, Noordwijk, The Netherlands